AN EVALUATION OF THE NATURAL RADIOACTIVITY IN THE SOILS OF OKAHANDJA AND KARIBIB, NAMIBIA.

A MINI THESIS

SUBMITTED IN PARTIAL FULFILMENT

OF THE REQUIREMENTS FOR THE DEGREE OF

MASTER OF SCIENCE IN NUCLEAR SCIENCE

OF

THE UNIVERSITY OF NAMIBIA

BY

WILFRED MIDZI

201406379

APRIL 2018

Supervisor: Professor J Oyedele, Department of Physics, University of Namibia

ABSTRACT

The natural radioactivity and associated hazards in the soils of the towns of Karibib and Okahandja have been studied by gamma spectroscopy. Each town was divided into ten geographical areas and five soil samples were collected across each area. These samples were processed and placed in well-labelled 500 ml plastic bottles. A High Purity Germanium detector (HPGe) was used to measure the gamma ray spectra of the samples. The intensities of selected gamma lines were used to calculate the activity concentrations of the gamma emitting radionuclides ^{238}U, ^{232}Th, and ^{40}K. The average activity concentrations of ^{238}U, ^{232}Th, and ^{40}K in Karibib are 29.4 ± 5.8 Bq/kg, 49.0 ± 8.6 Bq/kg, and 824.3 ± 153.5 Bq/kg respectively while they are 40.9 ± 8.6 Bq/kg, 57.9 ± 19.4 Bq/kg, and 562.4 ± 125.4 Bq/kg respectively in Okahandja. Consequently, the average activity concentrations of ^{238}U and ^{232}Th are much higher in Okahandja than in Karibib, while the average activity concentration of ^{40}K is much higher in Karibib than in Okahandja. These concentrations were used to calculate the absorbed dose rates and effective dose rates in air in the two towns. The average absorbed dose rate in air in Okahandja is 77.3 ± 18.0 nGy/hr while that in Karibib is 77.6 ± 10.9 nGy/hr. However, the resulting average effective dose rate in Okahandja and Karibib are the same and equal to 9.5 x 10^{-2} mSv/yr. The average absorbed dose rate in air in each of the two towns is relatively high than the world average of 51 nGy/hr. However, the corresponding average effective dose rate in both towns is much below the recommended maximum permissible dose rate of 1.0 mSv/yr. This result implies that the two towns have normal background radiation. Also, the results of 163.0 ± 22.6 Bq/kg and 167.1 ± 40.1 Bq/kg obtained for the Radium equivalent activities, Ra_{eq}, in Karibib and Okahandja respectively are much lower than the recommended maximum value of 370 Bq/kg thus confirming that both towns have

normal background radiation. Furthermore, the average external hazard indices determined for Karibib and Okahandja are respectively 0.4 ± 0.1 and 0.5 ± 0.1. These values are again far less than the recommended safe level of unity. This result further confirms that radiological hazard is negligible in Karibib and Okahandja. The results obtained in this study would be useful in establishing a baseline data that will serve as a reference to ascertain possible changes in environmental radioactivity due to nuclear and related activities in future.

TABLE OF CONTENTS

LIST OF TABLES

LIST OF FIGURES

ABBREVIATIONS

IAEA	International Atomic Energy Agency
ICRP	International Commission on Radiation Protection
HPGe	High Purity Germanium
LET	Linear Energy Transfer
NIED	National Institute for Education Development
UNAM	University of Namibia
UNSCEAR	United Nations Scientific Commission on the Effects of Atomic Radiation

ACKNOWLEDGEMENTS

I would like to thank Prof J Oyedele for supervising this project and for his guidance. He encouraged me to work hard and he was always available for consultation. Also, I would like to thank Mr S. Shimboyo and Mr E. Taapopi for their help in the project. The staff of the Physics department at UNAM were very supportive and I am grateful to them.

I am also grateful to my wife, Viola, and my kids, for their support during the project.

Finally I give all glory and honour to the Almighty God for His faithfulness and mercy.

DEDICATION

This work is dedicated to my wife, Viola, and my kids, Praise, David and Pearla. I love you guys.

DECLARATIONS

I, Wilfred Midzi, hereby declare that this study is my own work and is a true reflection of my research, and that this work, or any part thereof has not been submitted for a degree at any other institution.

……..	……	… …….
Name of Student	Signature	Date

CHAPTER 1

1. INTRODUCTION

1.1 Orientation of the Study

The radioactivity of naturally occurring unstable atoms are called “natural radioactivity” while those of the man-made unstable atoms are called “artificial radioactivity”. In nature there are many unstable atoms or nuclides. The radiation coming from these naturally occurring unstable nuclides is known as natural background radiation. Soil, rocks, water and air contain unstable nuclides that are a source of natural background radiation [1].

Determination of natural radioactivity levels in the soils of different towns and countries has been of interest to scientists worldwide [2–8]. Many studies have been carried out in different parts of the world to evaluate the natural radioactivity or the natural background radiation emanating from the natural environment [7,8]. The major sources of background radiation are cosmic radiation and radiation from natural radionuclides in the soils. Research has shown that soil radionuclide activity concentration is the main determinant of the natural background radiation [9]. The worldwide average annual radiation dose due to naturally occurring radiation sources, including radon, is 2.4 mSv [10]. However, many studies have shown that there are some areas in the world with high background radiation due to high radionuclide concentration in the soils [11]. High background radiation is a health hazard as it may increase the risk of cancer. A knowledge of the distribution of natural radionuclides and radiation levels in the soil is important for assessing the effects of exposure of human beings to background radiation [3]. It is therefore of interest to determine the concentrations and distributions of radionuclides in the soils of important towns in

Namibia. In fact, there have been a number of studies on the radioactivity in the soils of some towns in Namibia [12]. This study will investigate the natural radioactivity in the soils of the towns of Okahandja and Karibib in Namibia.

1.2 Statement of the Problem

There have been many studies on the concentrations of radionuclides in the soils of many towns in Namibia [4,12–14]. In particular the concentrations of radionuclides in the soils of most towns along the B1 road from Windhoek to Walvis Bay have been studied. Only the radioactivity in the soils of the towns of Okahandja and Karibib along the B1 road (between Windhoek and Walvis Bay) have not been studied. The natural radioactivity in the soils of the two towns may be very different from those of other towns since natural radioactivity depends on the geology of a given area. There is therefore interest in assessing the radiation levels in the soils of the towns. Furthermore, earlier studies on soil radioactivity in the Walvis Bay-Henties Bay coastal region (in western Namibia) have shown a trend in which the concentration of the radionuclide ^{40}K in the soils of the towns increases with decreasing latitude [14]. It is of interest to find out if the trend will continue to Karibib and Okahandja in western Namibia.

1.3 Objectives of the study

The objectives of this study are to

a) determine the concentrations and distributions of the radionuclides ^{238}U, ^{232}Th, and ^{40}K in the soils of the towns of Karibib and Okahandja;
b) determine the level of background radiation in Karibib and Okahandja;
c) ascertain whether the background radiation levels in the towns of Karibib and Okahandja are within acceptable limit;

d) provide a baseline data of activity concentrations for assessing the contribution of nuclear activities to environmental radioactivity in future;

e) To investigate whether the increase in the concentration of ^{40}K with decreasing latitude will be observed in Karibib and Okahandja.

1.4 Significance of the Study

Okahandja is an important town and it is 70 km north of Windhoek. It is known as the "Garden Town" of Namibia. The population of the town was 14 000 in 2001 but it rapidly increased to about 23 000 in 2011 [15]. The Von Bach dam that supplies water to the city of Windhoek is close to the town. Also the National Institute for Educational Development (NIED) is situated in Okahandja. Many foreign and local tourists pass through Okahandja on their way to the coastal cities of Swakopmund and Walvis Bay. Okahandja is particularly important to the Herero tribe as they gather annually in the town in August to commemorate their fallen heroes. The envisaged study will provide information on the background radiation level to which the inhabitants of Okahandja are exposed. A number of the inhabitants of the town are scientists, engineers, technicians, educationists, etc. and they will be interested in knowing if their town has normal or high background radiation.

Karibib is a town on the main road between Windhoek and Swakopmund, some 100 km west of Okahandja. It is almost halfway between the capital city, Windhoek, and the coastal resort areas of western Namibia. This town is therefore an ideal overnight or refreshment stop-over for both foreign and local tourists travelling to the western coast of Namibia. It has a population of about 5 100 [15]. The Navachab gold mine is located 10 km from the town and it is the major source of employment for the populace of Karibib. Many workers of the gold mine live in Karibib. Marble deposits are also found in Karibib and a company processing marble and granite is based in the town.

The headquarters of the Namibian Air force is also situated in Karibib [16]. It is therefore of interest to determine the level of background radiation to which the inhabitants of the town are exposed. The study will provide a baseline data of activity concentrations for assessing the contribution of nuclear activities to environmental radioactivity in future.

CHAPTER 2

2. LITERATURE REVIEW

2.0 Introduction

In this chapter the literature that forms the basis of this research will be reviewed. The literature will be taken from books, published articles and scientific journals. There will first be a discussion of basic nuclear structure and the interaction of radiation with matter. This will be followed by discussions on radioactivity in soils and the biological effects of radiation. Finally, a review of the literature on international and local studies on soil radioactivity will be presented.

2.1.0 Radioactivity

Radioactivity, first discovered by Antonio Henri Becquerel in 1896, is a phenomenon in which radiation is given off by the nuclei of elements said to be unstable [17]. This radiation can be in the form of particles or electromagnetic waves [18]. It is a spontaneous nuclear transformation in unstable atoms that results in the formation of new elements. These transformations are characterized by one of several different mechanisms, including alpha-particle emission, beta-particle and positron emission, and orbital electron capture. Each of these reactions may or may not be accompanied by gamma radiation [19].

Radioactivity, also known as radioactive decay, nuclear decay, nuclear disintegration and nuclear transformation, is a spontaneous process by which an unstable parent nucleus emits a particle or electromagnetic radiation and transforms into a more stable daughter nucleus that may or may not be stable [19]. The unstable daughter nucleus may decay further in a decay series until a stable nuclear configuration is reached. Radioactive decay is usually accompanied by emission of energetic particles or γ ray

photons or both [20]. In 1895 Wilhelm Conrad Roentgen discovered a new phenomenon that he called the X-rays [21]. Soon after, Henri Becquerel decided to study the correlation between newly discovered X-rays and the fluorescence phenomena of uranium salts. He discovered that once exposed to ultraviolet photons (sun light), the uranium salts radiate visible light (the fluorescence phenomenon). However, due to bad weather in Paris, Becquerel was not able to expose the samples to sun light for a few weeks, during which time he left them in a closet. Later he found that the plates were exposed and concluded that a new type of radiation was emitted from the non-fluorescence uranium and correctly speculated that some materials at rest emitted radiation in a spontaneous fashion without the addition of any external energy. Becquerel called this new radiation "U rays", later renamed radioactivity [21].

2.1.1 Basic constituents of an atom

The constituent particles forming an atom are protons, neutrons and electrons. Protons and neutrons are known as nucleons and form the nucleus of the atom. Protons have a positive charge, neutrons are neutral and electrons have a negative charge mirroring that of a proton. In comparison to electrons, protons and neutrons have a relatively large mass exceeding the electron mass by a factor of almost 2000 [20].

The following general definitions apply to atomic structure:

- Atomic number Z is the number of protons or number of electrons in an atom.
- Atomic mass number A is the number of nucleons in an atom, i.e. the number of protons Z plus the number of neutrons N in an atom: $A = Z + N$.
- Atomic mass is the mass of a specific isotope expressed in atomic mass unit u, where 1 u is equal to one twelfth of the mass of the ^{12}C atom (unbound, at rest and in the ground state) or 931.5 MeV/c^2 [20].

The atomic mass is smaller than the sum of the individual masses of the constituent particles because of the intrinsic energy associated with binding the particles (nucleons) within the nucleus. On the other hand, the atomic mass is larger than the nuclear mass M because the atomic mass includes the mass contribution of Z orbital electrons while the nuclear mass M does not. The binding energy of orbital electrons to the nucleus is ignored in the definition of the atomic mass [20].

2.1.2 Basic nuclear structure

According to the Rutherford–Bohr atomic model, most of the atomic mass is concentrated in the atomic nucleus consisting of Z protons and (A – Z) neutrons where Z is the atomic number and A is the atomic mass number of a given nucleus [20]. With regards to the relative values of atomic number Z and atomic mass number A of nuclei, the following conventions apply:

- An element may be composed of atoms that all have the same number of protons, i.e. have the same atomic number Z, but have a different number of neutrons (have different atomic mass numbers A). Such atoms of identical Z but differing A are called isotopes of a given element.
- A nuclide is an atomic species characterized by its nuclear composition (A, Z and the arrangement of nucleons within the nucleus). The term ‘nuclide’ refers to all atomic forms of all elements. The term ‘isotope’ is narrower and only refers to various atomic forms of a given chemical element [20].
- Unstable nuclides are radioactive and are called radionuclides. Their decay products ('daughter' products) are called radiogenic nuclides. Figure 2.1 shows a graph of stability of nuclides.

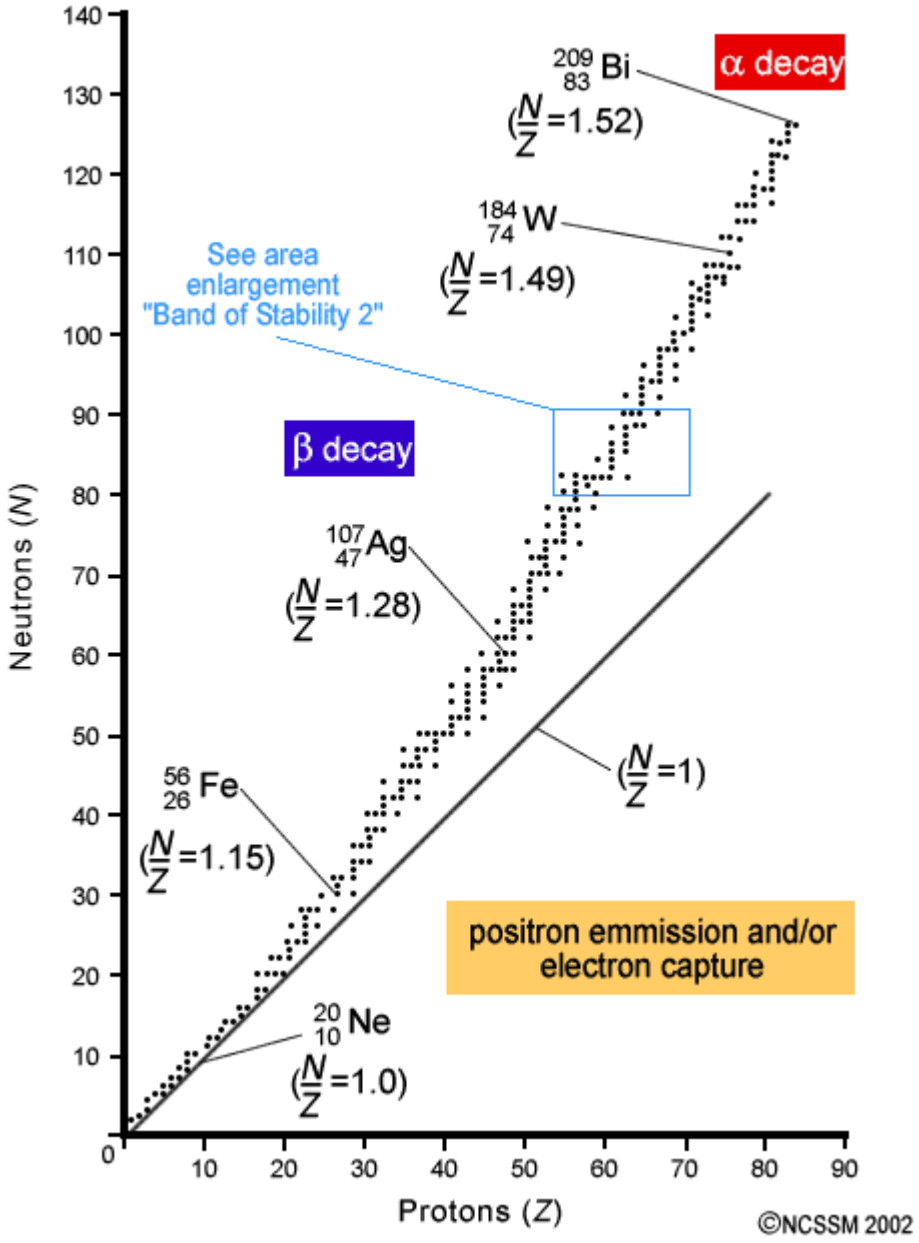

Figure 2.1. Stability of nuclides by (Z, N) [22].

From the graph in Figure 2.1 it is of interest to find out why some nuclides decay while others are stable. The question of nuclear stability depends on numbers. The number is related to the neutron to proton ratio (N/Z) [23]. From the graph of the plot of Z proton number against N neutron number, the region where stable nuclei are found is called the belt of nuclear stability. The belt is narrow and very close to 1:1 N = Z ratio. Lying outside the belt means nuclides have too many protons or neutrons to be stable, therefore the nuclide will undergo some decay to be stable. Investigation of the N/Z ratio is an important method to determine nuclear stability. Detailed analysis reveals that the numbers 2, 8, 20, 28, 50, 82 and 126 seem to impart special stability to nuclides that contain these number of protons and or neutrons. Because of this characteristic, they are sometimes referred to as *magic numbers*.

2.1.3 Modes of radioactive decay

Radioactive nuclides, either naturally occurring or artificially produced by nuclear activation or nuclear reactions, are unstable. They reach more stable nuclear configurations through various processes of spontaneous radioactive decay that involve transformation to a more stable nuclide and emission of energetic particles. A closer look at radioactive decay processes shows that they are divided into six categories, consisting of:

(i) alpha (α) decay,

Alpha decay occurs when an unstable radionuclide emits a helium nucleus that consists of two protons and two neutrons as shown in Figure 2.2.

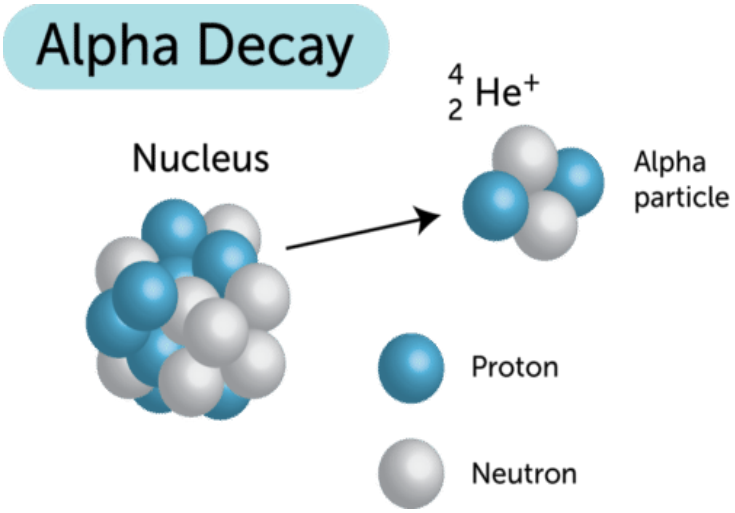

Fig 2.2 Alpha decay[24]

(ii) beta (β) decay encompassing three related decay processes (beta minus, beta plus and electron capture)

Beta minus decay occurs when a radioactive nuclide rich in neutrons converts one of its neutrons to proton and ejects a fast moving electron as shown in Figure 2.3. In Beta plus decay the radioactive nuclide which is rich in protons, converts a proton to a neutron and a positron as shown in Figure 2.3. In electron capture, an inner atomic electron is captured by a proton in the nucleus, transforming it into a neutron, and a neutrino is released as shown in Figure 2.4.

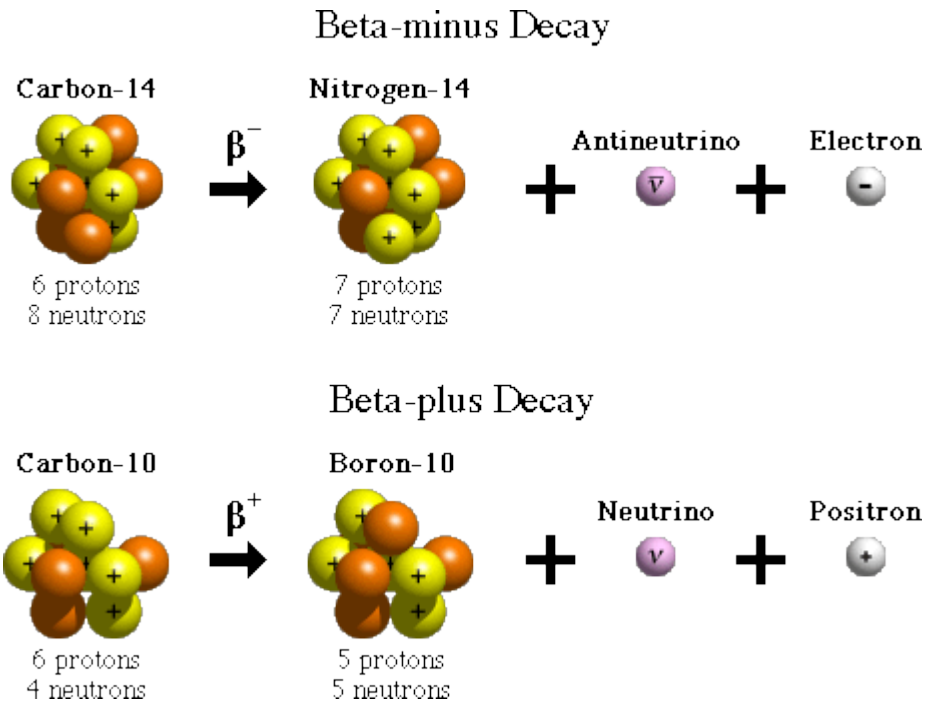

Fig 2.3 Beta-minus and Beta -plus decay [25]

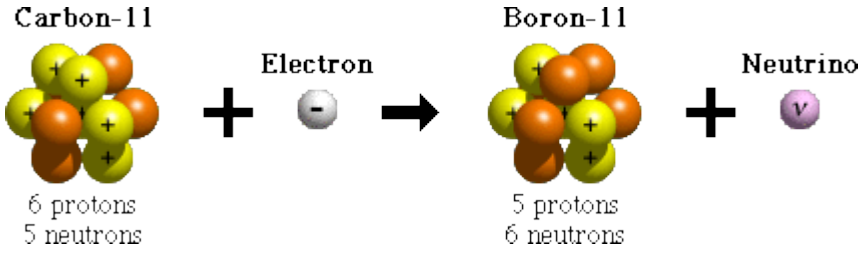

Fig 2.4 Electron capture [25]

(iii) Gamma (γ) decay encompassing two competing decay processes (pure γ decay and internal conversion).

In pure gamma decay an unstable radionuclide dissipates energy by emitting gamma rays, however there is no change in the number of protons and neutrons in the nuclide as shown in Figure 2.5. Internal conversion is a radioactive decay process wherein an excited nucleus interacts electromagnetically with one of the orbital electrons of the

atom. This causes the electron to be ejected from the atom [26]. Thus, in an internal conversion process, a high-energy electron is emitted from the radioactive atom, but not from the nucleus. Since an electron is lost from the atom, a hole appears in an electron shell which is subsequently filled by other electrons that descend to that empty, lower energy level, and in the process emit characteristic X-ray(s), Auger electron(s), or both. The atom thus emits high-energy electrons and X-ray photons, none of which originate in the nucleus as illustrated in Figure 2.6.

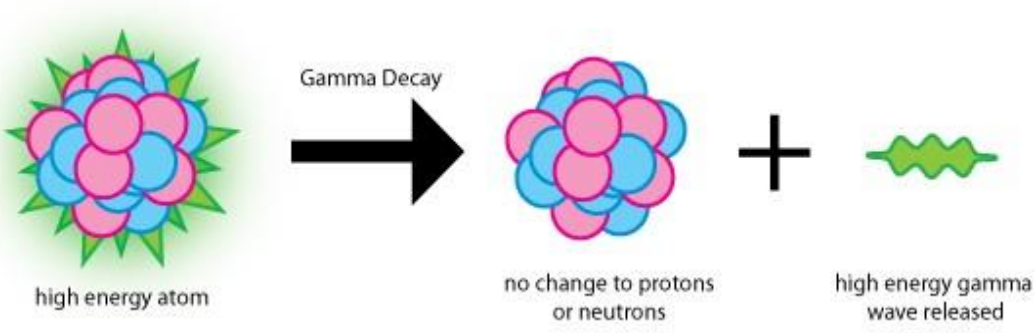

Fig 2.5. Pure gamma decay [27].

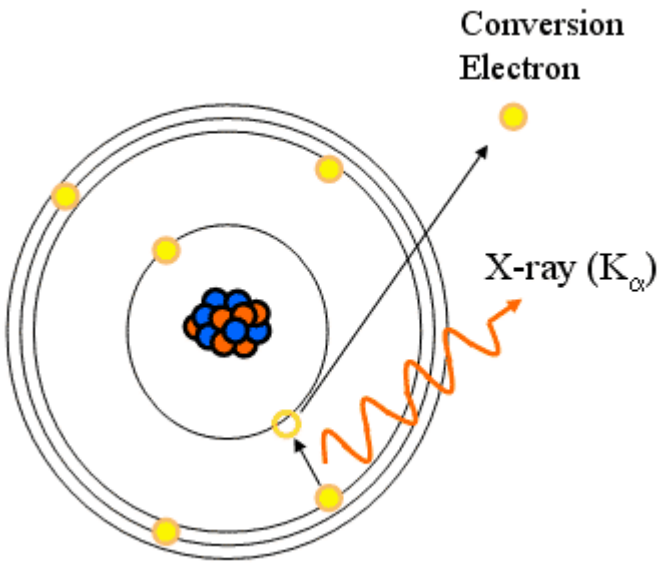

Fig 2.6 Electron conversion [28].

(iv) Spontaneous fission.

The spontaneous breakdown of some heavy nuclei to smaller nuclei and some nuclear particles as shown in figure 2.7 is called spontaneous fission.

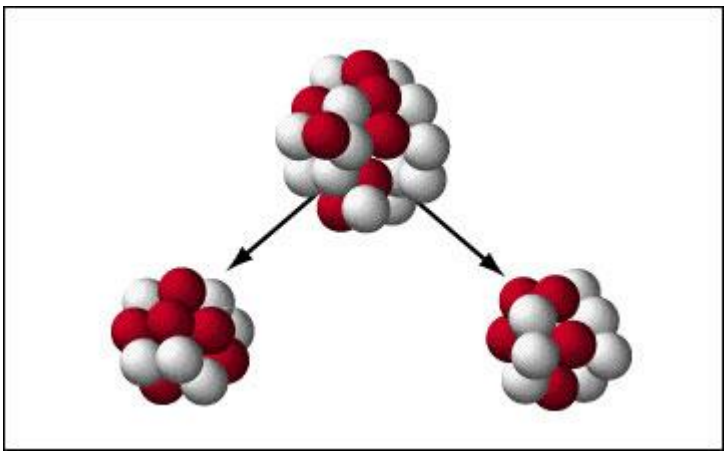

Fig 2.7 Spontaneous fission of a nucleus [29].

(v) Proton decay

Proton decay occurs when an unstable nuclide that is rich in protons converts one of its protons to a neutron in the nucleus and emits a positron and a neutrino in the process. The emitted positron combines with an electron and annihilates producing two anti-parallel photons with an energy of 511 KeV as illustrated in figure 2.8 below.

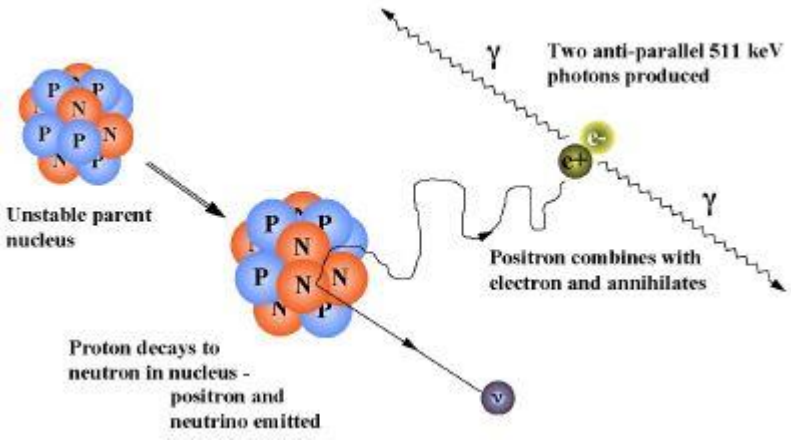

Fig 2.8 Proton decay [30]

(vi) Neutron emission.

Neutron decay is a type of radioactive decay of atoms containing excess neutrons. In this decay a neutron is simply ejected from the nucleus as illustrated in Figure 2.9. Neutron emission is one of the ways an atom reaches its stability.

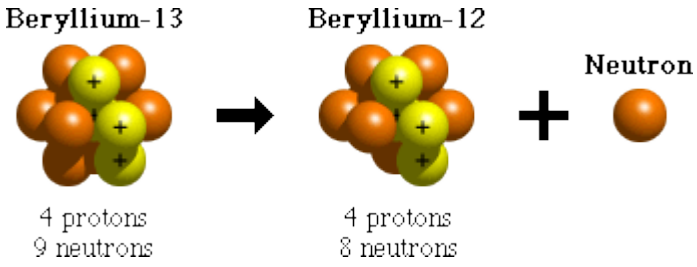

Fig 2.9 Neutron emission[25]

Nuclides with an excess number of neutrons are referred to as neutron-rich nuclides similarly, nuclides with an excess number of protons are referred to as proton-rich nuclides [31]. The following features are notable:

- For a slight proton–neutron imbalance in the nucleus, radionuclides decay by β decay characterized by transformation of a proton into a neutron in β^+ decay, and transformation of a neutron into a proton in β^- decay.
- For a large proton–neutron imbalance in the nucleus, the radionuclides decay by emission of nucleons: α particles in α decay, protons in proton emission decay and neutrons in neutron emission decay.
- For very large atomic mass number nuclides (A > 230), spontaneous fission, which competes with α decay, is also possible. Excited nuclei decay to their ground state through γ decay. Most of these transformations occur immediately upon production of the excited state by either α or β decay. However, a few

exhibit delayed decays that are governed by their own decay constants and are referred to as metastable states (e.g. ^{99m}Tc).

Nuclear transformations are usually accompanied by emission of energetic particles (charged particles, neutral particles, photons, etc.). The particles released in the various decay modes are as follows:

- Alpha particles in α decay;
- Electrons in β^- decay;
- Positrons in β^+ decay;
- Neutrinos in β^+ decay;
- Antineutrinos in β^- decay;
- Gamma rays in γ decay;
- Atomic orbital electrons in internal conversion;
- Neutrons in spontaneous fission and in neutron emission decay;
- Heavier nuclei in spontaneous fission;
- Protons in proton emission decay.

2.2.0 Interaction of ionising radiation with matter

Ionising radiation can be divided into two groups, namely directly ionising radiation and indirectly ionising radiation. When an X- or γ-ray beam passes through a medium, interaction between photons and matter can take place with the result that energy is transferred to the medium. The initial step in the energy transfer involves the ejection of electrons from the atoms of the absorbing medium [20]. These high-speed electrons transfer their energy by producing ionization and excitation of the atoms along their paths. If the absorbing medium consists of body tissues, sufficient energy may be

deposited within the cells, destroying their reproductive capacity. However, most of the absorbed energy is converted into heat, producing no biological effect [3].

The process by which a neutral atom acquires a positive or a negative charge is known as ionization. Removal of an orbital electron leaves the atom positively charged, resulting in an ion pair. The stripped electron, in this case, is the negative ion and the residual atom is the positive ion. In some cases, an electron may be acquired by a neutral atom which then becomes the negative ion.

2.2.1 Interaction of directly ionising radiation with matter

Ionising radiation interacts with matter by:

- Interaction with the electron cloud of the atom, or by
- Interaction with the nucleus of the atom.

Charged particles such as electrons, protons, and α particles are known as directly ionizing radiation provided they have sufficient kinetic energy to produce ionization by collision as they penetrate matter [20]. A mono-energetic, parallel beam of charged particles has a well-defined range in a given material, whereas uncharged particles are attenuated more or less exponentially, without having a well-defined range [32]. When charged particles such as alpha-particles and free electrons interact with atoms, they lose energy in two ways, ionisation slowing down and radiative slowing down. Charged particles interact continuously and quite intensely, display a well-defined range, and do not penetrate nearly as deeply as uncharged particles[18].

2.2.2 Ionisation slowing down of charged particles

Coulombic interactions of charged particles with atomic electrons, can impart energy to the atom and excite it to a higher energy state. If the energy transfer of the charged particle to the atomic electrons is sufficiently high, one or more electrons may be

detached from the atom. This is called ionisation. In every ionisation event, a small amount of energy is transferred from the charged particle to the atom being ionised, so that the energy of the moving particle decreases, i.e. it is slowed down [32]. This process is called ionisation slowing down. It can be shown that the linear energy transfer (LET, i.e. the energy transferred per unit path length) of a heavy charged particle by the mechanism of ionisation slowing down, obeys the approximate relationship

$$dE/dx = LET = z^2 Z/v \quad \ldots\ldots (2.1)$$

where z is the charge of the projectile, Z is the atomic number of the medium in which the interaction takes place and *v* is the speed of the heavy charged particle. The linear energy transfer rate is a measure of the intensity with which the particle interacts with matter [19], and the ionisation density, i.e. the number of ion pairs produced per unit path length [21].

Analysing the equation

- The z^2 term shows that the higher the charge, z, on a charged particle, the more intensely it will interact, i.e. the more energy will be transferred and the more ion pairs will be produced per unit path length.
- The Z term shows that the higher the atomic number Z of the medium in which the charged particle slows down, the more intense the interaction will be, i.e. the more energy will be transferred per unit path length.
- The $1/v$ term shows that slower-moving charged particles will interact more intensely than fast-moving charged particles

2.2.3 Radiative slowing down

The second mechanism by which charged particles are slowed down will now be discussed. If a charged particle which is free, (i.e. not bound in a potential well) enters the vicinity of an atomic nucleus, it will be deflected from its original direction, by the electric field of the nucleus. This causes a rapid change in the direction as well as the speed of movement of the electrically charged projectile. When an unbound, free, electrically charged particle is decelerated, it emits ionising photons known as bremsstrahlung ("braking radiation") [32]. In contrast, charged particles such as atomic electrons that are bound inside a potential well, have quantised energies and do not emit bremsstrahlung when they are accelerated. This process by which charged particles lose energy and slow down, is called radiative slowing down. The faster the deceleration, the more bremsstrahlung is produced.

The intensity M of bremsstrahlung production is given by the approximate relationship [33].

$$I = \frac{z^2 Z^2}{m^2} \quad \ldots\ldots (2.2)$$

where z is the charge of the projectile, m is its mass and Z is the atomic number of the medium. From equation (2.2) the following can be deduced about bremsstrahlung production and radiative slowing down:

- Bremsstrahlung production and radiative slowing down does not play a significant role for heavy charged particles (e.g. α particles), as a result of the $1/m^2$ term. However, radiative slowing down with associated bremsstrahlung production, will play an important role in the attenuation of low-mass charged particles such as electrons.

- The slowing down of charged particles in a medium with a high atomic number Z will produce much more bremsstrahlung compared to a medium with a low Z, on account of the Z^2 term.

2.2.4 Interaction of indirectly ionising radiation with matter

Uncharged particles such as neutrons and photons are indirectly ionizing radiation because they liberate directly ionizing particles from matter when they interact with matter. Ionizing photons interact with the atoms of a material or absorber to produce high-speed electrons by three major processes: photoelectric effect, Compton effect, and pair production [18].

2.2.5 Photoelectric Effect

The photoelectric effect is a phenomenon in which a photon interacts with an atom and ejects one of the orbital electrons from the atom as shown in figure 2.10. In this process, the entire energy ($h\nu$) of the photon is first absorbed by the atom and then transferred to the atomic electron. The kinetic energy of the ejected electron (called the photoelectron) is equal to $h\nu - E_B$, where E_B is the binding energy of the electron [34]. Interactions of this type can take place with electrons in the K, L, M, or N shells. After the electron has been ejected from the atom, a vacancy is created in the shell, thus leaving the atom in an excited state. The vacancy can be filled by an outer orbital electron [34].

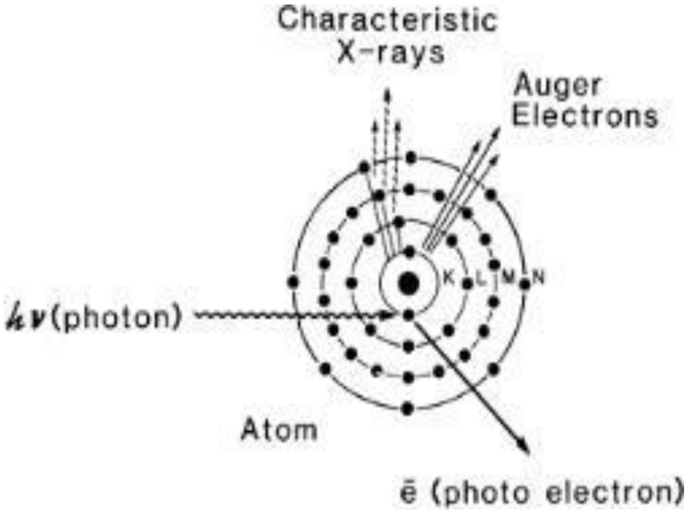

Fig. 2.10 Photoelectric effect [18]

At small values of gamma ray energy, the photoelectric effect dominates as shown in figure 2.11. The mechanism is also enhanced for materials of high atomic number Z. The probability of producing a photoelectron when light strikes an atom is strongly dependent on the atomic number *Z* and the energy *hν* of the photons. It is largest for high-*Z* materials. The probability varies as:

$$\tau_{(photoelectric)} = constant \times \frac{Z^4}{(h\nu)^3} \quad \ldots\ldots\ldots\ldots\ldots (2.3)$$

where Z is the atomic number, *hν* is the energy of the incident photon. The proportionality to higher powers of the atomic number Z is the main reason for using of high Z materials, such as lead or depleted uranium in gamma ray shields [32].

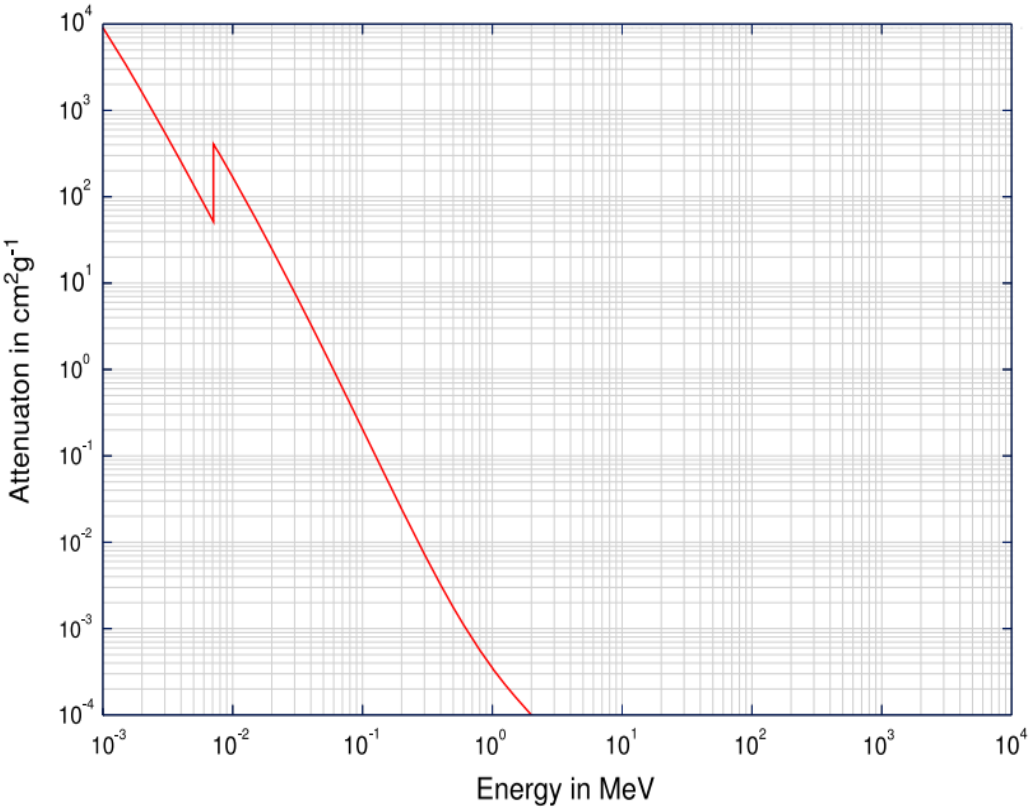

Fig 2.11 Cross section of Photoelectric effect [35].

2.2.6 Compton Effect

In the Compton Effect, the photon interacts with an atomic electron as though it were a "free" electron. The term free here means that the binding energy of the electron is much less than the energy of the bombarding photon [34]. In this interaction, the electron receives some energy from the photon and is emitted at an angle ϕ. The photon, with reduced energy, is scattered at an angle θ as shown in figure 2.12.

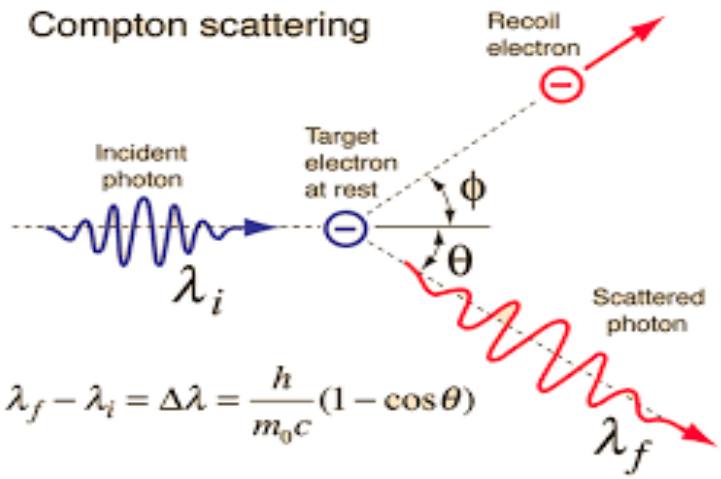

Fig 2.12 Compton scattering [36]

In Compton scattering, the incident gamma-ray photon is deflected through an angle Θ with respect to its original direction. This deflection results in a decrease in energy (decrease in photon's frequency) of the photon and is called the Compton Effect [37]. The probability of Compton scattering per one interaction with an atom increases linearly with atomic number Z, because it depends on the number of electrons, which are available for scattering in the target atom [37]. The cross section of Compton scattering is shown in Figure 2.13.

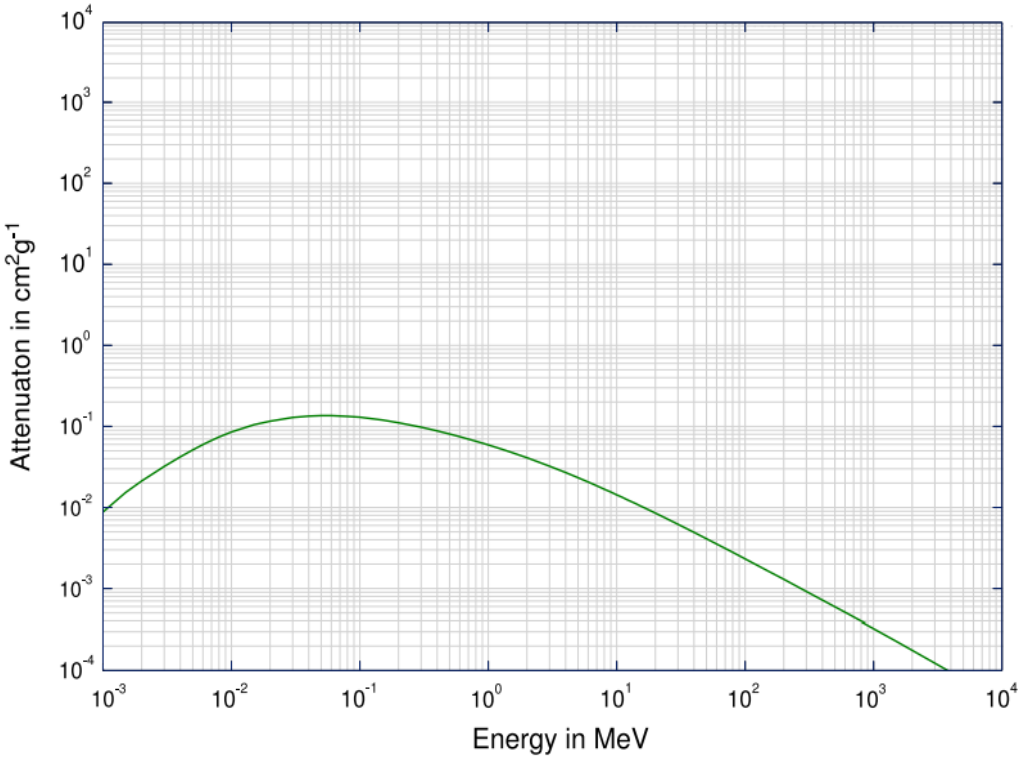

Fig 2.13 Cross section of Compton effect [38].

2.2.7 Pair Production

If the energy of the photon is greater than 1.02 MeV, the photon may interact with matter through the mechanism of pair production. In this process, the photon interacts strongly with the electromagnetic field of an atomic nucleus and gives up all its energy thereby creating a pair consisting of a negative electron (e-) and a positive electron (e+) as shown in figure 2.14. Since the rest mass energy of the electron is equivalent to 0.51 MeV, a minimum energy of 1.02 MeV is required to create the pair of electrons. Thus, the *threshold energy* for the pair production process is 1.02 MeV [18]. Figure 2.15 shows the cross section of pair production.

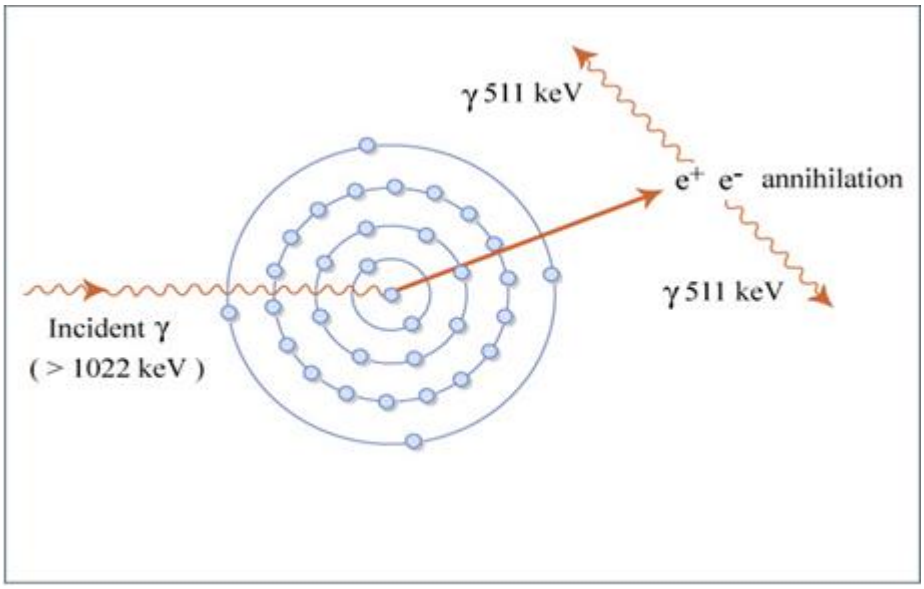

Fig.2.14 Illustration of pair production [39]

In general the cross section increases approximately with the square of atomic number and increases with photon energy, but this dependence is much more complex.

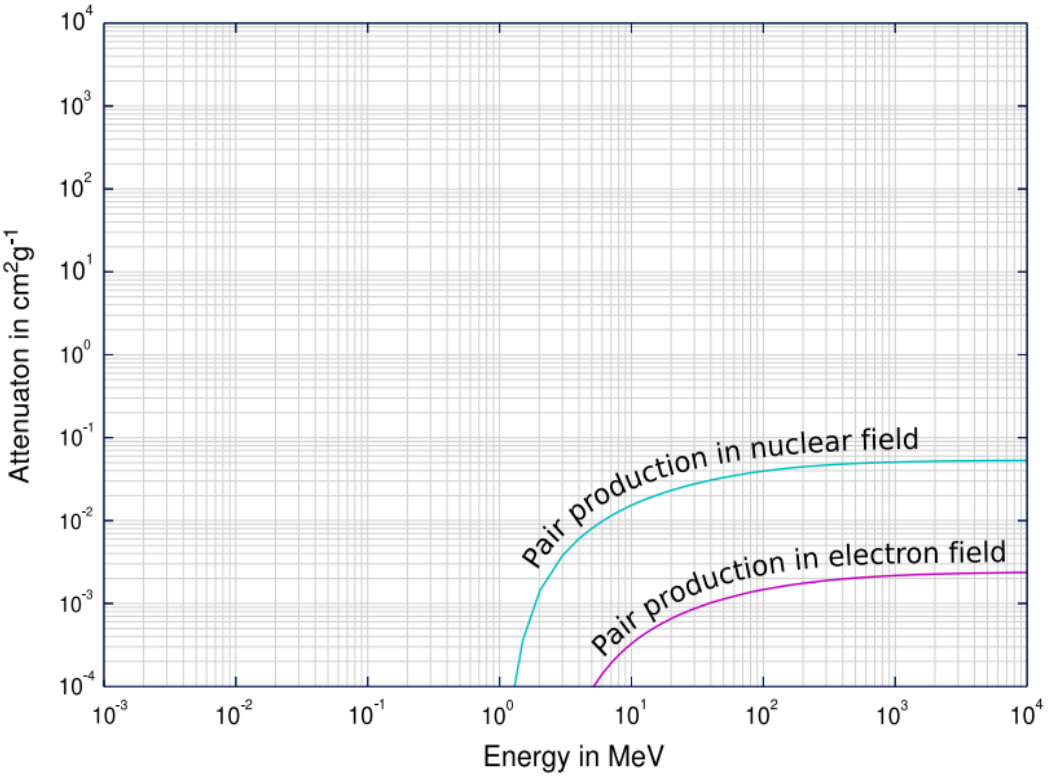

Fig.2.15 Cross section of pair production in nuclear field and electron field [40].

Since the probability of occurrence of photoelectric effect and pair production is a function of a power of Z while Compton scattering is nearly independent of Z for low Z materials, the Compton Effect is dominant for all energies. As Z increases, photoelectric effect becomes dominant at low energies, while pair production becomes dominant at high energies as shown in figure 2.16 below.

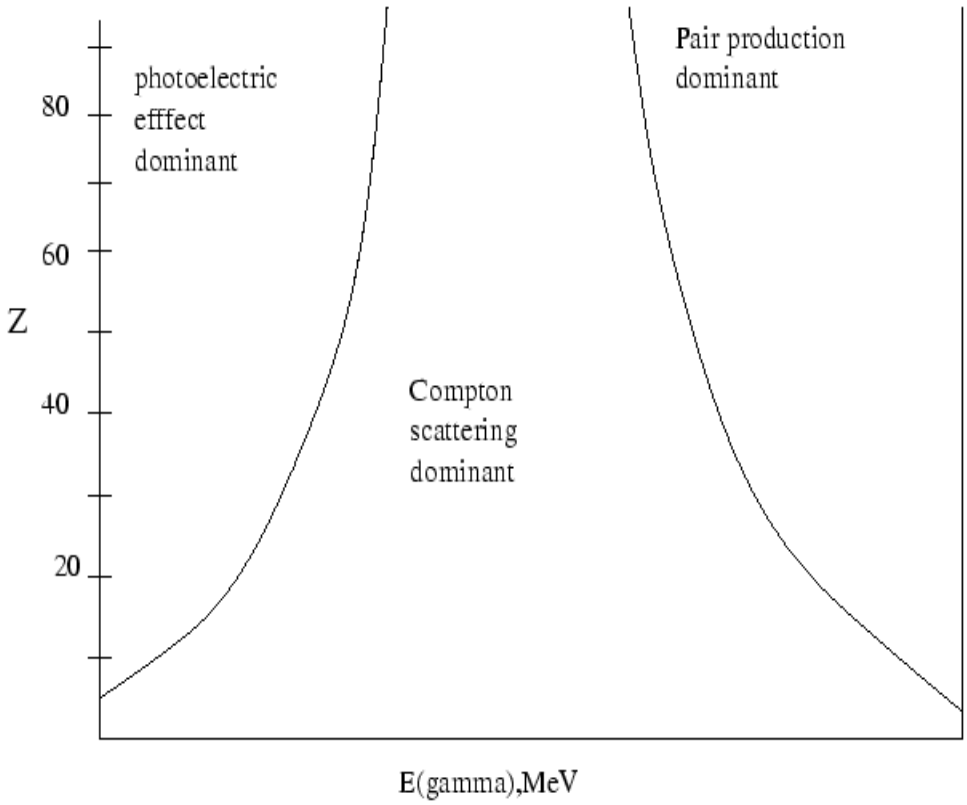

Fig.2.16Energy dependence of photoelectric effect, Compton scattering and pair production [41].

2.2.8 Interaction of neutrons with matter

The neutron is indirectly ionising [34], and the ionisation is produced by charged particles such as recoil nuclei and nuclear reaction products, produced by the neutrons [18]. The production of secondary ionising photons by neutrons will result in the release of energetic electrons, and these can deposit energy at a considerable distance from the interaction centers of the neutrons [31]. There is negligible interaction between neutrons and the electron cloud of atoms. The neutron is a particle without any net charge and is therefore not affected by the strong nuclear force [37]. Because the neutron has no charge it only interacts through direct collisions. Since the neutron is approximately 1840 times heavier than the electron [20], it will experience virtually no energy loss through collisions with electrons. Therefore the only substantial energy loss of neutrons are through interaction with atomic nuclei**.** When neutrons impinge on a medium, the nuclear reactions that can take place will depend on the energy of the neutron and the cross-sections for the nuclear reactions [19]. Neutrons are scattered or absorbed by nuclei [21]. Scattering is the deflection of neutrons from their original direction and energy. Neutrons can also be captured or absorbed by the nucleus. When a nucleus absorbs a neutron, γ-photons are, as a rule, emitted when the excited product nucleus reverts to its ground energy state [19]. At high incident energies, neutrons produce charged particles such as alpha particles and protons, by nuclear reactions with nuclei. The secondary radiation produced in this manner causes ionisation. When a high-energy neutron is scattered by an atomic nucleus, the nucleus recoils [32].

2.3.0 Measurement of ionising radiation

From the previous discussions on the different types of interactions of ionising radiation with matter, it is evident that all the types of interactions have one aspect in common, an electron is ejected from one of the orbitals of the absorbing atom, and a

positive ion is produced. The formation of an ion and a high energy electron in the material that is exposed to nuclear radiation, is called primary ionization. All subsequent effects are the results of primary ionization. The high energy electron produced in the primary ionization event travels further in the material. It can interact with other atoms in the material to further ionize the material, this is called secondary ionization. The process continues until all the electrons produced have lost their kinetic energy.

Radiation detectors exploit the ionizing effect of radiation in absorbing material to measure the radiation incident on the material [19,37]. A large number of detector types have been developed since the discovery of radioactivity, some of which are no longer in use. There is currently a wide variety of detector types available, but three broad categories can be distinguished.

2.3.1 Gas ionization detectors.

Several of the oldest and most widely used types of radiation detectors are based on the effects produced when a charged particle passes through a gas. The primary modes of interaction involve ionization and excitation of gas molecules along the particle track [37]. Although the excited molecules can at times be used to derive an appropriate signal (as in the gas scintillators), the majority of gas-filled detectors are based on sensing the direct ionization created by the passage of the radiation. The gas ionization detectors that will be discussed are the ion chambers, proportional counters and Geiger tubes, all derive, in somewhat different ways, an electronic output signal that originates with the ion pairs formed within the gas filling the detector [37]. All the ionization caused by a single particle of (α, β, γ) inside a closed volume of gas, is collected by applying a suitable electrical voltage across the container. The average energy needed to produce an electron – ion pair is 30 ± 10eV, with a weak dependence

on the gas used and the energy of the incident particle [17]. The electrons are attracted by the positive electrode, and are swept from the gas before they can recombine with the positive ions. The container is often in the form of a long cylinder or a thick pancake with a thin window on the one side, and is normally filled with a special counting gas. Gas detectors are used primarily for the detection of α and β particles as shown in Figure 2.17.

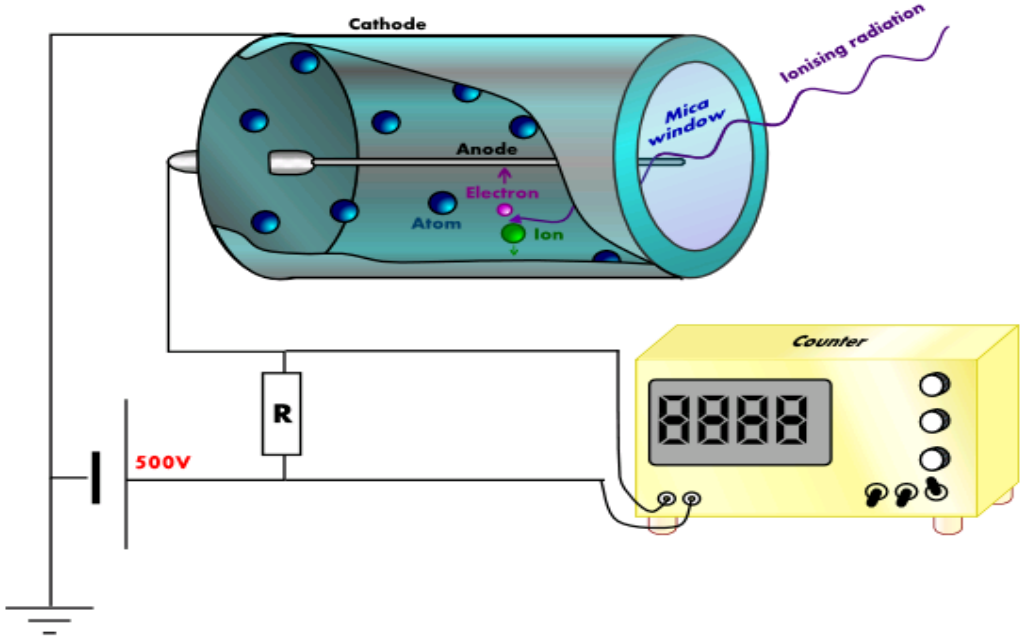

Fig 2.17 Gas filled radiation detector [42]

Depending on the applied voltage across the electrodes, and hence the electrical field strength, a gas-filled radiation detector can be engineered to be either an Ionization chamber, Proportional counter or a Geiger-Muller counter [20].

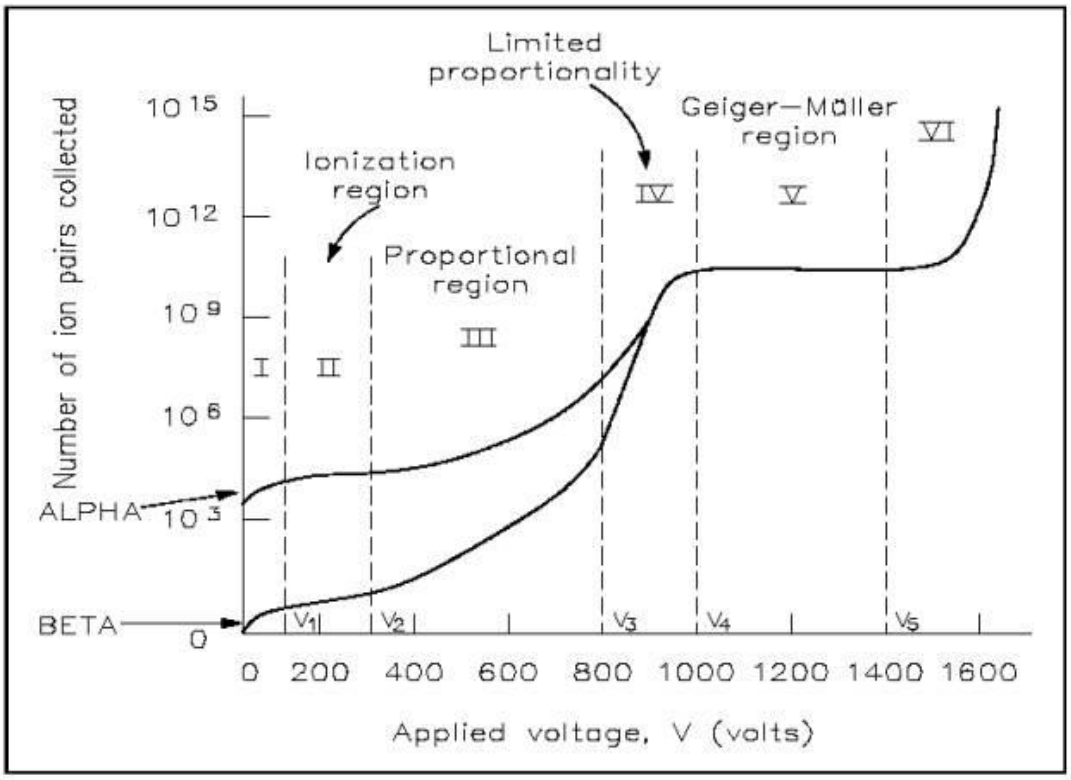

Fig.2.18 The "Six region" characteristic curve for gas filled radiation detectors [43]

Figure 2.18 shows the "six region" characteristic curve for gas filled detectors.

Region 1, is the recombination region. In this region the applied voltage is insufficient to collect all of the ion pairs before some of them recombine. This region is not used.

Region 2, is known as the ionisation chamber region. In this region as the voltage across the electrodes is increased, a voltage range is reached at which essentially all of the ion pairs created in the gas by the ionising radiation, are collected before they can recombine. Instruments operating in this region are called Ionisation Chambers.

Region 3, is known as the Proportional counter region. As the voltage across the electrodes of a gas-filled detector is increased beyond the ion chamber region, the electrons formed by the primary ionisations pick up enough energy during acceleration in the strong electrical field close to the thin central anode wire, to enable them to

produce further ion pairs via secondary ionisation. The electrons liberated during secondary ionisation are also accelerated, they gather enough energy to cause further ionisation. The large number of ionisation events formed in the chain reaction is known as an avalanche**,** and creates a single, large electrical output pulse. As the result of gas multiplication, the proportional counter is able to detect individual incident radiations as pulses – hence the name "counter."

Region 4, is known as the Limited proportionality region. This region is not used as the instrument is unstable and calibration is not possible.

Region 5, is the Geiger Muller region. In this region the instrument is operated at high voltages. Inert gases are used as the counting gas. The internal gas pressure is often lower than the atmospheric pressure. Generated electrons are accelerated towards the anode and they produce secondary electrons, a large avalanche of electrons is produced generating a strong electrical signal. A Geiger-counter can detect individual particles and photons.

Region 6, is known as the Continuous discharge Region. In this region the voltage is too high which causes arcing and breakdown of the detector gas.

2.3.2 Scintillation Detectors

"A scintillation detector is a transducer that changes the kinetic energy of an ionizing particle into a flash of light. Historically, one of the earliest means of measuring radiation was by scintillation counting. Rutherford, in his classical experiments on scattering of alpha particles, used a zinc sulphide crystal as the primary detector of radiation; he used his eye to see the flickers of light that appeared when alpha particles struck the zinc sulphide. Today, the light is viewed electronically by photomultiplier

tubes or photodiodes whose output pulses may be amplified, sorted by size, and counted" [19]. Table 2.1 lists some of the substances used for this purpose.

Table 2.1 Scintillating materials [19]

PHOSPHOR	*DENSITY ($g.cm^{-3}$)*	*WAVELENGTH OF MAXIMUM EMISSION (A°)*	*RELATIVE PULSE HEIGHT*	*Decay Time (µs)*
NaI (Tl)	3.67	4100	210	0.25
CsI (Tl)	4.51	Blue	55	1.1
KI (Tl)	3.13	4100	50	1
Anthracene	1.25	4400	100	0.032
Trans-Stibene	1.16	4100	60	0.0064
Plastic		3550 - 4500	28 - 48	0.003 - 0.005
Liquid		3550 - 4500	27 - 49	0.002 - 0.008
p - Terphenyl	1.23	4000	40	0.005

2.3.3 Semiconductor Detectors

A semiconductor is a material that can act as an insulator or as a conductor [19]. Detectors fabricated using semiconductor material are termed semiconductor detectors. Semiconductor detectors are fabricated from either elemental or compound crystal material having a band gap in the range of approximately 1 to 5 eV [37]. The group IV elements Silicon and Germanium are the most widely used semiconductors. Semiconductor detectors have a P-I-N diode structure in which the intrinsic (I) region is created by depletion of charge carriers when a reverse bias is applied across the diode [19]. When a photon interacts within the depletion region, charge carriers (holes and electrons) are freed and are swept to their respective collecting electrode by the electric field. The resultant charge is integrated by a sensitive preamplifier and converted to a voltage pulse with an amplitude proportional to the original photon energy [44].

2.3.4 High Purity Germanium (HPGe) Detector

"Germanium semiconductor detectors were first introduced in 1962 and are now the detectors of choice for high energy-resolution γ-ray studies. These detectors directly collect the charges produced by the ionization of the semiconductor material. One electron-hole pair is produced on the average for every 3 eV absorbed from the radiation. These pairs drift under an external electric field to the electrodes where they generate the pulse. The high number of information carriers leads to a small percentage fluctuation and this is the reason for the high energy-resolution of Ge detectors. However, the detector cannot simply consist of the semiconductor material and two electrodes because there are inherent impurities in these materials. Both Si and Ge have a valence 4 and when an impurity of valence 3 (acceptor) or 5 (donor) exists in the crystal, it lowers the energy necessary to create electron-hole pairs and this tends to create too much noise. The Ge crystal with acceptor impurities is called p-type (Ge) material and the same with donor impurities is called n-type (Ge) material" [45]. The solution is to create a p–n junction at one electrode and to polarize it so that no current passes through when there is no ionizing radiation (this is called reverse biasing or using non-injecting or blocking electrodes) [37]. This creates a region called the depletion layer as shown in Figure 2.19 where few charge carriers remain, resembling a pure semiconductor. With a sufficient voltage, the electric field can create a large enough depleted volume to make a viable detector. The intrinsic region (depleted volume) is sensitive to ionizing radiation particularly X-rays and γ-rays [45].

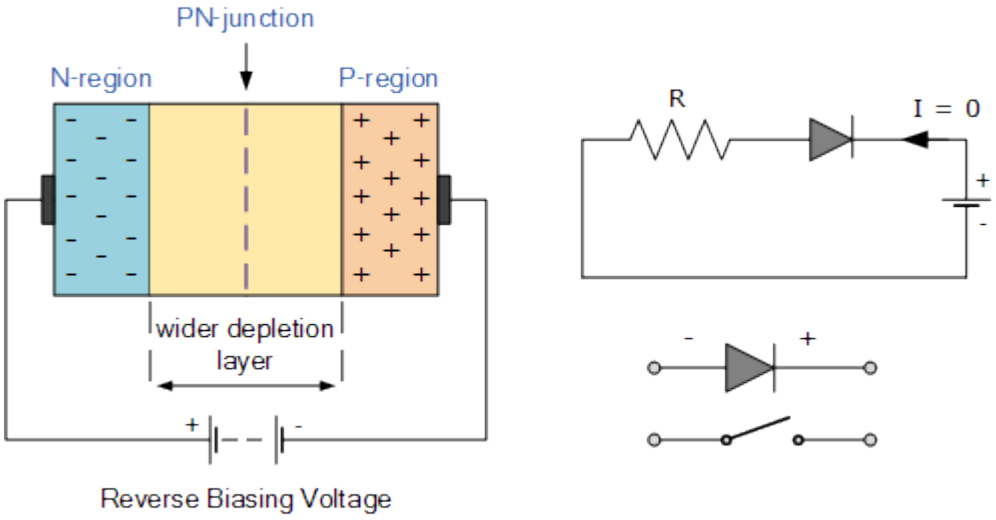

Fig 2.19 PN junction [46].

"The performance of a detector depends on its depletion depth, which is inversely proportional to the net impurity concentration in the detector material. A step forward was achieved when higher purity Ge material could be fabricated, with impurity concentration of 10^{10} atoms cm^{-3} instead of 10^{13} atoms cm^{-3}, eliminating the need for Li compensation. This means that the material has a higher resistivity which is proportional to the square of the depletion layer's thickness. This paved the way for the manufacture of larger and much more efficient detectors. The major characteristics of the HPGe detector are high atomic number, low impurity concentration (large depletion depth), low ionizing energy required to produce an electron-hole pair, high conductivity, compact size, first time response, high resolution, low efficiency and relative simplicity of operation" [45].

2.3.5 Interaction of Gamma radiation with detector crystal

Gamma-ray (γ-ray) detection is based on the effect of a γ-ray interacting with matter as discussed earlier [45]. The three important types of interaction of a γ-ray with matter to be considered are (i) the photoelectric effect, (ii) the Compton Effect, and (iii) the pair-production. In the photoelectric process, the γ- or X-ray gives all of its energy to the recoil electron." As a result, the recoil electrons ejected from the shell of atoms and hence produces the electron-hole pairs in the detector that yield the output pulse. This output pulse from the detector is proportional to the energy of the γ- or X-ray that made the interaction. In the spectrum, these events will show up as full-energy photo-peaks. The Photo electric effect is significant for the incident gamma energy of 0-150 keV" [45].

"The Compton cross section is the dominant one for all energies except the very lowest ($E_\gamma \leq 150$ keV) and the very highest ($E_\gamma = 8.5$ MeV). The Compton Effect too contributes strongly to the full energy peak by multiple Compton scattering under the condition that the last interaction is a photoelectric one and that all the preceding Compton interactions take place in the Ge crystal. In large-volume detectors the probability of multiple Compton scattering increases. If the last interaction does not occur by the photoelectric effect or if one of the multiple Compton interactions takes place outside the sensitive volume of the detector, the pulse will contribute to the Compton continuum. The pair-production process can also provide a total absorption of the γ-ray energy. The gamma enters the detector and creates an electron-positron pair. From the law of conservation of mass and energy, it follows that the initial gamma ray must have energy of at least 1.02 MeV because it takes that much energy to create both the negative and positive electrons" [45].

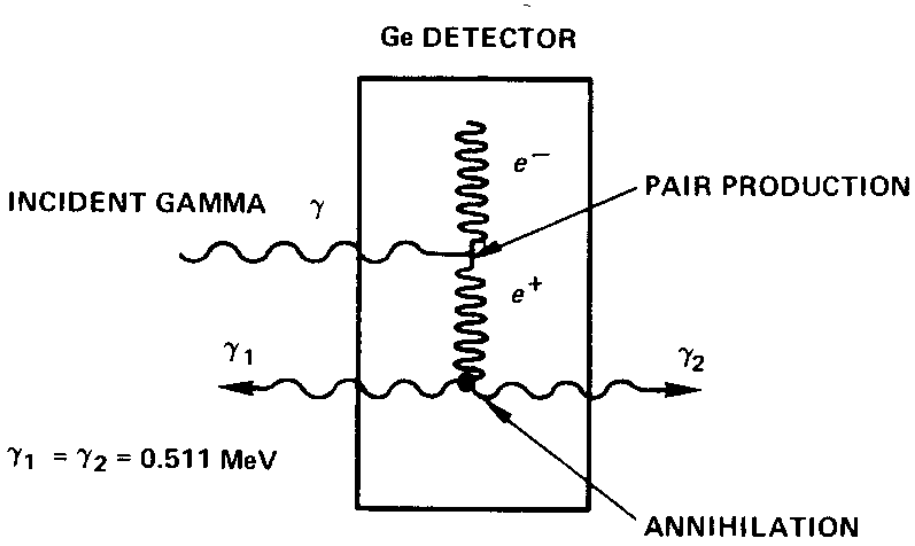

Fig.2.20 Pair production in Ge detector [45].

Figure 2.11 illustrates what happens in the detector in the pair-production process. "In the figure, the e^- (ordinary electron) will produce a pulse whose magnitude is proportional to the energy of e^- (Ee^-). The positron will also produce a pulse proportional to Ee^{+}. Since these two pulses are produced simultaneously, the output pulse from the detector would be the sum of the two pulses. When the positron annihilates in the detector, the annihilation radiation γ_1 and γ_2 is produced. If both γ_1 and γ_2 escape from the boundaries of the detector without making further interactions, then energy of exactly 1.02 MeV escapes from the detector and is subtracted from the total energy that entered in the detector. Sometimes only one of the gammas, make a photoelectric interaction in the detector while the other escapes. In such cases, the total energy absorbed by the detector is 0.511 MeV less than the original incident γ-energy. It is also possible that both gammas make photoelectric interactions without escaping, leaving all of the incident γ-energy in the detector. Therefore, in the measured spectrum three peaks can be obtained for each γ-energy" [45]. These peaks are called

full-energy peak, single-escape peak, and double-escape peak, and they will be separated by 0.511 MeV increments[47].

2.4.0 Units used to describe ionisation dose

Radiation exposures are measured in terms of the quantity called absorbed dose, which equals the ratio of energy imparted to the mass of the exposed body or organ. The unit of absorbed dose is joules per kilogram (J/kg) [48]. For convenience this unit has been given the special name gray (Gy) [48]. "Ionizing radiation can consist of electromagnetic radiation, such as X-rays or gamma rays (γ-rays), or of subatomic particles, such as protons, neutrons, and α-particles. X- and γ-rays are said to be sparsely ionizing, because they produce fast electrons, which cause only a few dozen ionizations when they traverse a cell. Since the rate of energy transfer is called linear energy transfer (LET), they are also termed low-LET radiation. In contrast, the heavier particles are termed high-LET radiations because they transfer more energy per unit length as they traverse the cell. Since the high-LET radiations are capable of causing more damage per unit absorbed dose, a weighted quantity, equivalent dose, or its average over all organs, effective dose, is used for radiation protection purposes. For low-LET radiation, equivalent dose equals absorbed dose. For high-LET radiation such as neutrons, α-particles, or heavier ion particles equivalent dose or effective dose equals the absorbed dose multiplied by a factor, the quality factor or the radiation weighting factor, to account for their increased effectiveness. Since the weighting factor for radiation quality is dimensionless, the unit of equivalent dose is also joules per kilogram. However, to avoid confusion between the two dose quantities, the special name Sievert (Sv) has been introduced for use with equivalent dose and effective dose" [48]. Table 2.2 show some of the radiation units used.

Table 2.2 : Units of dose [48].

Unit	*Symbol*	*Conversion Factors*
Becquerel (SI)	Bq	1 disintegration/s = 2.7 x 10^{-11} Ci
Curie	Ci	3.7 x 10^{10} disintegrations/s = 3.7 x 10^{10}Bq
Gray (SI)	Gy	1 J/Kg = 100 rads
Rad	rad	0.01 Gy = 100 erg/g
Sievert	Sv	1 J/Kg = 100 rem
Rem	rem	0.01 Sv

2.5.0 Biologic effects of ionising radiation

2.5.1 Interaction of ionising radiation with biologic matter

The previous sections discussed how radiation interacts with matter. In this section the interaction of radiation with biologic matter and its effects will be reviewed. "At the microscopic level, incident rays or particles may interact with orbital electrons within the cellular atoms and molecules to cause excitation or ionization. When ionisation takes place electrons are ejected from the cellular atoms or molecules. This gives rise to a flux of electrons that are energetic and unbound and are capable of migrating away from the site of their production and, through a series of interactions with other atoms and molecules, they give up their energy to the surrounding medium" [20]. "The important characteristic of ionizing radiation is the localized release of large amounts of energy. The energy dissipated per ionizing event is about 33 eV, which is more than enough to break a strong chemical bond; for example, the energy associated with a C==C bond is 4.9 eV" [34]. "This energy absorption process gives rise to radicals and other chemical species and it is the ensuing chemical interactions involving these which are the true causatives of radiation damage. It is important to note that, irrespective of the nature of the primary radiation (which may be composed of particles and/or electromagnetic waves), the mechanism by which energy is transferred from the primary radiation beam to biological targets is always via the secondary electrons

which are produced. The initial ionization events are the precursors to a chain of subsequent events which may eventually lead to the clinical (macroscopic) effects of radiation damage" [20].

2.5.2 Direct and Indirect Action of Radiation on DNA Molecule

"The biologic effects of radiation result principally from damage to deoxyribonucleic acid (DNA), which is the critical target. When any form of radiation (x- or γ-rays, charged or uncharged particles) is absorbed in biologic material, there is a possibility that it will interact directly with the critical targets in the cells. The atoms of the target itself may be ionized or excited, thus initiating the chain of events that leads to a biologic change. This is called direct action of radiation, it is the dominant process if radiations with high linear energy transfer (LET), such as neutrons or α-particles, are considered. Alternatively, the radiation may interact with other atoms or molecules in the cell (particularly water) to produce free radicals that are able to diffuse far enough to reach and damage the critical targets. This is called indirect action of radiation. Figure 2.21 illustrates the direct and indirect interactions of radiation with DNA. A free radical is an atom or molecule carrying an unpaired orbital electron in the outer shell" [34].

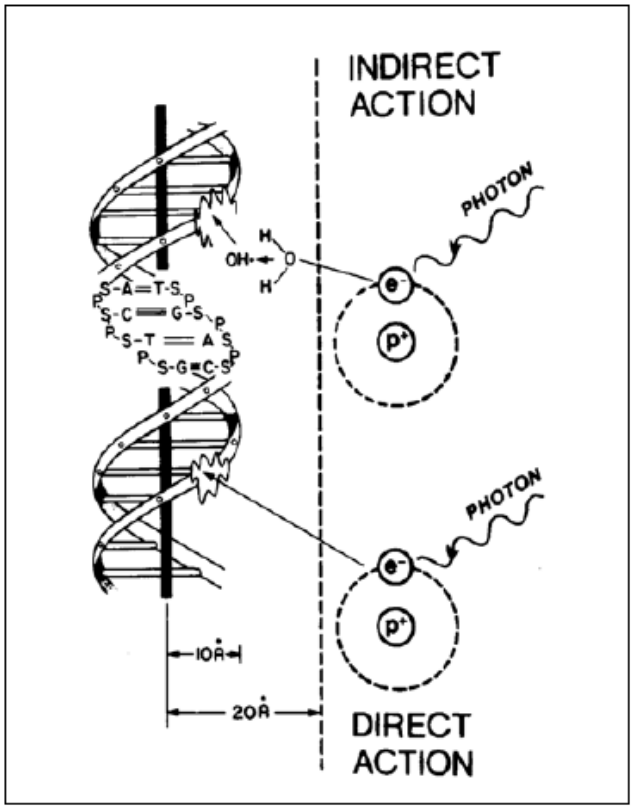

Fig 2.21 Direct and Indirect interactions of radiation with DNA [34].

"The structure of DNA is shown schematically. In direct action, a secondary electron resulting from absorption of an x-ray photon interacts with the DNA to produce an effect. In indirect action, the secondary electron interacts with, for example, a water molecule to produce a hydroxyl radical (OH·), which in turn produces the damage to the DNA. The DNA helix has a diameter of about 20 Å (2 nm). It is estimated that free radicals produced in a cylinder with a diameter double that of the DNA helix can affect the DNA. Indirect action is dominant for sparsely ionizing radiation, such as x-rays" [34].

Irradiation of any biological system generates a succession of processes that differ enormously in time scale. This is illustrated in the Figure 2.22.

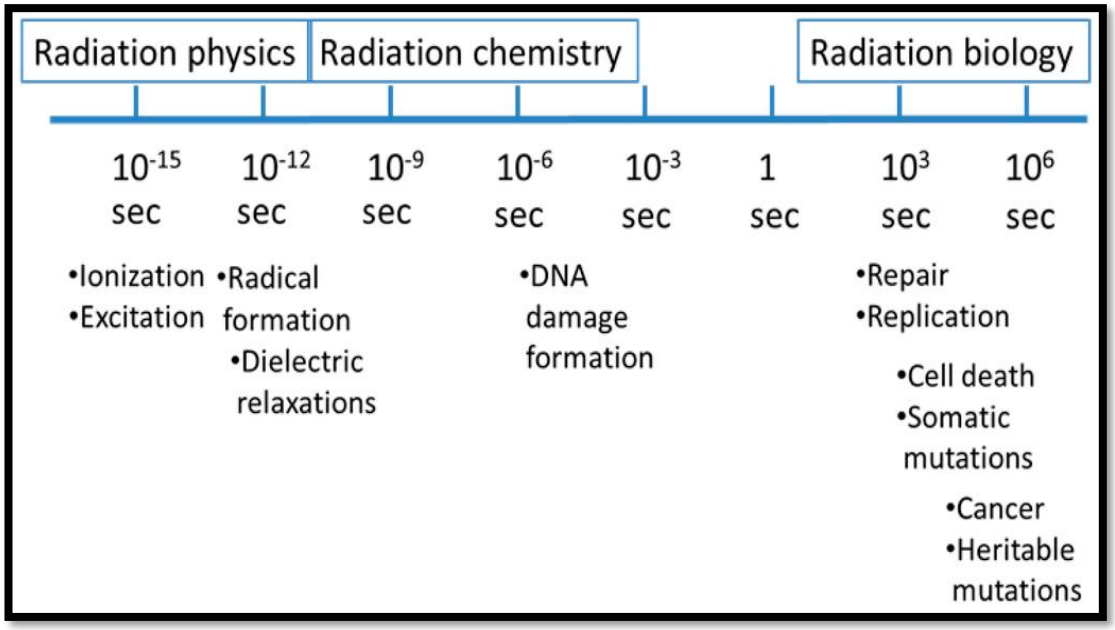

Fig. 2.22 Time-Scale Effects in Radiation Biology that lead to biological effects of ionizing radiation. Above the scale bar are shown the corresponding research fields that investigate the events [49].

2.5.3 Health effects of Ionising Radiation.

Most adverse health effects of radiation exposure may be grouped in two general categories:

1- deterministic effects (harmful tissue reactions) due in large part to the killing or malfunction of cells following high doses; and

2- Stochastic effects, i.e., cancer and heritable effects involving either cancer development in exposed individuals owing to mutation of somatic cells or heritable disease in their offspring owing to mutation of reproductive (germ) cells [50].

2.5.4 Deterministic effects

“The induction of tissue reactions is generally characterised by a threshold dose. The reason for the presence of this threshold dose is that radiation damage (serious

malfunction or death) of a critical population of cells in a given tissue needs to be sustained before injury is expressed in a clinically relevant form. Above the threshold dose the severity of the injury, including impairment of the capacity for tissue recovery, increases with dose" [50]. "Early tissue reactions to radiation in cases where the threshold dose has been exceeded may be of the inflammatory type resulting from the release of cellular factors, or they may be reactions resulting from cell loss. Late tissue reactions (months to years) can be of the generic type if they arise as a direct result of damage to that tissue. By contrast other late reactions may be of the consequential type if they arise as a result of early cellular damage" [51].

2.5.5 Stochastic effects

"These effects result from an alteration in the genome of a cell, which, in the case of cancer gives rise to a clone of uncontrolled, rapidly dividing cells. Various mechanisms might be involved in mutation of the DNA. These may include the activation of an oncogeny (a cancer-causing gene), the inactivation of a tumour-suppressor gene or the loss of function of a repair-mutator gene "[52]. The severity of the cancer is independent of the dose, but the probability of developing cancer is proportional to the dose received.

2.5.6 Differences between stochastic effects and deterministic effects

The crucial differences between tissue reactions, and stochastic effects of ionising radiation, are summarised in Table 2.3

Table 2.3. Key differences between deterministic and stochastic effects of ionising radiation

Deterministic Effects	***Stochastic Effects***
Caused by the death of cells after irradiation	Caused by changes in cells that do not die after irradiation
There is a clear, unambiguous causal relationship between exposure and the observed effect. Effects include tissue reaction, radiation disease, radiation wounds, etc.	Effects are , Risk that cancer may develop after a period of latency, and risk of hereditary damage transferred to progeny
Threshold effect: A certain minimum dose must be exceeded before the particular effect is observed; no tissue reaction if dose is below the threshold	No threshold dose for risk
Above the threshold, the seriousness of the injury is proportional to the magnitude of the dose	Seriousness of cancer is independent of the dose, but the probability or risk of cancer is proportional to the dose.
Strongly dependant on the dose rate	Practically independent of the dose rate

2.5.7 Effects of low dose ionising radiation

According to IAEA TECDOC-870, there is no firm evidence from human low-dose epidemiological studies which unequivocally demonstrates an increase in cancer incidence with exposure to low-dose ionising radiation [52]. However ICRP -103 publication alludes to the thought that DNA damage response or repair and the induction of gene chromosomal mutations can contribute significantly to judgements on the radiation-associated increase in the incidence of cancer at low doses.[50]". Generally, scholars hold the view that there is no threshold dose that may induce these effects. However, the probability of the effects increase with increased dose. There are however different schools of thoughts with regards to effects of low-dose ionising radiation. The most prominent assumption accepted by most official bodies is the Linear No Threshold (LNT) hypothesis [52]. According to this hypothesis, the cancer risk is directly proportional to the magnitude of dose down to zero dose.

2.5.8 Effects of High Dose Ionising Radiation

The degree of killing of cells in a population increases with the radiation dose [19]. Table 2.4 shows the effects of high dose ionising radiation. If enough cells are killed in an organ or tissue, the function of the organ or tissue is impaired. In extreme cases the organism itself may die. With larger doses, there may be a substantial degree of cell killing, sufficient to result in detectable tissue changes. Cell killing plays a crucial role in tissue injury, and causes tissue reactions. The response of tissue to cell killing is determined by cell survival [34]. "Since a given fraction of cells must be killed in order to reach the level of clinical manifestation, tissue reactions are only observed above a certain dose threshold. Tissue reactions from exposure to ionising radiation occur as a result of the death of cells. If the dose and dose rate are large enough, so many cells will die and the tissue can no longer function properly" [50].

Table 2.4 Effects of high dose ionising radiation

Whole Body Absorbed dose (Gy)	***Principal Effect Contributing to Death***	***Time of Death After Exposure (days)***
3 - 5 Gy	Damage to Bone - marrow	30 - 60 days
5 - 15 Gy	Damage to Gastro-intestinal tract	7-20 days
5 - 15 Gy	Damage to lungs and kidneys	60 -150 days
> 15 Gy	Damage to nervous and vascular systems	

2.6.0 Low Dose Ionising Radiation.

According to the Biologic Effects of Ionising Radiation BEIR report V11 committee low dose is characterised as any dose in the range from near to zero to about 100 mSv. The annual worldwide background exposure from natural sources of low-LET radiation is about 1 mSv [48].

2.6.1 Natural Sources of Radiation

The exposure of human beings to ionizing radiation from natural sources is a continuing and inescapable feature of life on earth. For most individuals, this exposure exceeds that from all man-made sources combined. There are two main contributors to natural radiation exposures: high-energy cosmic ray particles incident on the earth's atmosphere and radioactive nuclides that originated in the earth's crust and are present everywhere in the environment, including the human body itself. Both external and internal exposures to humans arise from these sources [1].

2.6.2 Cosmic radiation

The earth is continually bombarded by high-energy particles that originate in outer space. These cosmic rays interact with the nuclei of atmospheric constituents, producing a cascade of interactions and secondary reaction products that contribute to cosmic ray exposures that decrease in intensity with depth in the atmosphere, from aircraft altitudes to ground level. The cosmic ray interactions also produce a number of radioactive nuclei known as cosmogenic radionuclides [1]. Table 2.5 gives information on some cosmogenic radionuclides of natural origin

Table 2.5 : Cosmogenic radionuclides

ELEMENT	*ISOTOPE*	*HALF-LIFE*	*DECAY MODE*
Hydrogen	H^{3}	12.33 years	beta (100%)
Carbon	C^{14}	5730 years	beta (100%)
Krypton	K^{81}	2.29×10^{5}	Electron Capture (100%)

2.6.3 Terrestrial Radiation

Naturally occurring radionuclides of terrestrial origin (also called primordial radionuclides) are present in various degrees in all media in the environment, including the human body itself. Only those radionuclides with half-lives comparable to the age of the earth, and their decay products, exist in significant quantities in these materials. Irradiation of the human body from external sources is mainly by gamma radiation from radionuclides in the ^{238}U and ^{232}Th series and from ^{40}K. These are the radionuclides that will be of major concern in this project. Table 2.6 give more information on some terrestrial radionuclides

TABLE 2.6. Terrestrial radionuclides

ELEMENT	*RADIONUCLIDE*	*HALF-LIFE*	*MAJOR RADIATIONS*
Potassium	^{40}K	1.28×10^9 years	Beta, gamma
Uranium	^{238}U	4.47×10^9 years	Alpha, beta and gamma (from decay daughters)
Thorium	^{232}Th	1.405×10^{10} years	Alpha, beta and gamma (from decay daughters)

The primordial radionuclides undergo transitions with long half-life, and produce several radioactive products in their respective transition cascades. Figure 2.23 shows the Uranium-238 decay chain.

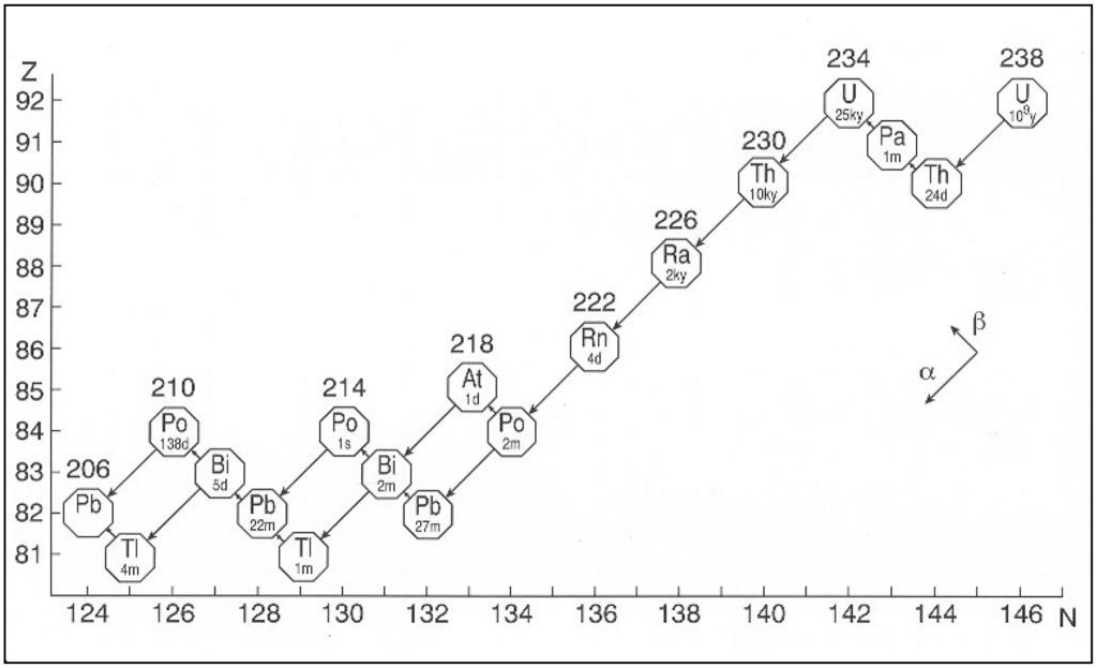

Fig.2.23 ^{238}U decay chain [53]

2.6.4 Radioactivity in Soils

"External exposures outdoors arise from terrestrial radionuclides present at trace levels in all soils. The specific levels are related to the types of rock from which the soils originate. Higher radiation levels are associated with igneous rocks, such as granite, and lower levels with sedimentary rocks. There are exceptions, however, as some shales and phosphate rocks have relatively high content of radionuclides. There have been many surveys to determine the background levels of radionuclides in soils, which can in turn be related to the absorbed dose rates in air. The latter can easily be measured directly, and these results provide an even more extensive evaluation of the background exposure levels in different countries. All of these spectrometric measurements indicate that the three components of the external radiation field, namely from the gamma-emitting radionuclides in the ^{238}U and ^{232}Th series and ^{40}K, make approximately equal contributions to the externally incident gamma radiation dose to individuals in typical situations both outdoors and indoors" [1].

2.6.5 Areas with High Background Radioactivity

Nearly eighty percent of the annual effective dose attributed to radiation exposure originates from background natural radiation, which is predominantly produced by cosmogenic and primordial radionuclides [54]. There are some areas of markedly high absorbed dose rates in air throughout the world that are associated with thorium-bearing and uranium-bearing minerals in the soil. In those areas, absorbed dose rates in air of several hundred nanograys per hour are not uncommon. There are various causes of these elevated exposure levels. Some result from monazite sand deposits, which have high levels of thorium, as observed in Guarapari in Brazil, Yangiang in China, the states of Kerala and Madras in India, and the Nile delta in Egypt [55–57]. The area of Ramsar in Iran is caused by ^{226}Ra deposited from waters flowing from hot springs [58]. Inhabitants of the world's high background natural radioactivity areas and radon prone areas receive radiation doses that are relatively higher than the doses in the normal background radiation areas (NBRAs) [11]. In areas of high natural background radiation, an increased frequency of chromosome aberrations has been noted repeatedly. The increases are consistent with those seen in radiation workers and in persons exposed to high dose levels, although the magnitudes of the increases are somewhat higher than predicted. No increase in the frequency of cancer has been documented in populations residing in areas of high natural background radiation [59].

2.6.6 Annual average background effective dose from natural radiation source

Natural ionising radiation is responsible for an average background effective dose of approximately 2.4 mSv per person per year [1]. Table 2.7 summarises the typical contributions of different sources of natural background radiation to the annual dose to the population [1].

Table 2.7 : Average worldwide exposure to natural radiation sources [1]

Source of Exposure	*Annual Effective dose in (mSv)*	*Percentage Contribution*
Total Cosmic and cosmogenic	0.39	16%
Total external Terrestrial radiation from indoors and outdoors	0.48	20%
Total inhalation exposure from Radon	1.26	52%
Total inhalation exposure from Potassium-40 and Uranium and Thorium series	0.29	12%
Total	**2.4**	

2.7.0 International studies on radioactivity in soils

In order to obtain a reference data for the natural environmental radioactivity and the associated exposure in the world, many studies have been carried out in many parts of the world and in different geological formations [60,61]. An evaluation of the radioactivity levels associated with naturally occurring radioactive materials was undertaken as part of a systematic study to provide a surface radiological map of the State of Kuwait [8]. Soil samples from across Kuwait were collected, measured and analysed. Two independent High-purity Germanium (HPGe) detectors were used for the gamma-ray spectrometric measurement of the samples. These studies provided soil activity concentration levels for primordial radionuclides, specifically members of the ^{238}U and ^{232}Th decay chains and ^{40}K. The ^{238}U and ^{232}Th radionuclides and ^{40}K activity concentration values ranged between 5.9 to 32.3 Bq/kg, 3.5 to 27.3 Bq/kg, and 74 to

698 Bq/kg, respectively. The calculated average specific activity concentrations of ^{238}U, ^{232}Th and ^{40}K in all the soil samples were 18, 15 and 385 Bq/kg respectively. These values are all below the worldwide mean values of 35, 40, and 400 Bq/kg, respectively. The measured annual dose rates for all samples gives rise to a mean value of 40.8 ± 3.0 μSv/yr which is less than the maximum permissible limit of 1 mSv per year while the internal and external hazard indices have been found to be 0.23 ± 0.02 and 0.19 ± 0.01 respectively.

A similar study was conducted in Thailand after the 2004 Tsunami. In the study, beach sand samples were collected from various locations along the Andaman coast of the Thai peninsula and a HPGe detector was used to detect radiation emitted by the samples [2]. The natural radioactivity levels of ^{226}Ra, ^{232}Th and ^{40}K measured in these samples were found to be in the range of 1.6 – 52.5 Bq/kg, 0.3 – 73.9 Bq/kg, and 2.8 – 11.9 Bq/kg, respectively, for the west coast and 3.5 – 83.1 Bq/kg, 4.5 – 42.0 Bq/kg, and 9.6 – 1376 Bq/kg, respectively, for the east coast. The radioactivity concentrations of ^{226}Ra, ^{232}Th and ^{40}K along the Andaman coast are comparable to that of the east coast, which was not exposed to the tsunami. The corresponding annual effective dose varies from 1.6 – 105.9 μSv/yr with a mean value of 59.1 - 70.3 μSv/yr, significantly lower than the world wide average as reported by United Nations Scientific Committee on the Effects of Atomic Radiation (UNSCEAR) [1].

2.8.0 National studies on radioactivity in soils

Namibia is rich in uranium especially in the western part of the country. A number of studies have been conducted to assess the radioactivity in the soils of some towns in Namibia. Soil samples from three major towns and a holiday settlement in uranium-rich western Namibia were analysed using an HPGe detector for radioactivity due to ^{238}U, ^{232}Th, and ^{40}K. The three major towns and holiday settlement in western Namibia are Walvis Bay, Swakopmund, Usakos, and Wlotzkasbaken respectively. The average activity concentrations of the radionuclides in the towns and settlement vary from a low of 18.6 ± 4.6 Bq/kg to a high of 69.6 ± 26.3 Bq/kg for ^{238}U, 23.8 ± 8.4 to 91.1 ± 41.0 Bq/kg for ^{232}Th and 460.3 ± 76.2 to 959.5 ± 194. Bq/kg for ^{40}K [14]. In order to evaluate the associated health hazard, the concentrations were used to calculate the mean annual effective dose, radium equivalent activity (Ra_{eq}) and external hazard index (H_{ex}) for the towns and settlement. The values of 0.11 mSv, 195.3 Bq/kg and 0.53 obtained respectively for the mean annual effective dose, Ra_{eq} and H_{ex} are, however, below their permissible limits, thus implying that radiation hazard is negligible in the towns [14]. It should be mentioned that studies on natural radioactivity in the soils have been conducted at a uranium mine (the Rossing Uranium Mine) and at a dumping site Kupferberg, landfill in Namibia [4,13]. The results obtained show that radiation hazard is also negligible in the mine and dumpsite.

CHAPTER 3

3. RESEARCH METHODOLOGY

3.1 Introduction

The first section of this chapter will discuss the study setting which will be followed by sample collection and sample preparation. The preceding sections will then be followed by discussing the detector system and the chapter will conclude by evaluating the activity concentration and calculation of radiation hazard indices.

3.2 Study Area

Okahandja is a town in Namibia in the Otjozondjupa region. It is situated in the central part of Namibia as shown in figure 3.1. The coordinates of the city are 21˚59'S 16˚55'E. The town has a population of about 24000 [15]. Okahandja falls within the central plains landscape and lies between 1000 m and 1200 m above sea level [62]. The dominant soil type in Okahandja is a mixture of *Lithic Leptosols, Eutric Regosols and Chromic Cambisols*. Lithic means 'very thin and shallow soils' and *Leptosols* means 'soils which typically form in actively eroding land scapes, especially in hilly or undulating areas [62]. The soils are course textured and characterised by their limited depth caused by the presence of a continuous hard rock highly calcareous'. Eutric means 'fertile soils with high base saturation' and Regosol are 'soils with medium to fine textured of actively eroding land scapes'. *Chromic* means 'soils with bright colours' and *Cambisols* means ' soils that were formed quite recently in geological time, mainly from medium and fine textured parent material deposited during sporadic flooding [62].

Karibib is a town in the Erongo region in the western part of Namibia. It is about 100 km away from Okahandja on the B2 road to Walvis Bay. It is well known for its marble

and granite deposits. The coordinates of the town are 21˚56'17"S, 15˚51'16"E. Karibib and most of the Erongo Region falls within the Central-western Plains landscape [62].. Much of the area lies between 500 m and 1,000 m above sea level, and consists of metamorphic rocks [62]. The dominant soil type in this sub-biome is a mixture of different soil types of *Petric Calcisols* and Rock outcrops. Petric means "soils with a solid layer at a shallow depth that remains hard even when wet" and Calcisols are soils "found in depressions or other low-lying areas of the landscapes and typically contain accumulations of calcium carbonate, often in a cemented form called *calcrete*" [62]. Karibib is located at an altitude of 1,137m above sea-level. According to the geological map of Namibia, the dominant soils found in the town are as shown in Fig 3.2.

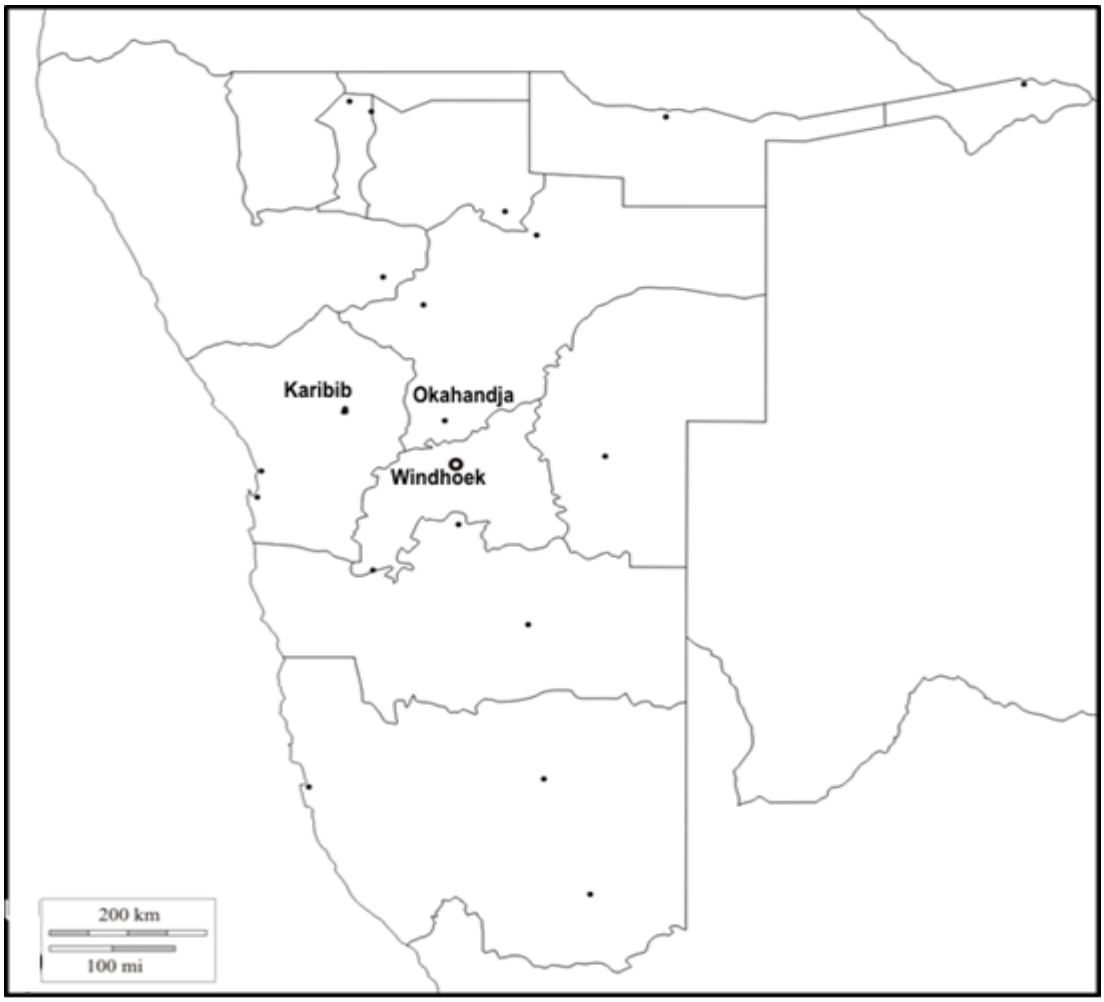

Fig 3.1Map of Namibia showing the locations of Okahandja and Karibib [63]

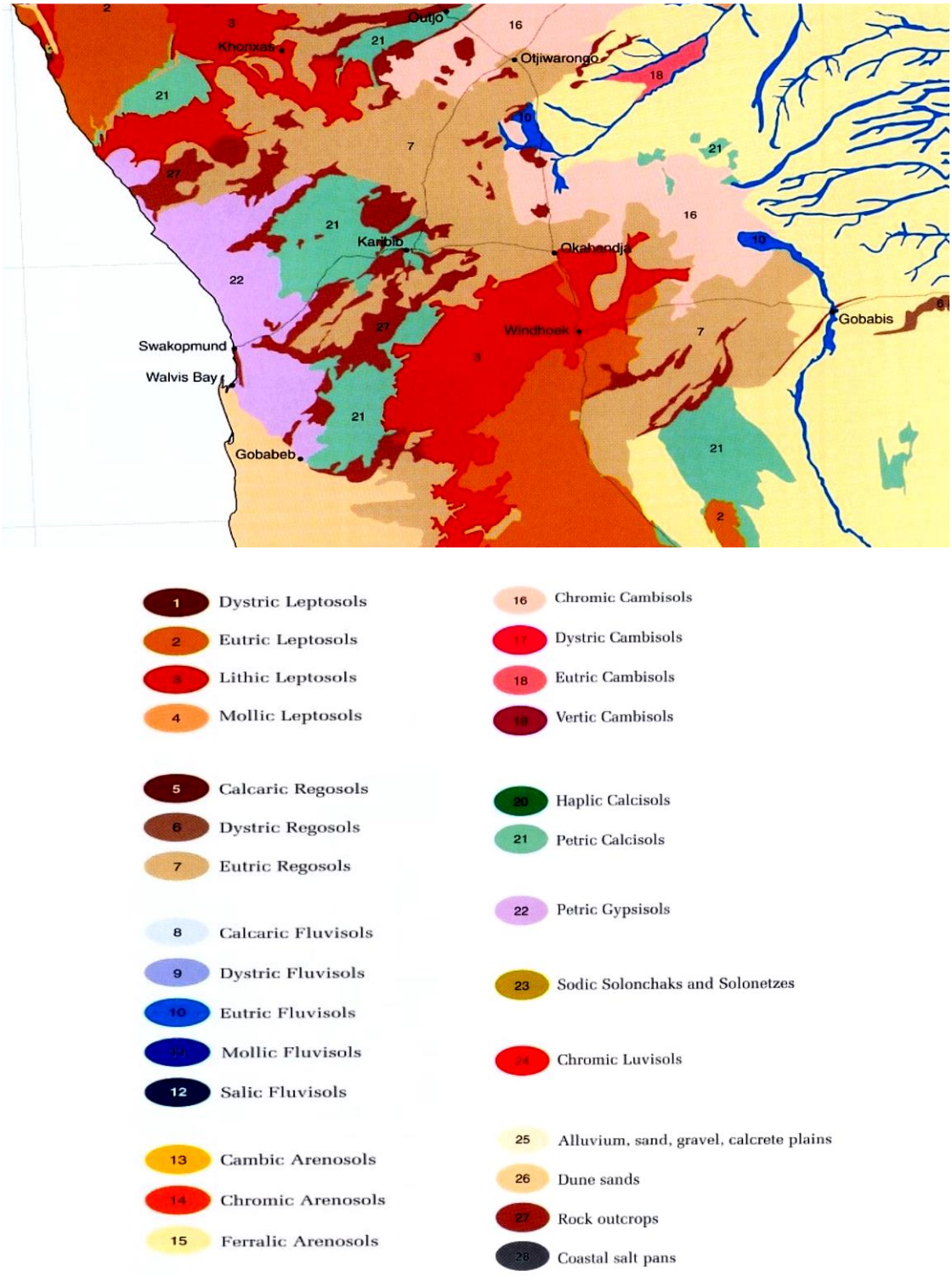

Fig 3.2 Dominant soils of Namibia [62]

3.3 Sample Collection

Soil sample collection and preparation were done according to the usual procedure described in reference [4,12–14]. A total of 50 soil samples were collected from ten geographical areas in each of the two towns as shown in Figure 3.3.and 3.4. In each geographical area, soil samples were collected at five sites across the area. All the sites chosen were away from roads, buildings, railway lines, industrial or agricultural sites and rivers. Soil samples were collected from undisturbed areas with a natural morphology. The samples were collected at a depth of about 2cm - 5cm below the soil surface. Gloves, dust masks, spades and digging equipment were employed to collect 50 samples of about 1kg across each town. They were then placed in labelled plastic bags corresponding to the areas and sites where they were collected. All samples were then transported from the site(s) to the nuclear science laboratory in the Department of Physics of the University of Namibia (UNAM) in Windhoek for processing.

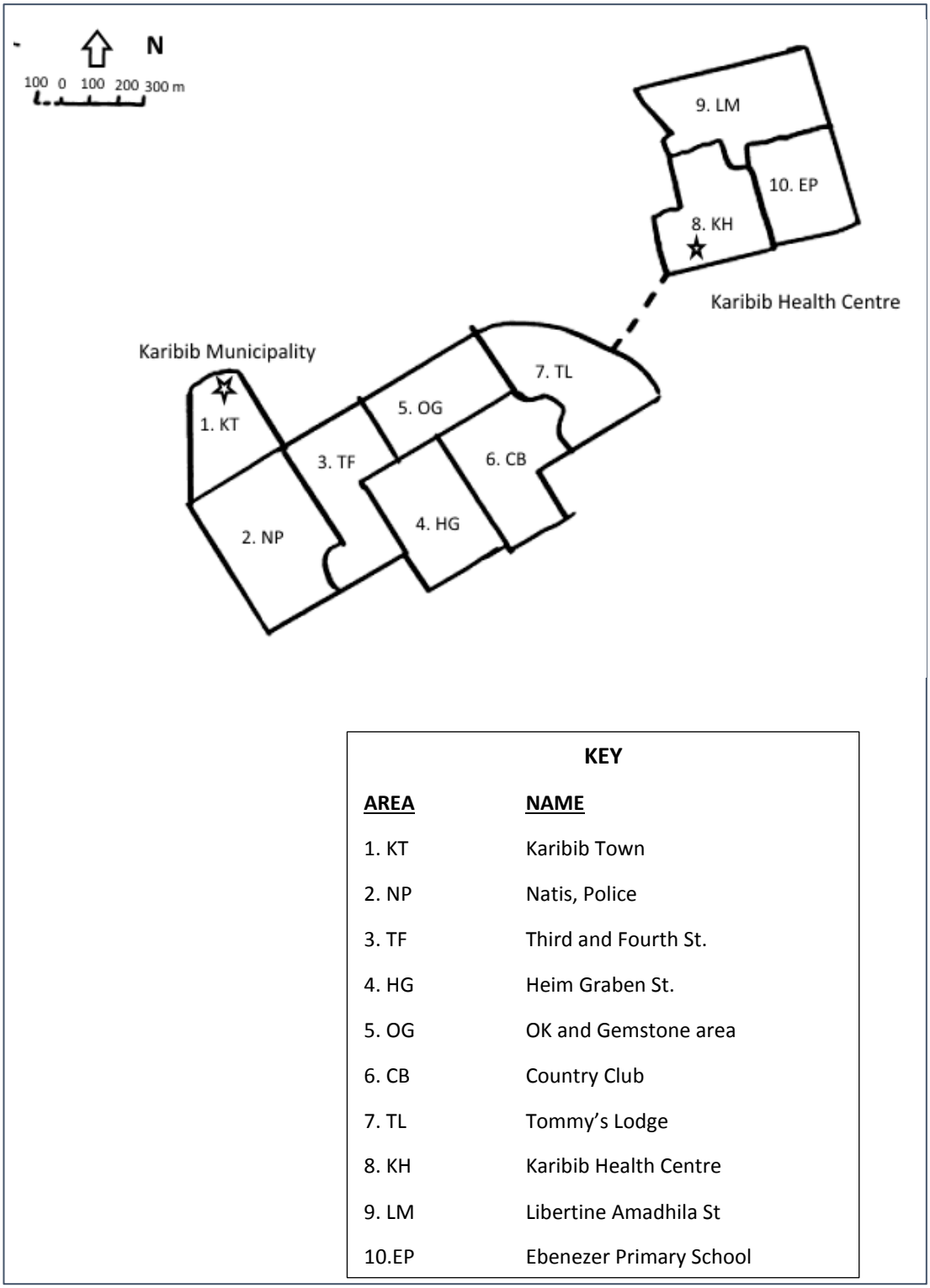

KEY	
AREA	**NAME**
1. KT	Karibib Town
2. NP	Natis, Police
3. TF	Third and Fourth St.
4. HG	Heim Graben St.
5. OG	OK and Gemstone area
6. CB	Country Club
7. TL	Tommy's Lodge
8. KH	Karibib Health Centre
9. LM	Libertine Amadhila St
10.EP	Ebenezer Primary School

Figure 3.3 Map showing the geographical areas where soil samples were collected in Karibib

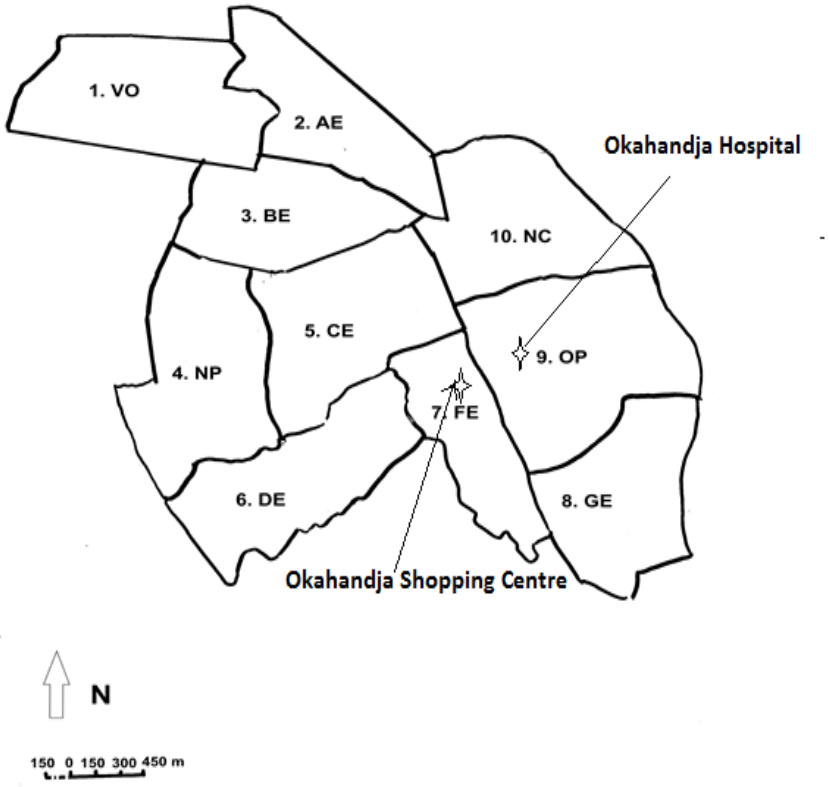

KEY

AREA	NAME
1. VO	Veddersdal, Okahandja (Extension 11)
2. AE	Okahandja (Extension 2)
3. BE	Okahandja (Extension 6)
4. NP	Nau-aib Proper
5. CE	Okahandja (Extension 8)
6. DE	Okahandja (Extension 9, 10)
7. FE	Okahandja Extension 1, 7)
8. GE	Okahandja Extension 4
9. OP	Okahandja Proper
10. NP	Nied, Okahandja Country Club

Figure 3.4 Map showing the geographical areas where soil samples were taken in Okahandja.

Figure 3.5. UNAM Staff members who were part of the team of collecting soil sample. From left; Mr. S Shimboyo, Mr. E. Taapopi and Prof. J.A Oyedele.

3.4 Sample Preparation

Soil samples were left to dry for a period of two weeks at room temperature as shown in figure 3.6. The dried soil samples were pulverised and sieved through a 2 mm mesh screen. The sieved soil was weighed to 500 g which was then placed in 500 ml plastic bottles and sealed as shown in Figure 3.7 and 3.8. The plastic bottles used are similar to those of the reference material. The sealed plastic bottles were left for about a month so that there can be radioactive equilibrium between ^{226}Ra and ^{232}Th and their progeny. After the one month period the soil samples were ready for counting on the HPGe detector.

Figure 3.6 Drying of soil samples

Figure 3.7 Determination of the weight of a soil sample using an electronic scale.

Figure 3.8 Soil samples in plastic bottles ready for counting.

3.5 Detector System

The detector system used in this study included a high-resolution HPGe coaxial detector, high-voltage power supply, preamplifier, amplifier and a multichannel analyser (MCA) as shown in figure 3.9 – 3.14. The HPGe coaxial detector used had a measured energy resolution of 1.0 keV FWHM at 1.22 keV and 1.9 keV FWHM at 1332 keV, with 25% relative efficiency (Canberra model GC2519). The detector was placed inside a Canberra Model 737 lead shield having a thickness of 10 cm. In addition, it had a graded 1.5 mm copper and 1.0 mm tin lining with an outer jacket of 9.5 mm thick low carbon steel. A Model 7915-30 Cryostat was used to supply liquid nitrogen (LN_2) to the detector, with a Model 2002C Pre-amplifier as shown in Figure 3.10. Liquid nitrogen (LN_2) was used to cool the detector to reduce thermal noise in the detector. There was a constant supply of LN_2 during measurements. A Model 9660

Digital Signal Processor, an Acquisition Interface Module (AIM 556A) and a Multichannel Analyser (MCA) were used. A Genie® 2000 software (V3.2.1) was used to analyse the spectra acquired in the measurements.

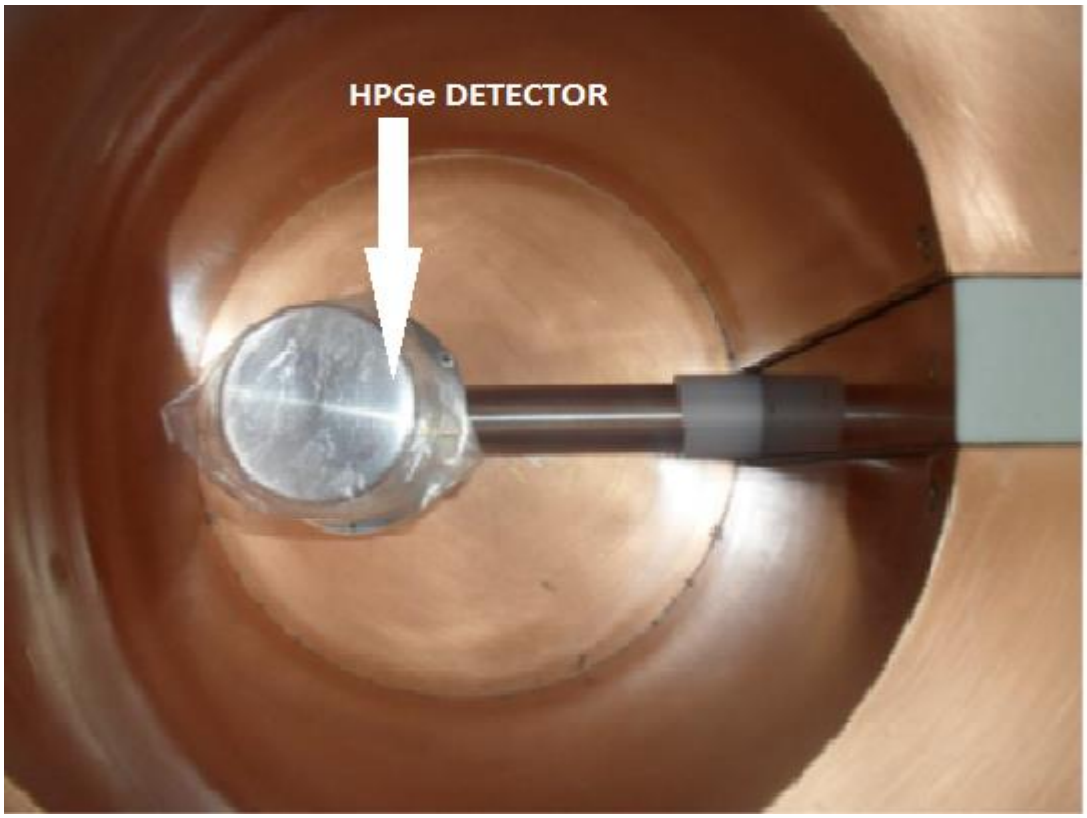

Figure 3.9 The HPGe detector in a Lead shield

The high-purity germanium detector (HPGe) used in this study is basically a cylindrical germanium crystal with an n-type contact on the outer surface, and a p-type contact on the surface of an axial well as shown in Figure 3.11. The Germanium has a net impurity level of around 10^{10} atoms per cubic centimetre so that with moderate reverse bias, the entire volume between the electrodes is depleted, and an electric field extends across this active region. Photon interaction within this region produces charge carriers which are swept by the electric field (produced by the high voltage supplied over the crystal lattice) to their collecting electrodes, where a charge sensitive

preamplifier converts this charge into a voltage pulse proportional to the energy deposited in the detector as shown in Figure 3.12 and 3.13 [44].

Figure 3.10 Lead shield and Cryostat

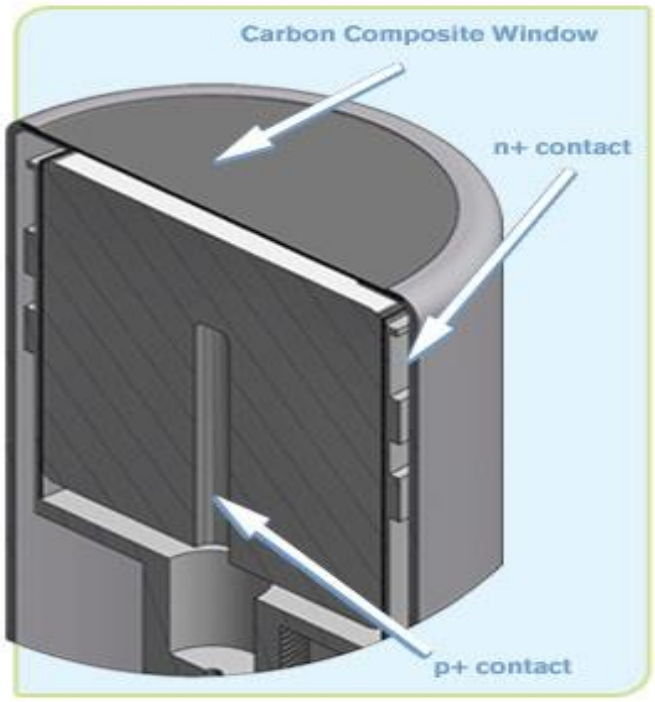

Figure 3.11 Cross sectional view of HPGe Detector [44]

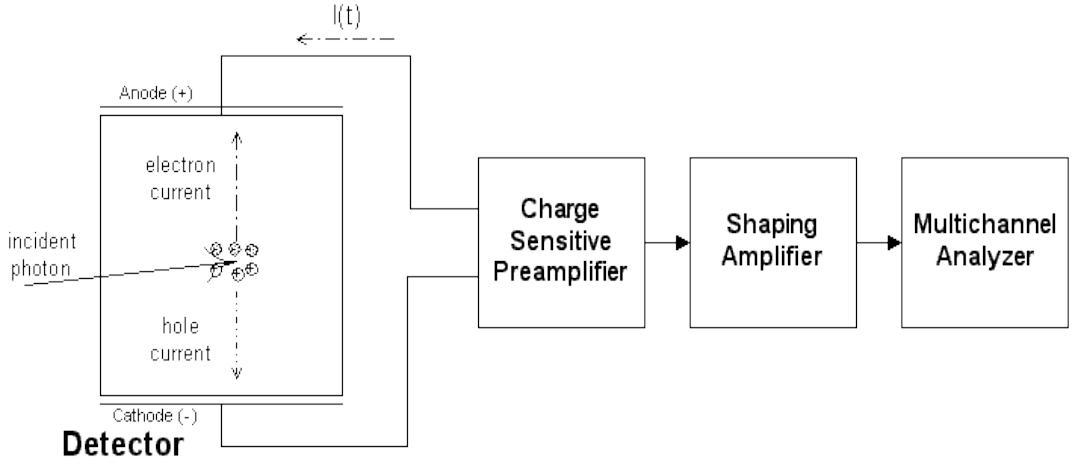

Figure 3.12 Block diagram of a typical gamma spectroscopy system [64]

Figure 3.13 System electronics of HPGe detector

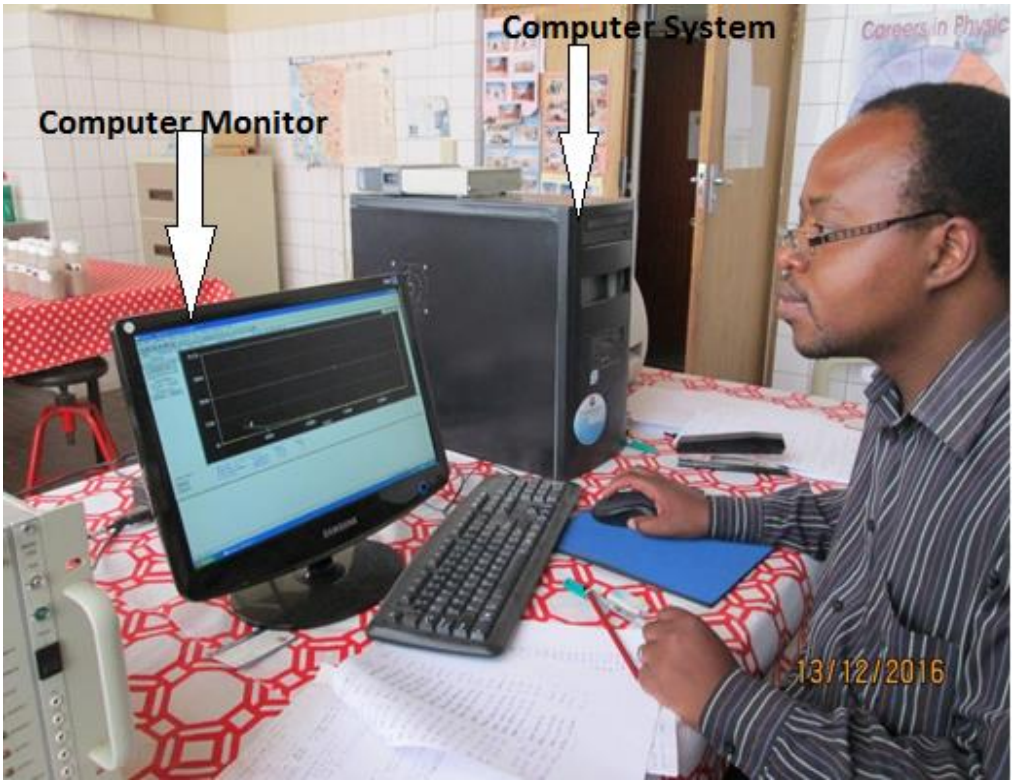

Figure 3.14 Data acquisition and display computer system using Genie 2000 software

3.6 Calibration of the HPGe Detector

Energy calibration of the detector was performed to obtain a relationship between the position of the photo peak in the spectrum and the gamma-ray energy. Identifying the gamma rays within a measured spectrum requires matching the energies of the gamma rays with those emitted by known radionuclides. The process involved using standard point sources with known energy peaks whose gamma ray energies spans over the entire energy range of interest. ^{137}Cs, ^{22}Na and ^{60}Co point sources were used to calibrate the detector. Each point source was placed on the detector and counted for 1800 seconds. Energy calibration was done to obtain a relationship between the peak position in the spectrum and the corresponding gamma-ray energy as shown in Table 3.1. The table shows the measured values of point sources used. A graph of the energy calibration curve is shown in figure 3.15.

Table 3.1 Point sources used for energy calibration

Radionuclide	Peak Energy (keV)
^{137}Cs	661.66
^{60}Co	1173.24 and 1332.50
^{22}Na	1274.54

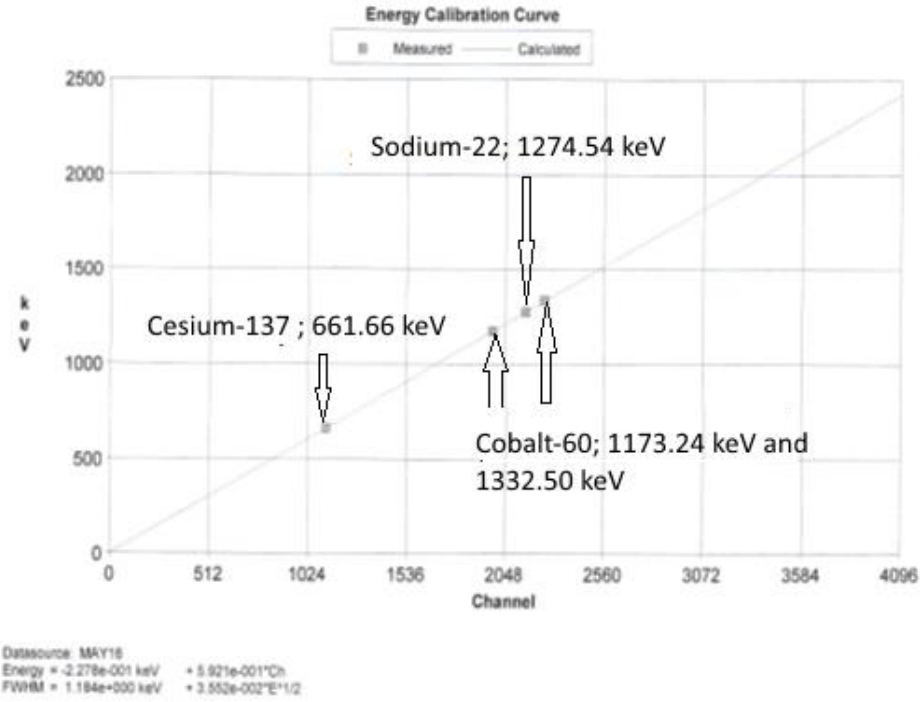

Figure 3.15 Energy Calibration Curve

3.7 Background counting

It is essential to determine how much background radiation is present before commencing with soil sample measurements. This because the detector is sensitive to all particles interacting inside its active volume so that it measures the radiation coming from the sample as well as from the environment (natural background radiation). The background radiation was measured by placing a 500 ml empty bottle on the detector and counting the radiation in the environment for 10800 seconds as shown in Figure 3.16. The results of the measurement shows that there are no energy peaks corresponding to ^{40}K, ^{232}Th and ^{238U} peaks in the background radiation.

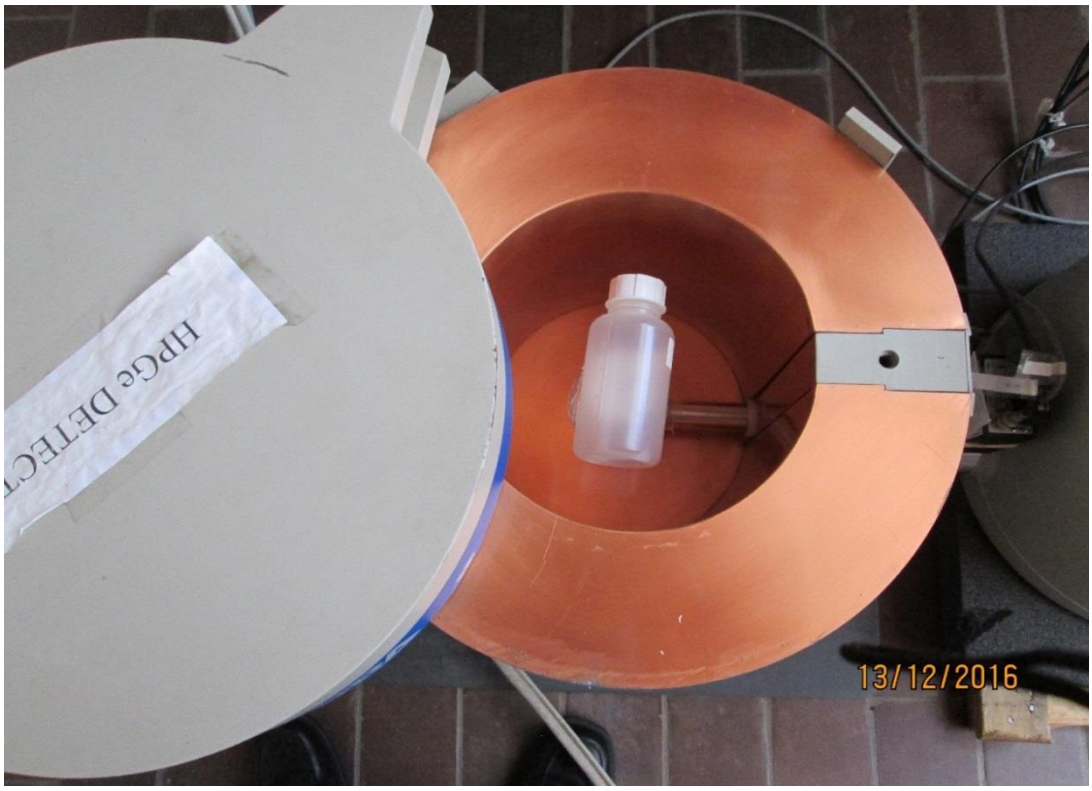

Figure 3.16 HPGe Detector with empty bottle ready for background counting

3.8 Measurement on reference materials

After the completion of the background measurements IAEA certified reference materials or standards RGK-1, RGTh-1 and RGU-1 were analysed using the HPGe detector. The reference materials contained 500 g of ^{40}K, ^{232}Th and ^{238}U respectively as shown in Figure 3.17. The standards were placed one at a time on the detector and the radiation emitted was counted for 10800 seconds and recorded. The energy peak, channel number and number of counts were recorded. The Gene 2000 Gamma Acquisition software was used to determine accurately the peak energy and net area of each relevant peak. The data obtained were used to determine the concentration of the particular radionuclide in the standard.

Figure 3.17 IAEA certified reference material RGK-1, RGTh-1 and RGU-1

3.9 Measurement on soil samples.

Soil sample counting commenced after the IAEA standard source counting was completed. The outside of the bottles containing the soil sample were cleaned and then placed on the detector as shown in figure 3.18. Each soil sample was counted for 10800 seconds just as in the case of the IAEA standards. Also, the date of the measurement, the sample number, the start and stop times and counting period were recorded for each sample. The data obtained was saved on a computer. Measurements were made on about five samples every week day (from 07:00 to 22:00 hours). The relatively high number of samples analysed per day was due to time constraint for all the measurements and non-steady supply of LN_2. The 50 soil samples from Karibib were first analysed after which the three IAEA standards were again analysed to check the stability of the detector. Okahandja soil samples were then analysed and the three IAEA standards were analysed again to make sure that the detector stability did not change during the measurements of all samples. Figure 3.18 shows an example of soil sample spectrum.

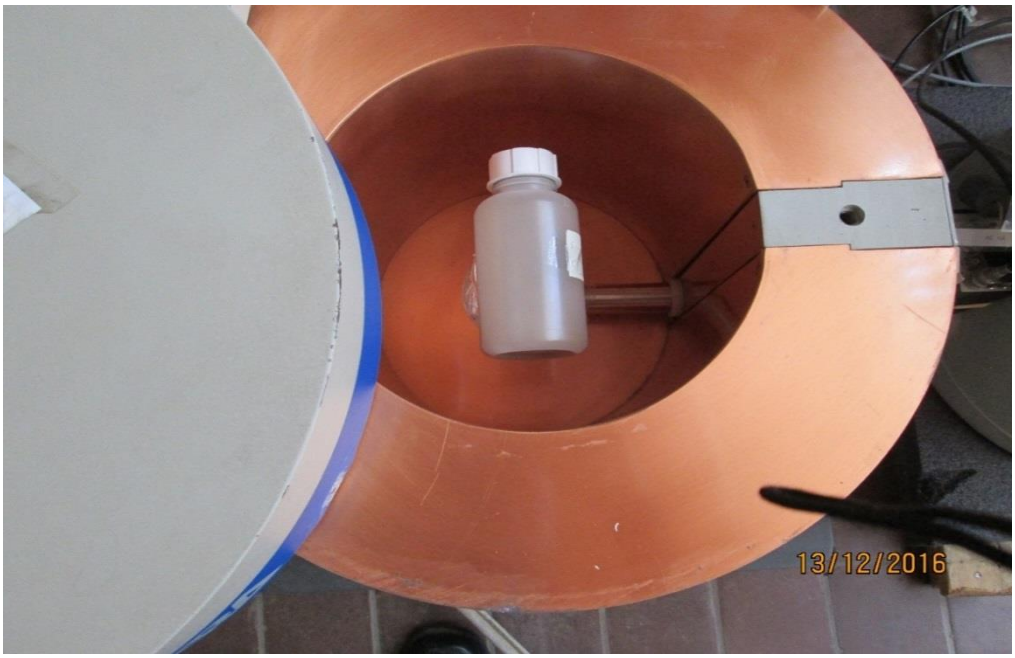

Figure 3.18 HPGe Detector with soil sample ready for counting

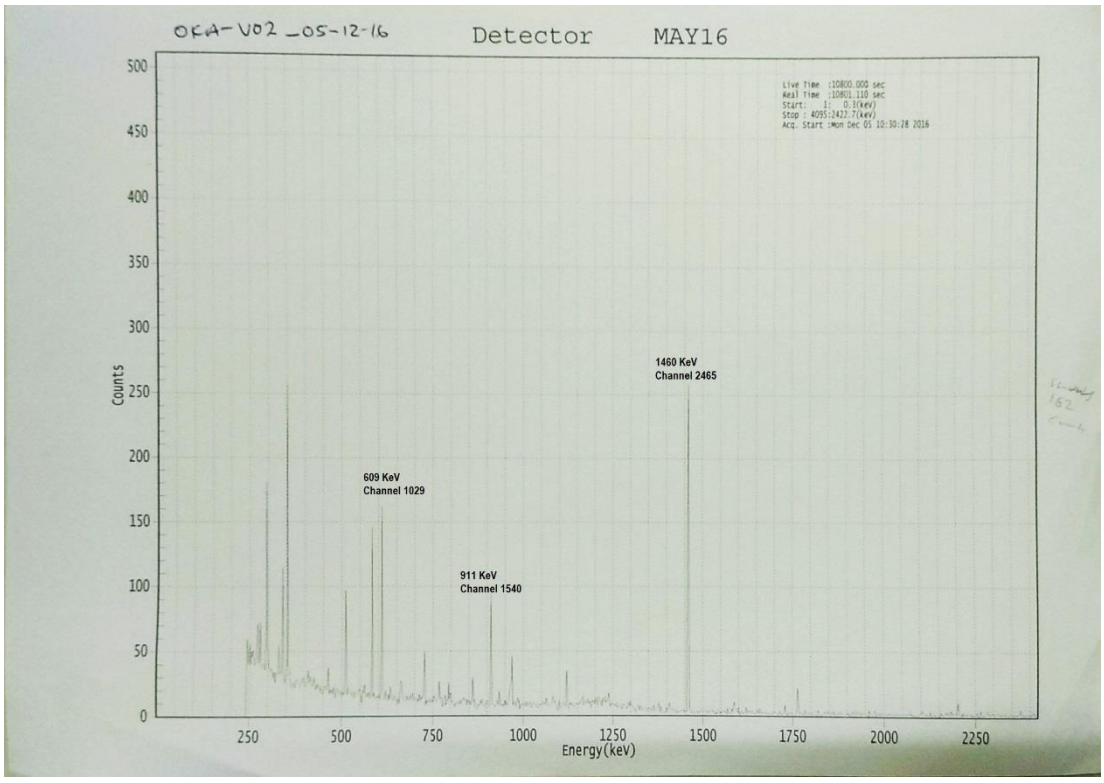

Figure 3.19 Example of soil sample spectrum from HPGe detector system

3.10 Determination of Activity Concentration

According to Beck et al, the number of counts obtained under a photo peak in a spectrum is related to the activity concentration of the radionuclide producing the peak in the soil [65]. The activity concentrations of ^{40}K, ^{232}Th and^{238}Uin the soil samples were calculated from the corresponding photo peaks in the spectra. The activity concentration of ^{238}U was evaluated from the intensity of 609 keV gamma transition line of ^{214}Bi while the activity concentration of ^{232}Th was determined using the 911 keV gamma line of ^{228}Ac. The 1460.75 keV gamma ray of ^{40}K was used to determine the activity concentrations of the ^{40}K. The net peak area *A* is proportional to specific activity concentration *C* of the radionuclide. That is

$A \propto C \; or$

$A = kC \; therefore$

$k = {}^{A}/_{C}$ ……3.1

where *k* is a constant for a given element

Therefore, for a given element X (e.g. ^{238}U) in a standard source

$$k^X_{standard} = \frac{A^X_{standard}}{C^X_{standard}} \text{ ……3.2}$$

Similarly, for element X (e.g. ^{238}U), in the sample

$$k^X_{sample} = \frac{A^X_{sample}}{C^X_{sample}} \text{ ……3.3}$$

rearranging equation 3.3

$$C^X_{sample} = \frac{A^X_{sample}}{k^X_{sample}}$$

Since $k^X_{standard} \equiv k^X_{sample}$ for a given element X, therefore

$$C^X_{sample} = \frac{A^X_{sample}}{k^X_{standard}} \text{ ……3.4}$$

Equation 3.4 shows that the activity concentration of a particular radionuclide X in a given soil sample can be determined from the net peak area of the corresponding photo peak divided by constant k calculated for the standard source. For example to determine the concentration of ^{238}U in a given sample, the following equation applies

$$Concentration\ of\ U^{238} in\ sample = \frac{net\ peak\ area\ of\ U^{238} in\ sample}{k_{standard}^{238_U}} \ldots\ldots\ldots\ldots\ldots\ldots\ldots\ldots\ldots\ldots 3.5$$

3.11 Radiation Hazard and Indices calculation.

The quantity used to measure the "amount" of ionizing radiation is the absorbed dose, or simply known as dose [34]. The absorbed dose rate is determined from the activity concentrations of the radionuclides ^{40}K, ^{232}Th and ^{238}U in the soil. UNSCEAR(2000) report provides guidelines on how to calculate the absorbed dose rate (D) due to gamma radiation in air at 1m above the ground [1]. In this study the absorbed dose rate (D) was calculated using the formula [1,4,66].

$$D(nGy/h) = 0.462C_U + 0.621C_{Th} + 0.0417C_K \ldots\ldots\ldots\ldots\ldots\ldots\ldots\ldots\ldots\ldots\ldots 3.6$$

where C_U, C_{Th}, C_K are the activity concentrations of ^{238}U , ^{232}Th and ^{40}K respectively in the sample.

To estimate the annual effective dose, the conversion coefficient from absorbed dose in air to effective dose (0.7 Sv Gy^{-1}) and an outdoor occupancy factor (0.2) proposed by UNSCEAR, 2000 are used [1]. That is, the annual effective dose rate (in mSv yr^{-1}) was calculated using the formula,

$$Effective\ Dose\ Rate\ \left(\frac{mSv}{yr}\right)$$

$$= D\left(\frac{nGy}{hr}\right) \times 8760\ \left(\frac{hr}{yr}\right) \times 0.7 \times (10^3 mSv/10^9)\eta Gy \times 0.2 \ldots\ldots\ldots\ldots 3.7$$

A widely used hazard index (reflecting external exposure) called the external hazard index, H_{ex}, is defined as

$$H_{ex} = \frac{C_U}{370} + \frac{C_{Th}}{259} + \frac{C_K}{4810} \ldots\ldots\ldots\ldots 3.8$$

The value of the index (H_{ex}) must be less than unity for the radiation hazard to be negligible [67].

The Radium equivalent activity is a radiological index that represents the activity levels of ^{238}U, ^{232}Th and ^{40}K as a single quantity, it takes into account the radiation hazards associated with each component [67]. The recommended maximum value of Radium equivalent activity is 370 Bq/kg [14]. The Radium equivalent activity (Ra_{eq}) is given by the expression

$$Ra_{eq} = C_U + 1.43C_{Th} + 0.077C_K \ldots\ldots\ldots\ldots 3.9$$

where C_U, C_{Th} and C_K are the activity concentrations of ^{238}U, ^{232}Th and ^{40}K respectively.

A computer program was written in Python language to calculate all the above parameters (in equations 3.7, 3.8 and 3.9).

CHAPTER 4

4. RESULTS AND DISCUSSIONS

4.0 Introduction

In this chapter, the results of the measurements of natural radioactivity in the soils of Karibib and Okahandja are respectively presented and discussed. The results obtained from the two towns are also compared with each other in the chapter.

4.1 Natural radioactivity in Karibib

4.1.1 Radionuclide concentrations in Karibib

The mean activity concentrations of ^{238}U, ^{232}Th and ^{40}K in the soil samples collected from each of the ten geographical areas in Karibib (Figure 3.3) are summarized in Table 4.1 and shown in Figure 4.1. Also, the concentrations of ^{238}U, ^{232}Th and ^{40}K measured in each of the 50 soil samples collected from the town are shown in Appendix 1 and the statistics of the results obtained in the measurements are shown in Table 4.2. As could be observed in the Table and Figure, the activity concentration of ^{238}U is highest in the NP area with an average of 32.7 ± 2.1 Bq/kg (and varies from 31.0 to 36.2 Bq/kg) but lowest in the CB area with an average of 26.1 ± 3.3 Bq/kg (and varies from 21.6 to 29.5 Bq/kg). The difference between the minimum and maximum (or range of) activity concentrations of ^{238}U in all the samples is 28.8 Bq/kg as shown in Table 4.2 (column 2). The average activity concentration of ^{238}U from all the soil samples across the town of Karibib is 29.4 ± 5.8 Bq/kg as shown in column 2 of Table 4.1. This value is lower than the worldwide average activity concentration of 35 Bq/kg for ^{238}U in soil [1]. Similarly, the activity concentration of ^{232}Th is highest in the TF area with an average of 55.4 ± 6.1 Bq/kg (and varies from 45.3 to 61.6 Bq/kg) while it is lowest in the KH area with an average of 40.9 ± 11.6 Bq/kg (and varies from 29.0

to 54.7 Bq/kg) as could be observed in Table 4.1 (column 3) and Figure 4.1. Also, the difference between the minimum and maximum (or range of) activity concentrations of ^{232}Th in all the 50 samples is 40.9 Bq/kg as shown in Table 4.2 (column 3). The average activity concentration of ^{232}Th from all the samples across Karibib is 49.0 ± 8.6 Bq/kg as could be observed in Table 4.1 (column 3). These results shows that the average activity concentration of ^{232}Th in the soil of Karibib is higher than the worldwide average activity concentration of 30 Bq/kg reported by UNSCEAR [1].This observation is in contrast to that made on ^{238}U in which the average activity concentration of ^{238}U is lower than the worldwide average. In the case of ^{40}K its activity concentration is highest in the EP area with an average of 1007.4 ± 108.8 Bq/kg (and varies from 815.8 to 1079.0 Bq/ kg) but it is lowest in the TF area with an average of 704.2 ± 87.1 Bq/kg (and varies from 579.0 to 784.2 Bq/kg) as could be seen in Table 4.1 column 4. However, while the average activity concentration of ^{40}K has its lowest value in the TF area, the average activity concentration of ^{232}Th has its highest value in the TF area as could be observed in Figure 4.1. The average activity concentration of ^{40}K from all the samples collected across Karibib is 824.3 ± 153.5 Bq/kg as could be seen in Table 4.1 (column 4). This average activity concentration of ^{40}K (from all the soil samples) is twice higher than the worldwide average activity concentration of 400 Bq/kg [1]. As could be seen in Figure 4.1 the activity concentration of ^{40}K (in each of the geographical areas) is much greater than those of ^{238}U and ^{232}Th while the activity concentration of ^{232}Th is higher than that of ^{238}U. It therefore follows that, among the three primordial radionuclides, ^{40}K has the highest activity concentration while ^{238}U has the least activity concentration in the soil of Karibib. These results are consistent with those obtained in some other towns in western Namibia [14].

Table 4.1 Average activity concentrations of ^{238}U, ^{232}Th and ^{40}K in different geographical areas of Karibib. The range of values is given in parenthesis.

Area	*Radionuclide Concentration [Bq/kg]*		
	^{238}U	^{232}Th	^{40}K
KT	30.3 ± 7.1 (24.4 - 42.3)	53.1 ± 5.2 (43.8 - 56.5)	857.9 ± 104.4 (736.8 – 994.7)
NP	32.7 ± 2.1 (31.0 - 36.2)	43.8 ± 5.3 (36.9 - 49.0)	753.7 ± 60.2 (694.7 - 821.1)
TF	26.2 ± 4.2 (21.2 – 30.7)	55.4 ± 6.1 (45.3 – 61.6)	704.2 ± 87.1 (579.0 – 784.2)
HG	30.3 ± 6.5 (23.1 - 39.0)	47.8 ± 5.6 (39.1 - 53.7)	801.1 ± 109.2 (621.1 – 879.0)
OG	27.8 ± 5.2 (20.5 – 34.0)	45.7 ± 9.1 (39.1 – 60.7)	707.4 ± 74.8 (605.3 – 805.3)
CB	26.1 ± 3.3 (21.6 – 29.5)	48.3 ± 7.8 (38.4 – 55.9)	783.2 ± 67.3 (731.6 – 884.2)
TL	30.9 ± 10.8 (14.3 – 43.1)	51.9 ± 14.6 (33.1 – 69.9)	801.1 ± 240.1 (505.3 – 1168.4)
KH	27.8 ± 7.5 (19.8 – 39.5)	40.9 ± 11.6 (29.0 – 54.7)	822.1 ± 206.9 (621.1 – 1057.9)
LM	31.9 ± 3.3 (27.6 - 36.4)	49.9 ± 2.5 (46.5 - 52.5)	1005.3 ± 57.5 (926.3 - 1057.9)
EP	30.6 ± 4.2 (25.9 - 36.5)	53.1 ± 6.3 (43.5 - 60.4)	1007.4 ± 108.8 (815.8 - 1079.0)
Average of all samples	**29.4 ± 5.8 (14.3 – 43.1)**	**49.0 ± 8.6 (29.0 – 69.9)**	**824.3 ± 153.5 (505.3 – 1168.4)**

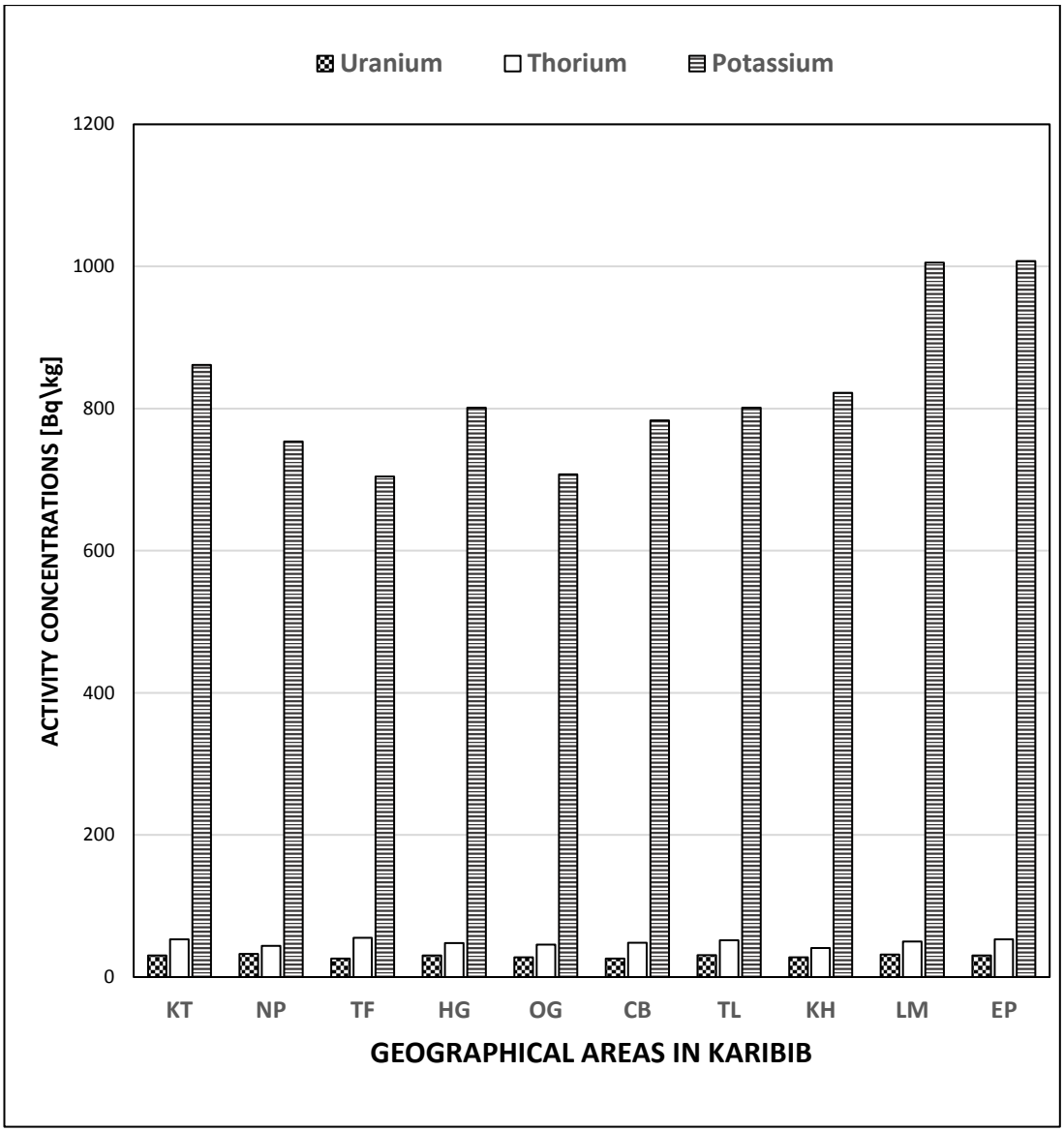

Figure 4.1: The mean activity concentrations of ^{238}U, ^{232}Th, and ^{40}K in the ten geographical areas of Karibib.

Table 4.2 Statistics of the results obtained in the measurement of radioactivity in the soils of Karibib

Descriptive Statistics	^{238}U conc (Bq/kg)	^{232}Th conc (Bq/kg)	^{40}K conc (Bq/kg)	Absorbed Dose rate (nGy/h)	Annual Effective Dose (mSv/y)	Radium Equivalent Activity (Raeq) (Bq/kg)	External Hazard Index (Hex)
Mean	29.4	49.0	824.3	77.6	0.095	163.0	0.4
Standard Error	0.8	1.2	21.7	1.5	0.002	3.2	0.01
Median	29.2	51.2	797.4	75.5	0.093	160.0	0.4
Standard Deviation	5.8	8.6	153.5	10.9	0.013	22.6	0.1
Kurtosis	0.3	-0.2	-0.6	0.5	0.541	0.7	0.8
Skewness	0.1	-0.2	0.3	0.5	0.496	0.5	0.5
Range	28.8	40.9	663.2	56.0	0.069	118.4	0.3
Minimum	14.3	29.0	505.3	54.9	0.067	114.5	0.3
Maximum	43.1	69.9	1168.4	110.8	0.136	232.9	0.6
Number of Samples	50	50	50	50	50	50	50

Figure 4.2 shows the frequency distributions of activity concentrations of (a) ^{238}U (b) ^{232}Th, and (c) ^{40}K in the 50 soil samples collected across Karibib. As could be observed in Table 4.2 (column 2) and figure 4.2 (a), the concentrations of ^{238}U in the soil samples have almost a normal distribution with a Skewness of 0.1. "Skewness is the degree of asymmetry, or departure from symmetry, of a distribution. If the frequency curve of a distribution has a longer tail to the right of the central maximum than to the left, the distribution is said to be skewed to the right or to have positive skewness. If the reverse is true, it is said to be skewed to the left, or have negative skewness" [68]. Also, the concentration of ^{238}U in most of the samples is between 20 Bq/kg and 38 Bq/kg. In fact, only 4 of the 50 samples have an activity concentration greater than 38 Bq/kg while only two samples have an activity concentration less than 20 Bq/kg. The most frequently occurring range of activity concentration of ^{238}U is 29 Bq/kg to 32 Bq/kg. As shown in Table 4.2 (column 3) and Figure 4.3 (b), the activity concentrations of ^{232}Th in the samples have almost normal distribution with a skewness of -0.2. Also,

the concentration of ^{232}Th in most of the samples is between 36 Bq/kg and 64 Bq/kg, and only one sample has an activity concentration greater than 64 Bq/kg while only three samples have an activity concentration smaller than 36 Bq/kg. The most frequently occurring range of activity concentration of ^{232}Th is 52 Bq/kg to 56 Bq/kg. Similarly, as could be seen in Table 4.2 (column 4) and Figure 4.2 (c), the activity concentrations of ^{40}K have almost a normal distribution with a positive skewness of 0.3. The concentration of ^{40}K in most of the samples is between 580 Bq/kg and 1060 Bq/kg. Only three samples have an activity concentration greater than 1060 Bq/kg and only two samples have a activity concentration smaller than 580 Bq/kg. The most frequently occurring range of activity concentration of ^{40}K is 740 Bq/kg to 820 Bq/kg.

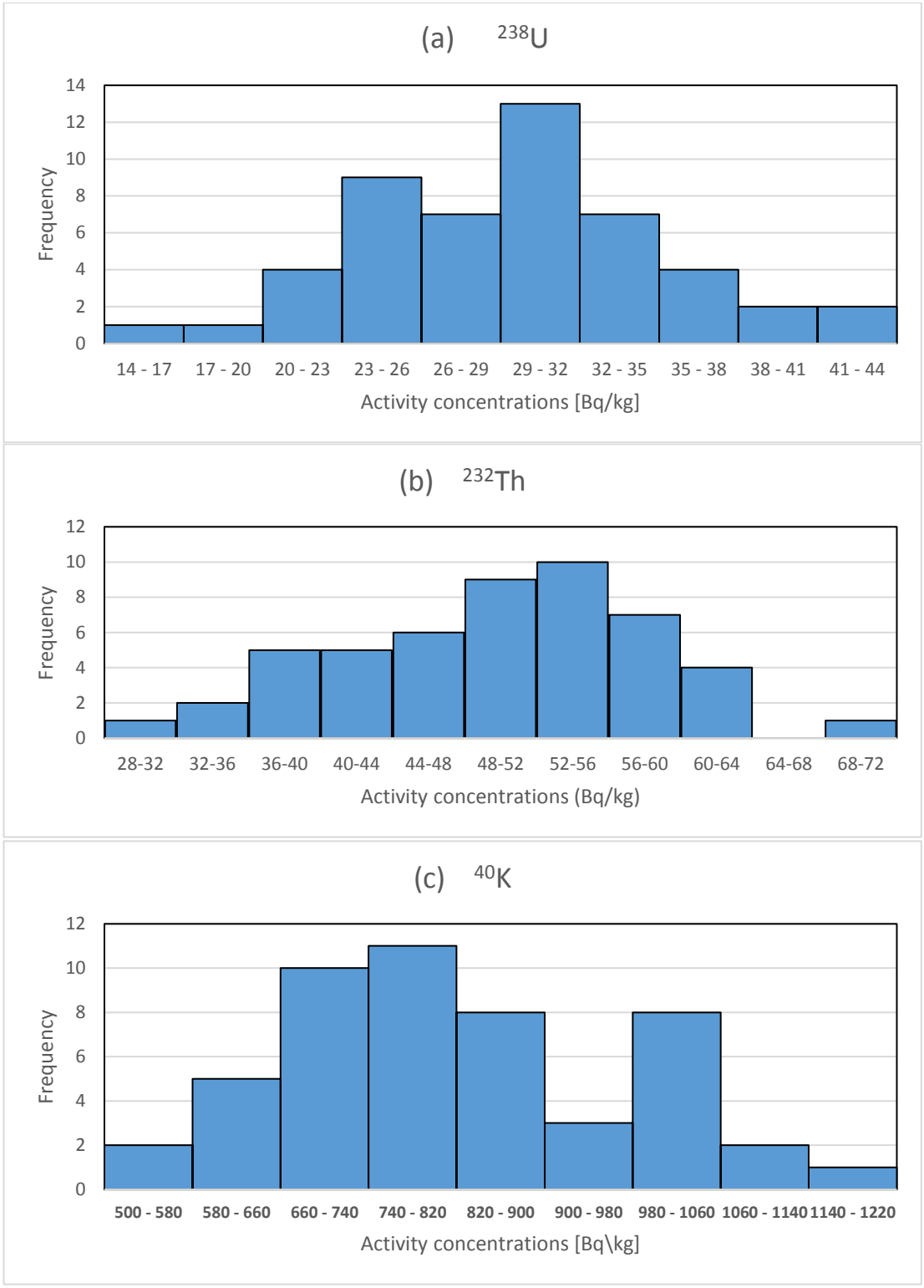

Figure 4.2 Frequency distributions of concentrations of a) ^{238}U, b) ^{232}Th, and c) ^{40}K in the soil samples of Karibib.

4.1.2 Absorbed dose rate and annual effective dose in Karibib

The mean absorbed dose rate in air and the mean annual effective dose in each of the ten geographical areas of Karibib are shown in Table 4.3 and Figure 4.3. As could be observed in Table 4.3 (column 2) and Figure 4.3 (a), the mean absorbed dose rate is highest in the EP area with an average value of 88.2 ± 7.3 nGy/h while it is lowest in the OG area with an average value of 69.9 ± 1.3 nGy/h. The relatively high value of the mean absorbed dose rate in the EP area is not surprising since the same area has a relatively high concentration of ^{40}K as discussed in section 4.1.1. The average absorbed dose rate from all the ten geographical areas in Karibib is 77.6 ± 10.9 nGy/h as shown in Table 4.3 (column 2) which is higher than the reported worldwide average value of 51 nGy/h [1,14]. As could be observed in Table 4.3 (column 3) and Figure 4.3 (b) the corresponding mean annual effective dose is highest in the EP area with a value of 0.108 ± 0.009 mSv (or 108 ± 9 μSv) while it is lowest in the OG area with a value of 0.086 ± 0.002 mSv. These results are not surprising since the EP and OG areas respectively have the highest and lowest absorbed dose rates. The average annual effective dose from all the ten geographical areas of Karibib is 0.095 ± 0.013 mSv (or 95 ± 13 μSv) which is below the maximum permissible annual dose of 1.0 mSv recommended for the public by ICRP [50]. This result implies that the town of Karibib has a normal background radiation.

Table 4.3 Mean absorbed dose rate, annual effective dose, radium equivalent activity and external hazard index in different geographical areas in Karibib. The range of values in each geographical area are given in parenthesis.

Area	*Absorbed dose rate (nGy/h)*	*Annual Effective dose (mSv)*	*Radium Equivalent Activity (Ra_{eq})*	*External Hazard Indices (H_{ex})*
KT	81.8 ± 8.9 (70.7 - 93.9)	0.100 ± 0.011 (0.087 - 0.115)	172.2 ± 18.4 (148.2 - 196.7)	0.47 ± 0.05 (0.40 - 0.53)
NP	73.0 ± 1.4 (70.5 - 74.2)	0.089 ± 0.02 (0.086 - 0.091)	153.3 ± 3.2 (148.6 - 156.9)	0.41 ± 0.01 (0.40 -0.42)
TF	74.9 ± 5.7 (67.6 - 80.7)	0.092 ± 0.007 (0.083 - 0.099)	159.7 ± 11.8 (145.5 - 172.1)	0.44 ± 0.03 (0.39 - 0.46)
HG	76.3 ± 8.3 (67.4 - 84.5)	0.094 ± 0.01 (0.083 - 0.104)	160.3 ± 17.2 (140.4 - 177.9)	0.43 ± 0.05 (0.38 - 0.48)
OG	69.9 ± 1.3 (68.6 - 71.4)	0.086 ± 0.002 (0.084 - 0.088)	147.6 ± 3.9 (143.6 - 153.9)	0.40 ± 0.01 (0.39 - 0.42)
CB	73.9 ± 7.5 (62.5 - 84.2)	0.091 ± 0.009 (0.078 - 0.103)	155.5 ± 16.6 (132.8 - 177.3)	0.42 ± 0.04 (0.36 - 0.48)
TL	78.9 ± 19.6 (67.6 - 110.8)	0.097 ± 0.024 (0.077 - 0.136)	166.7 ± 40.9 (129.7 - 232.9)	0.45 ± 0.11 (0.35 - 0.63)
KH	71.8 ± 18.1 (54.9 - 94.1)	0.088 ± 0.022 (0.067 - 0.115)	149.5 ± 37.9 (114.5 - 196.8)	0.40 ± 0.10 (0.31 - 0.53)
LM	86.8 ± 3.6 (83.6 - 92.6)	0.106 ± 0.004 (0.102 - 0.114)	180.7 ± 7.3 (174.8 - 192.9)	0.49 ± 0.02 (0.47 - 0.52)
EP	88.2 ± 7.3 (79.6 - 97.7)	0.108 ± 0.009 (0.098 - 0.120)	184.1 ± 15.3 (168.0 - 204.8)	0.50 ± 0.04 (0.45 - 0.55)
Average of all samples	**77.6 ± 10.9 (54.9 - 110.8)**	**0.095 ± 0.013 (0.067 - 0.136)**	**163.0 ± 22.6 (114.5 - 232.9)**	**0.44 ± 0.06 (0.31 - 0.63)**

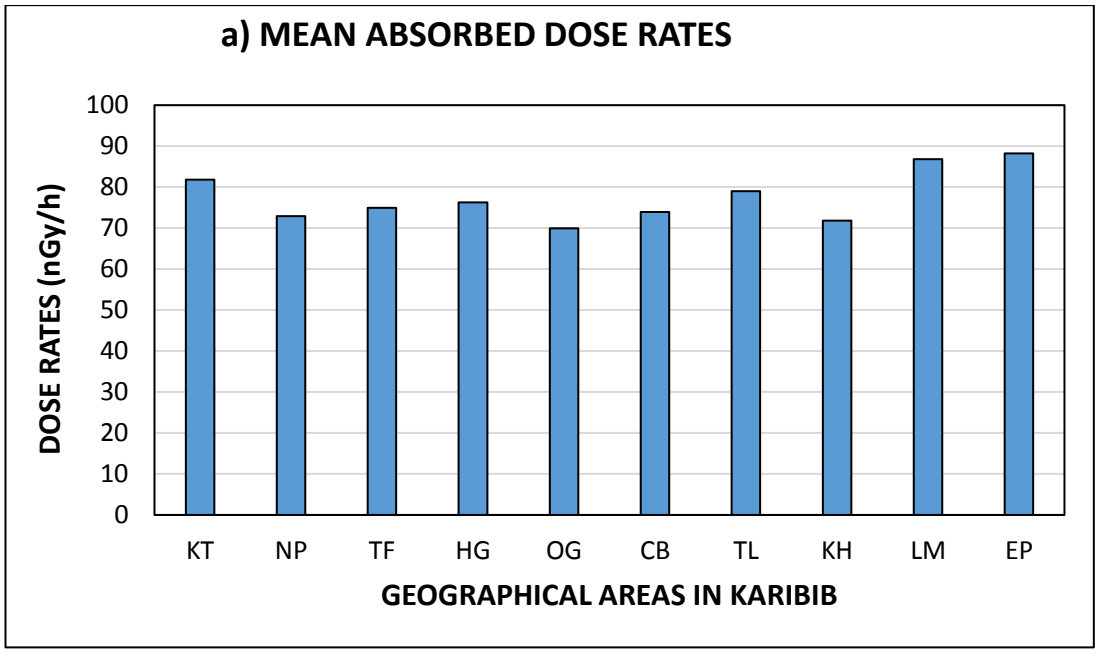

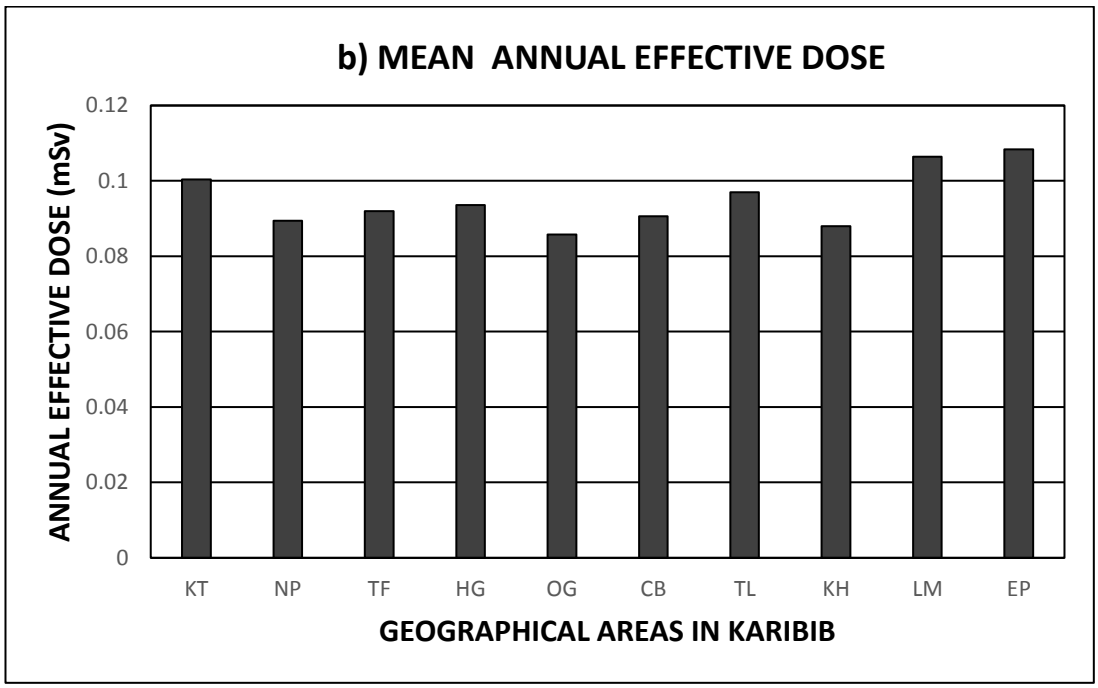

Figure 4.3: The mean absorbed dose rate (a) and the mean annual effective dose (b) in the ten geographical areas of Karibib.

Figure 4.4 shows the frequency distributions of (a) absorbed dose rates and (b) annual effective dose in Karibib. The absorbed dose rates have almost a normal distribution with a positive skewness of 0.5 as could be seen in Figure 4.4(a) and in Table 4.2 (column 5). The absorbed dose rate due to most of the samples is between 60 nGy/h and 96 nGy/h as could be observed in Figure 4.4 (a). Also, only two of the absorbed dose rates are greater than 96 nGy/h while only one absorbed dose rate is less than 60 nGy/h. The most frequently occurring range of absorbed dose rate is 66 to 72 nGy/h. As could be observed in Figure 4.4 (b), the annual effective dose due to most of the soil samples lies between 0.072 and 0.121 mSv. In fact, only one value of annual effective dose is greater than 0.121 mSv while only one value of annual effective dose is less than 0.072 mSv.

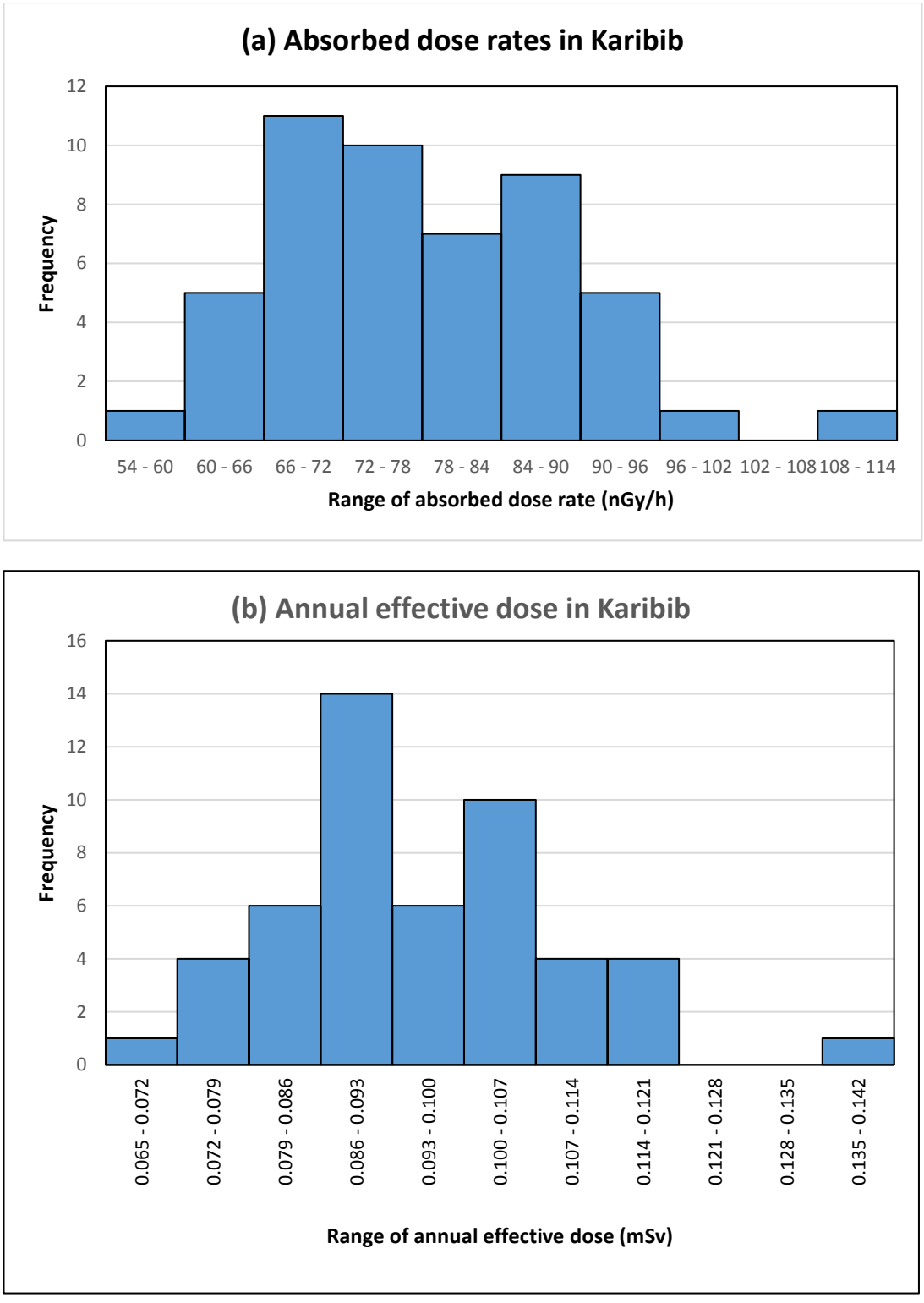

Figure 4.4: Frequency distributions of (a) absorbed dose rates and (b) annual effective dose in Karibib.

4.1.3 Radium equivalent activity and external hazard index in Karibib

The mean Radium equivalent activity and the external hazard index in the ten geographical areas of Karibib are presented in Table 4.3 (columns 4 and 5) and shown in Figure 4.5. As could be seen in Table 4.3 (column 4) and Figure 4.5(a), the Radium equivalent activity is highest in the EP area with an average value of 184.1 ± 15.3 Bq/kg while it is lowest in the OG area with an average value of 147.6 ± 3.9 Bq/kg. The average Radium equivalent activity from all the ten geographical areas in Karibib is 163.0 ± 22.6 Bq/kg. This value is below the recommended maximum of 370 Bq/kg so that radiation hazard is negligible in Karibib [1,14]. Similarly, the highest external hazard index is in the EP area with an average value of 0.50 ± 0.04 while it is lowest in the OG area with an average value of 0.40 ± 0.01 as shown in Figure 4.5 (b). The average external hazard index from all the ten geographical areas is 0.44 ± 0.06. This value is less than unity thus confirming that radiation hazard is negligible in Karibib as observed earlier in section 4.12 [67].

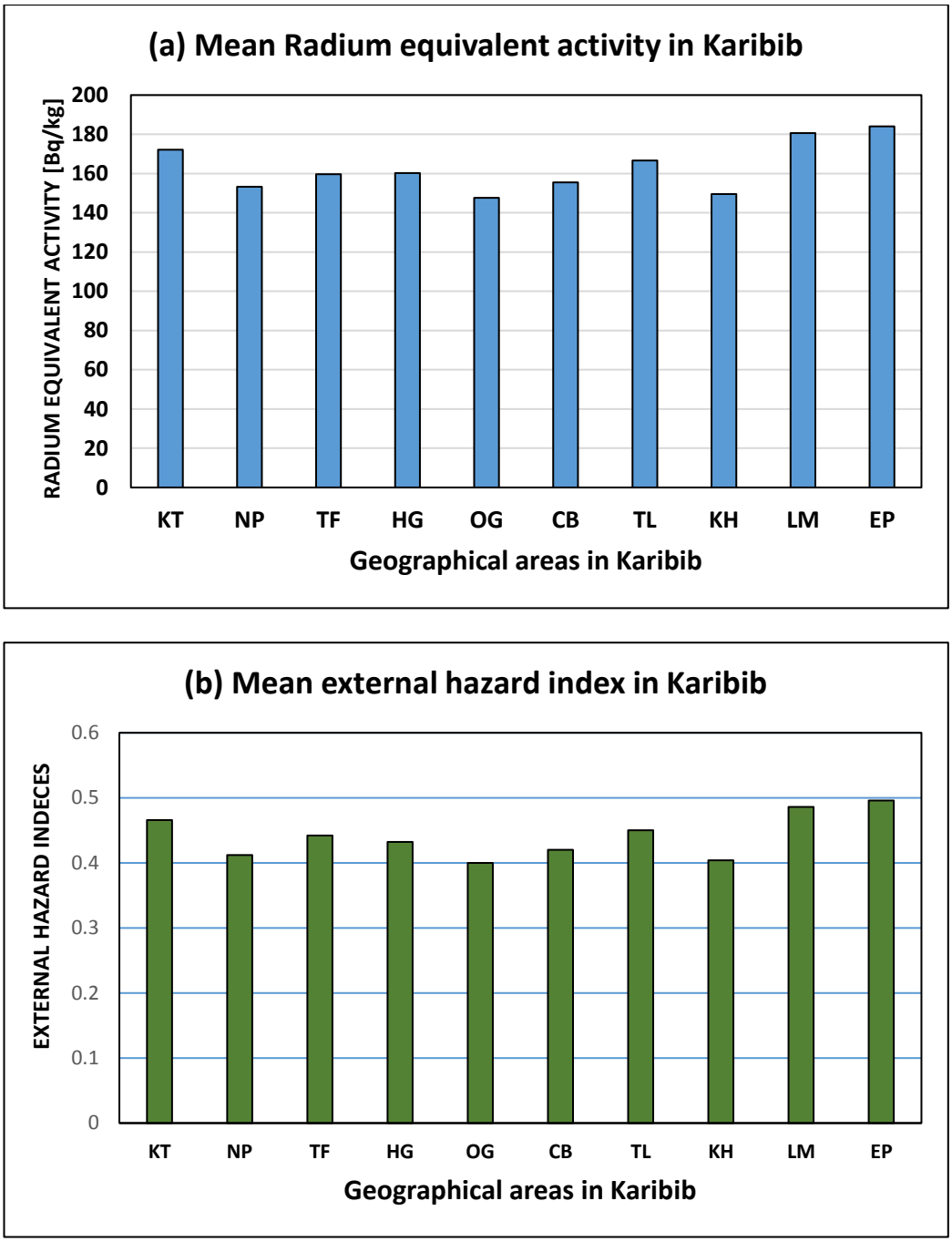

Figure 4.5: The mean Radium equivalent activity (a) and external hazard indices (b) in the ten geographical areas of Karibib.

The frequency distributions of Radium equivalent activity and external hazard index are presented in Table 4.2 (column 7and column 8) and shown in Figure 4.6. As could be observed in Figure 4.6 (a), most of the Radium equivalent activities calculated for the samples are between 125 Bq/kg and 202 Bq/kg. Only two samples have Radium equivalent activity greater than 202 Bq/kg and only one sample has Radium equivalent activity below 125 Bq/kg. Also, the most frequently occurring range of Radium equivalent activity is 147 to 158 Bq/kg. As could be seen in figure 4.6 (b), most of the calculated external hazard indices are between 0.39 and 0.54. Only two of the external hazard indices are above 0.54 while seven external hazard indices are below 0.39. The most frequently occurring range of external hazard index is 0.39 to 0.42. These relatively low values of H_{ex} again confirm that radiation hazard is negligible in Karibib.

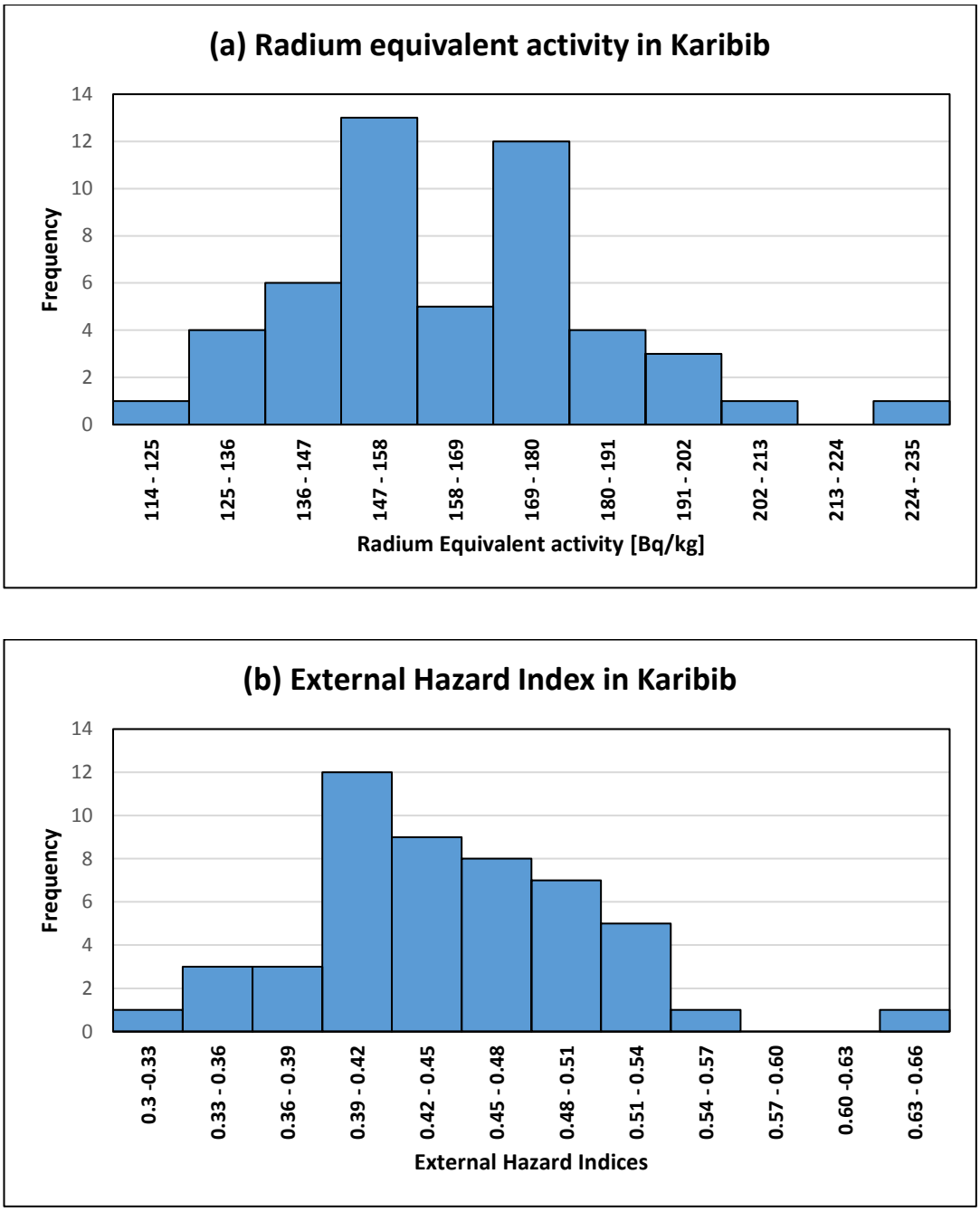

Figure 4.6: Frequency distribution of (a) Radium Equivalent activity and (b) External Hazard Index in Karibib.

4.2 Natural Radioactivity in Okahandja.

4.2.1 Radionuclide concentration in Okahandja

The mean activity concentrations of ^{238}U, ^{232}Th and ^{40}K in the soil samples collected from each of the ten geographical areas in Okahandja are summarized in Table 4.4 and shown in Figure 4.7. Also, the concentrations of ^{238}U, ^{232}Th and ^{40}K measured in each of the 50 soil samples are shown in Appendix 2, and the statistics of the results obtained in the measurements are shown in Table 4.5. As could be seen in the Table and Figure, the activity concentration of ^{238}U is highest in the FE area with an average of 50.6 ± 3.8 Bq/kg (and varies from 44.7 to 54.8 Bq/kg) but lowest in the VO area with an average of 31.3 ± 5.8 Bq/kg (and varies from 25.9 to 40.9 Bq/kg). The difference between the minimum and maximum (or range) of activity concentrations of ^{238}U in all the samples is 45.8 Bq/kg as could be seen in Table 4.5 (column 2). The average activity concentration of ^{238}U from all the soil samples collected across the town of Okahandja is 40.9 ± 8.6 Bq/kg as shown in Table 4.4 (column 2). This value is greater than the worldwide average activity concentration of 35 Bq/kg [1]. Similarly, the activity concentration of ^{232}Th is highest in the OP area with an average value of 72.2 ± 14.1 Bq/kg (and varies from 55.7 to 88.5 Bq/kg) but, interestingly, it is lowest in the VO area (as in the case of ^{238}U) with an average value of 44.4 ± 15.2 Bq/kg (and varies from 34.6 to 71.2 Bq/kg) as shown in Table 4.4 (column 3). The difference between the minimum and maximum (or range) of activity concentrations of ^{232}Th is 104.3 Bq/kg as shown in Table 4.5 (column 3). The average activity concentration of ^{232}Th from all the soil samples collected across the town of Okahandja is 57.9 ± 19.4 Bq/kg as shown in Table 4.4. This value is greater than the worldwide average activity concentration of ^{232}Th which is 30 Bq/kg [1]. The activity concentration of ^{40}K is highest in the FE area with an average value of 656.8 Bq/kg ± 55.6 (and varies from

579.0 to 726.3 Bq/kg) and lowest in the NP area with an average value of 348.4 ± 33.5 Bq/kg (and varies from 307.4 to 382.6 Bq/kg) as shown in Table 4.4 (column 4) and Figure 4.7. In fact, the average value of ^{40}K in the FE area is almost double that in the NP area. As could be seen in Table 4.4 (column 4) the average activity concentration of ^{40}K from all the soil samples is 562.4 ± 125.4. This average activity concentration of ^{40}K is higher than the worldwide average activity concentration of 400 Bq/kg [1]. It is apparent from Figure 4.7 that the activity concentration of ^{40}K is much larger than that of ^{238}U and ^{232}Th while the activity concentration of ^{232}Th is greater than that of ^{238}U across all the ten geographical areas of Okahandja. It therefore follows that, among the three primordial radionuclides, ^{40}K has the highest activity concentration in Okahandja while ^{238}U has the lowest activity concentration in the town.

Table 4.4 Average activity concentration of ^{238}U, ^{232}Th and ^{40}K in different geographical areas of Okahandja. The range of values is given in parenthesis.

Area	*Radionuclide Concentrations [Bq/kg]*		
	^{238}U	^{232}Th	^{40}K
VO	31.3 ± 5.8 (25.9 - 40.9)	44.4 ± 15.2 (34.6 - 71.2)	628.6 ± 167.2 (445.3 - 857.9)
AE	38.7 ± 3.5 (35.3 -43.2)	54.9 ± 3.4 (46.2 - 63.7)	535.5 ± 42.5 (470.5 - 573.7)
BE	43.4 ± 5.1 (35.5 - 48.4)	58.7 ± 20.6 (46.3 - 95.3)	593.4 ± 150.9 (460.5 - 815.8)
NP	34.7 ± 2.1 (29.7 - 40.0)	47.6 ± 7.5 (39.1 - 57.1)	348.4 ± 33.5 (307.4 - 382.6)
CE	37.3 ± 6.3 (30.2 - 44.7)	51.7 ± 8.7 (41.9 - 63.2)	523.4 ± 92.1 (420.0 - 657.9)
DE	40.8 ± 7.5 (32.0 - 47.3)	51.8 ± 11.2 (37.9 - 63.4)	526.5 ± 37.2 (474.2 - 573.7)
FE	50.6± 3.8 (44.7 - 54.8)	58.4 ± 13.3 (46.8 - 72.9)	656.8 ± 55.6 (579.0 - 726.3)
GE	50.1 ± 12.5 (41.0 - 71.7)	85.3 ± 38.6 (38.5 - 138.8)	651.2 ± 120.0 (482.1 - 768.4)
OP	44.6 ± 8.5 (32.6 - 51.0)	72.2 ± 14.1 (55.7 - 88.5)	635.3 ± 78.5 (513.2 - 726.3)
NC	37.8 ± 6.7 (29.3 - 44.2)	54.2 ± 8.8 (42.9 – 64.0)	524.7 ± 87.4 (417.9 - 636.8)
Average of all samples	**40.9 ± 8.6 (25.9 - 71.7)**	**57.9 ± 19.4 (34.6 - 138.8)**	**562.4 ± 125.4 (307.4 - 857.9)**

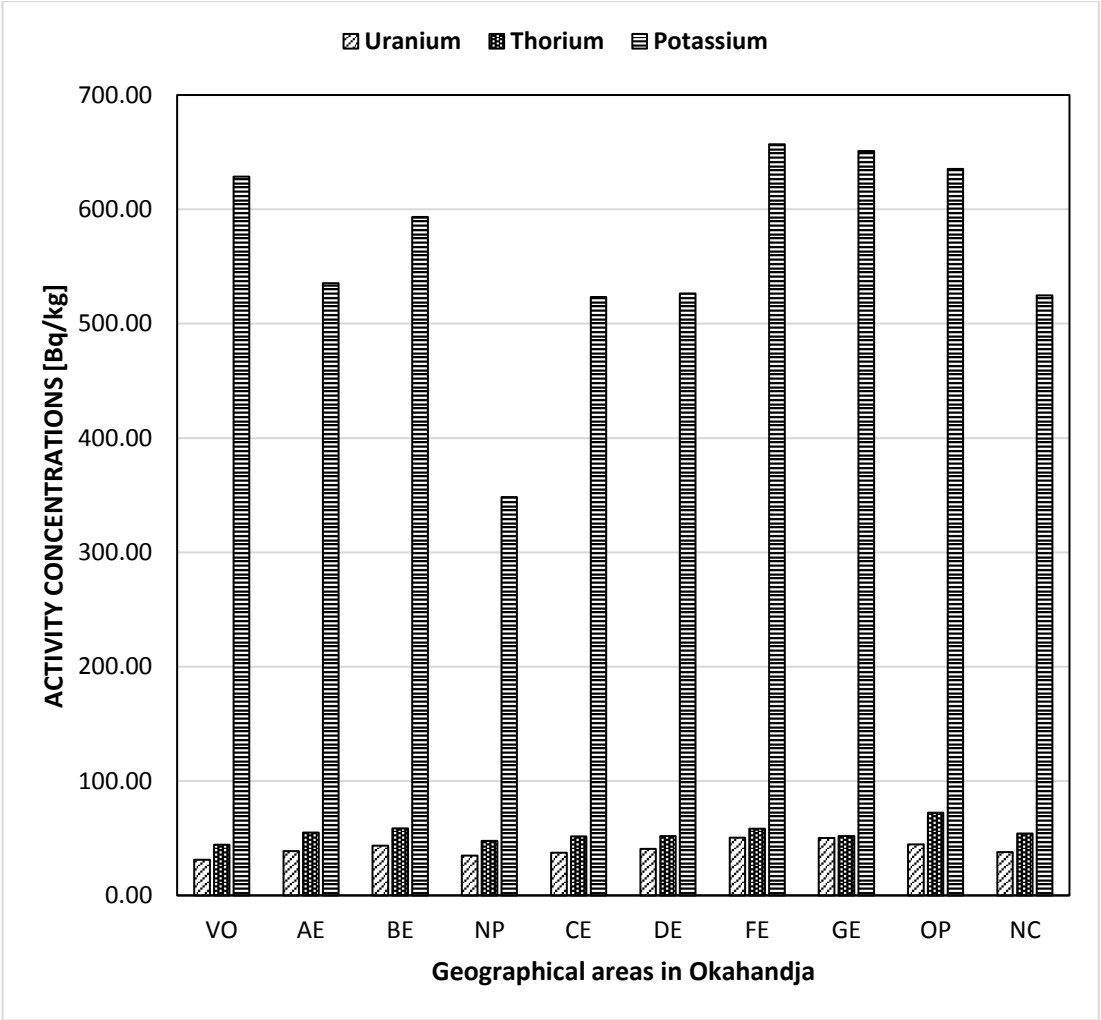

Figure 4.7: The mean activity concentrations of ^{238}U, ^{232}Th, and ^{40}K in the ten geographical areas of Okahandja.

Table 4.5 Statistics of results obtained in the measurement of radioactivity in the soils of Okahandja.

Descriptive Statistics	*^{238}U conc (Bq/kg)*	*^{232}Th conc (Bq/kg)*	*^{40}K conc (Bq/kg)*	*Absorbed Dose rate (nGy/h)*	*Annual Effective Dose (mSv)*	*Radium Equivalent Activity (Raeq) (Bq/kg)*	*External Hazard Index (Hex)*
Mean	40.9	57.9	562.4	77.3	0.095	167.1	0.5
Standard Error	1.2	2.7	17.7	2.5	0.003	5.7	0.0
Median	41.3	53.4	552.6	75.8	0.093	163.7	0.4
Standard Deviation	8.6	19.4	125.4	18.0	0.022	40.1	0.1
Kurtosis	1.7	5.4	-0.3	4.0	3.885	4.4	4.3
Skewness	0.8	1.9	0.2	1.5	1.513	1.6	1.6
Range	45.8	104.3	550.5	97.0	0.119	218.5	0.6
Minimum	25.9	34.6	307.4	51.8	0.063	110.5	0.3
Maximum	71.7	138.8	857.9	148.8	0.182	329.0	0.9
No of samples	50	50	50	50	50	50	50

Figure 4.8 shows the frequency distributions of activity concentrations of (a) ^{238}U, (b) ^{232}Th and (c) ^{40}K in the 50 soil samples collected across Okahandja. As could be observed in Table 4.5 (column 2) and in Figure 4.8 (a), the activity concentrations of ^{238}U in the soil samples have a frequency curve with Skewness of 0.8 and kurtosis of 1.7. Also, the activity concentration of ^{238}U in most of the soil samples is between 25 Bq/kg and 55 Bq/kg. In fact, only two of the 50 samples have an activity concentration greater than 55 Bq/kg. The most frequently occurring range of activity concentrations of ^{238}U is 45 Bq/kg to 50 Bq/kg. In the case of ^{232}Th, the activity concentrations of ^{232}Th in the soil samples have a frequency distribution with a skewness of 1.9 and a kurtosis of 5.4 as could be seen in Table 4.5 (column 3) and Figure 4.8 (b). Kurtosis is the degree of peakedness of a distribution, usually taken relative to a normal distribution [68]. A normal distribution has kurtosis of 3 it therefore means Figure 4.8 has a distribution that is more peaked than a normal distribution [68]. Also, the activity concentration of ^{232}Th in most of the soil samples is between 30 Bq/kg and 90 Bq/kg. Only three of the 50 soil samples have activity concentrations of ^{232}Th greater than 90

Bq/kg as shown in Figure 4.8 (b). The most frequently occurring range of activity concentrations of ^{232}Th is 40 Bq/kg to 50 Bq/kg. As could be observed in Table 4.5 (column 4) and Figure 4.8 (c), the activity concentrations of ^{40}K have almost a normal distribution with a Skewness of 0.2 and a negative kurtosis of 0.3. Also, the concentrations of ^{40}K in most of the soil samples are between 370 Bq/kg and 790 Bq/kg. In fact, only two samples have activity concentrations greater than 790 Bq/kg while only three samples have activity concentrations less than 370 Bq/kg. The most frequently occurring range of activity concentrations of ^{40}K is 510 Bq/kg to 580 Bq/kg.

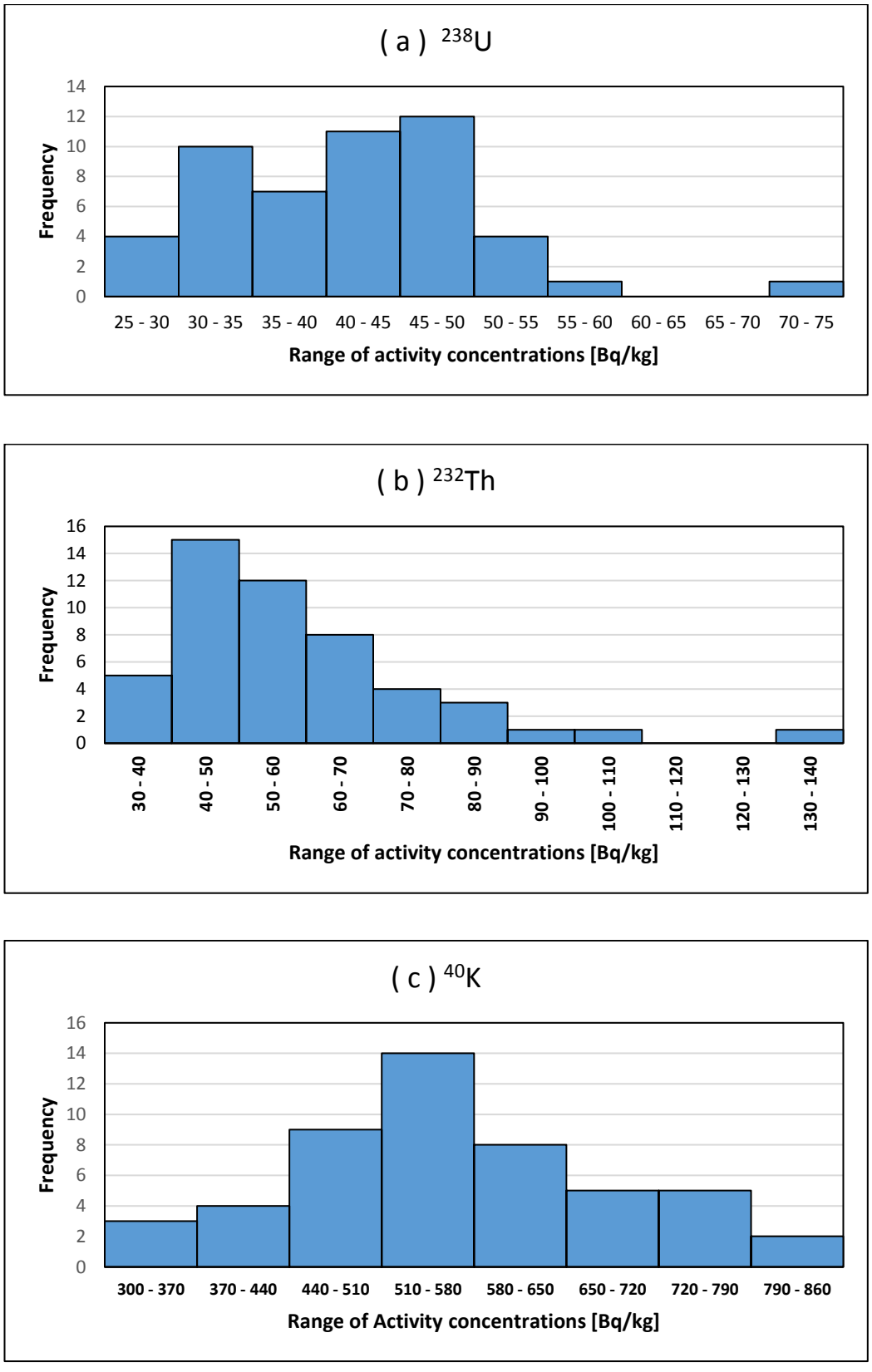

Figure 4.8 Frequency distributions of the activity concentrations of radionuclides in the soil samples of Okahandja. (a) ^{238}U, (b) ^{232}Th, and (c) ^{40}K

4.2.2 Absorbed dose rate and annual effective dose in Okahandja

The mean absorbed dose rates in air and the subsequent mean annual effective dose in the ten geographical areas of Okahandja are presented in Table 4.6 and shown in Figure 4.9. As could be observed in column 2 of Table 4.6 and Figure 4.9 (a), the mean absorbed dose rate is highest in the GE area with an average value of 101.8 ± 32.7 nGy/h while it is lowest in the NP area with an average value of 59.3 ± 6.1 nGy/h. The average absorbed dose rate from all the ten geographical areas is 77.3 ± 18.0 nGy/h. This value is higher than the reported worldwide average of 51 nGy/h [1,14]. Similarly, the corresponding mean annual effective dose is highest in the GE area with an average value of 0.125 ± 0.04 mSv (or 125 ± 40 μSv) while it is lowest in the NP area with an average value of 0.073 ± 0.007 mSv (or 73 ± 7 μSv) as could be observed in column 3 of Table 4.6 and Figure 4.9 (b). These results are not surprising since the GE and NP areas respectively have the highest and lowest absorbed dose rates. The average annual effective dose from all the ten geographical areas is 0.095 ± 0.022 mSv (or 95 ± 22 μSv) as could be seen in column 2 (bottom line) of Table 4.6. This average value is far below the maximum permissible annual dose of 1.0 mSv mentioned earlier in section 4.1.2 [50]. This result implies that the town of Okahandja has a normal background radiation.

Table 4.6 Mean absorbed dose rate, annual effective dose, radium equivalent activity and external hazard index in Okahandja.

Area	*Absorbed dose rate (nGy/h)*	*Annual Effective dose (mSv)*	*Radium Equivalent Activity (Ra_{eq})Bq/kg*	*External Hazard Index (H_{ex})*
VO	67.5± 15.3 (51.8 -91.9)	0.083 ± 0.011 (0.063 - 0.113)	143.2 ± 33.3 (110.5- 198.2)	0.39 ± 0.09 (0.30 - 0.54)
AE	73.4± 7.3 (63.8 - 81.2)	0.09 0 ± 0.009 (0.078 - 0.100)	158.5 ± 16.2 (137.6 - 176.4)	0.44 ± 0.53 (0.37 -0.48)
BE	80.3 ± 16.7 (66.6 - 108.2)	0.098 ± 0.021 (0.082 - 0.133)	173.1± 37.5 (142.7 - 237.0)	0.47± 0.10 (0.39 - 0.64)
NP	59.3 ± 6.1 (52.2 - 66.9)	0.073 ± 0.007 (0.064 -0.082)	129.7 ± 13.8 (113.1 - 146.8)	0.35 ± 0.04 (0.31 - 0.40)
CE	70.3 ± 11.4 (58.4 - 86.3)	0.086 ± 0.014 (0.072 - 0.106)	161.0 ± 24.5 (126.3 - 185.8)	0.41± 0.07 (0.34 - 0.50)
DE	72.2 ± 10.3 (60.0 - 80.0)	0.089 ± 0.03 (0.074 - 0.098)	155.5 ± 23.6 (127.7 - 173.9)	0.42 ± 0.06 (0.34 - 0.47)
FE	86.0 ± 7.6 (79.2 - 94.8)	0.105 ± 0.009 (0.097 - 0.116)	184.6 ± 18.5 (168.5 - 205.8)	0.50 ± 0.05 (0.46 - 0.56)
GE	101.8 ± 32.7 (67.2 - 148.8)	0.125 ± 0.04 (0.082 - 0.182)	222.2 ± 74.1 (142.3 - 329.0)	0.60 ± 0.2 (0.38 - 0.89)
OP	90.7 ± 13.5 (72.9 - 104.9)	0.111 ± 0.016 (0.089 - 0.129)	196.8 ± 29.7 (157.8- 229.1)	0.53 ± 0.08 (0.43 - 0.62)
NC	72.1 ± 8.8 (56.9 - 79.1)	0.088 ± 0.011 (0.07 - 0.097)	155.8± 19.5 (122.9 - 172.2)	0.42 ± 0.05 (0.33 - 0.47)
Ave all samples	**77.3 ± 18.0 (51.8 - 148.8)**	**0.095 ± 0.022 (0.063 - 0.182)**	**167.1 ± 40.1 (110.5 - 329.0)**	**0.45 ± 0.11 (0.3 - 0.9)**

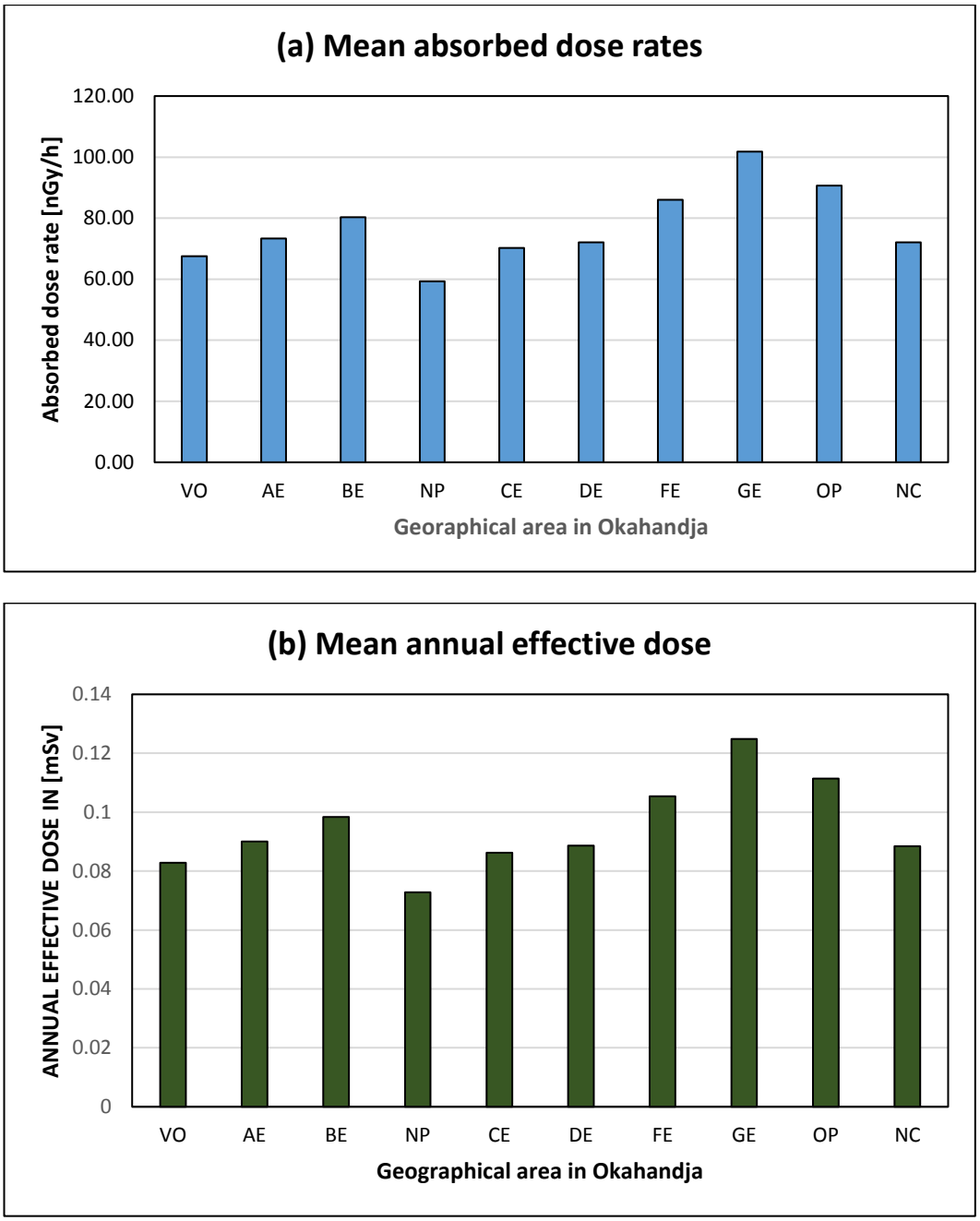

Figure 4.9: The mean absorbed dose rate (a) and the mean effective dose rate (b) in the ten geographical areas of Okahandja.

Figure 4.10 shows the frequency distributions of (a) absorbed dose rates and (b) annual effective dose in all the ten geographical areas of Okahandja. The absorbed dose rates have a frequency distribution with a skewness of 1.5 and a kurtosis of 4.0 as could be seen in Table 4.5 (column 5) and Figure 4.10(a). Most of the absorbed dose rates calculated for the samples are between 50 nGy/h and 110 nGy/h as shown in Figure 4.10 (a). Only two of the absorbed dose rates are greater than 110 nGy/h, and the most frequently occurring range of absorbed dose rate is 70 nGy/h to 80 nGy/h. Also, most of the corresponding effective dose are between 0.06 mSv and 0.132 mSv as shown in Figure 4.10 (b). In fact, only three values of the annual effective doses are greater than 0.132 mSv.

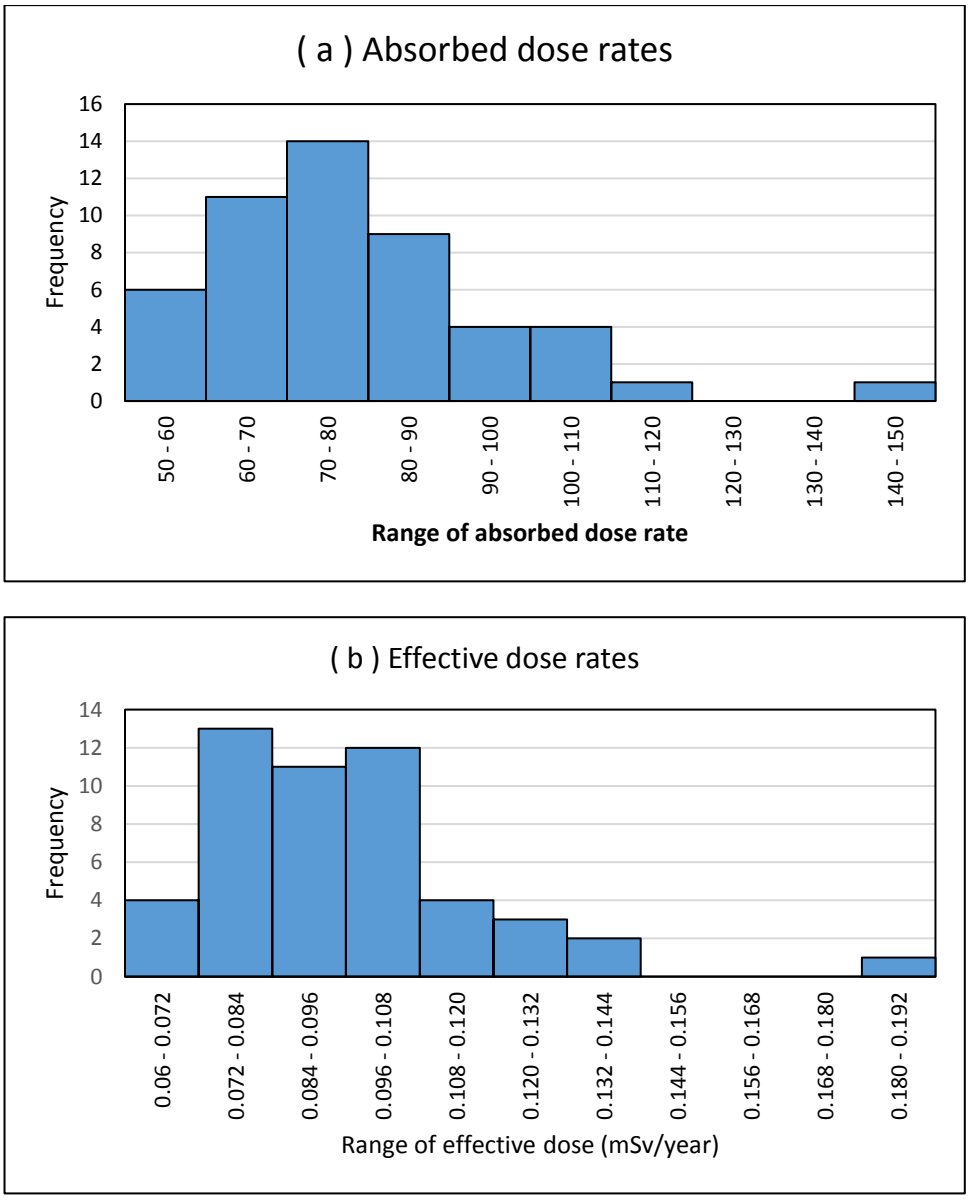

Figure 4.10: Frequency distribution of (a) absorbed dose rates and (b) effective dose rates in Okahandja.

4.2.3 Radium equivalent activity and external hazard indices in Okahandja

The mean Radium equivalent activity (Ra_{eq}) and the mean external hazard (H_{ex}) indices in the ten geographical areas in Okahandja are presented in Table 4.6 (columns 4 and 5) and shown in Figure 4.11. As could be observed in Table 4.6 (column 4) and Figure 4.11 (a), the Radium equivalent activity is highest in the GE area with an average value of 222.2 ± 74.1 Bq/kg while it is lowest in the NP area with an average value of 129.7 ± 13.8 Bq/kg. The average Radium equivalent activity from all the ten geographical areas is 167.1 ± 40.2 Bq/kg. This value is below the recommended maximum of 370 Bq/kg stated earlier in section 4.1.3 [1,14]. Similarly, the highest external hazard index is in the GE area with an average value of 0.60 ± 0.2 while it is lowest in the NP area with an average value of 0.35 ± 0.04 as could be observed in Table 4.6 (column 5) and Figure 4.11 (b). The average external hazard index from all the ten geographical areas is 0.45 ± 0.11 which is far less than unity [67]. The relatively low average values of Ra_{eq} and H_{ex} confirm that the town of Okahandja has a normal background radiation.

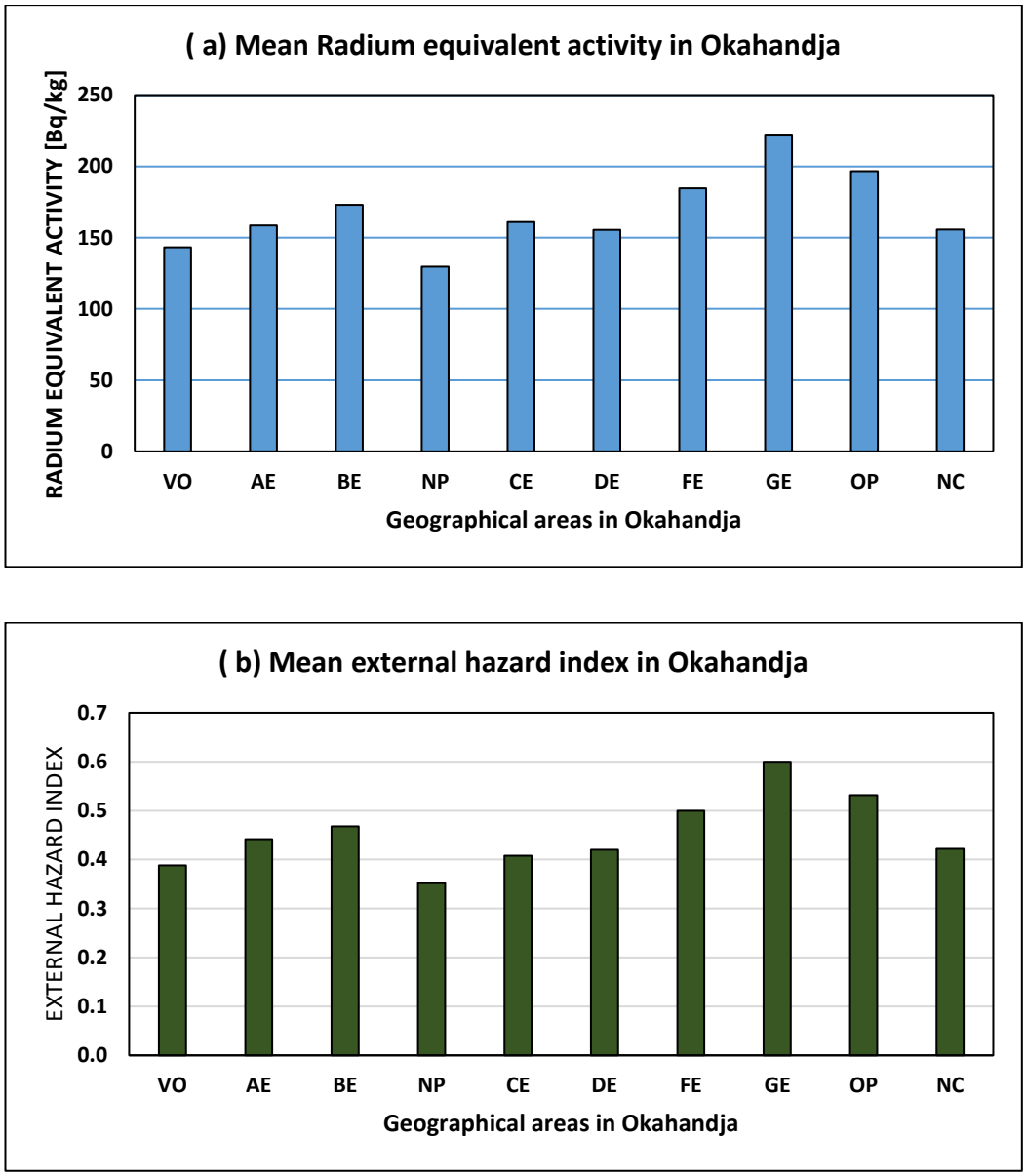

Figure 4.11: The mean Radium equivalent activity (a) and external hazard indices (b) in the ten geographical areas of Okahandja.

The frequency distributions of Radium equivalent activities and external hazard indices are presented in Table 4.5 (columns 7 and 8) and shown in Figure 4.12. As could be observed in Figure 4.12 (a), most of the Radium equivalent activities calculated for the samples are between 110 Bq/kg and 230 Bq/kg and only three of the activities are greater than 230 Bq/kg. Similarly, most of the calculated external hazard indices are between 0.3 and 0.6 as could be seen in Figure 4.12 (b). Only four of the

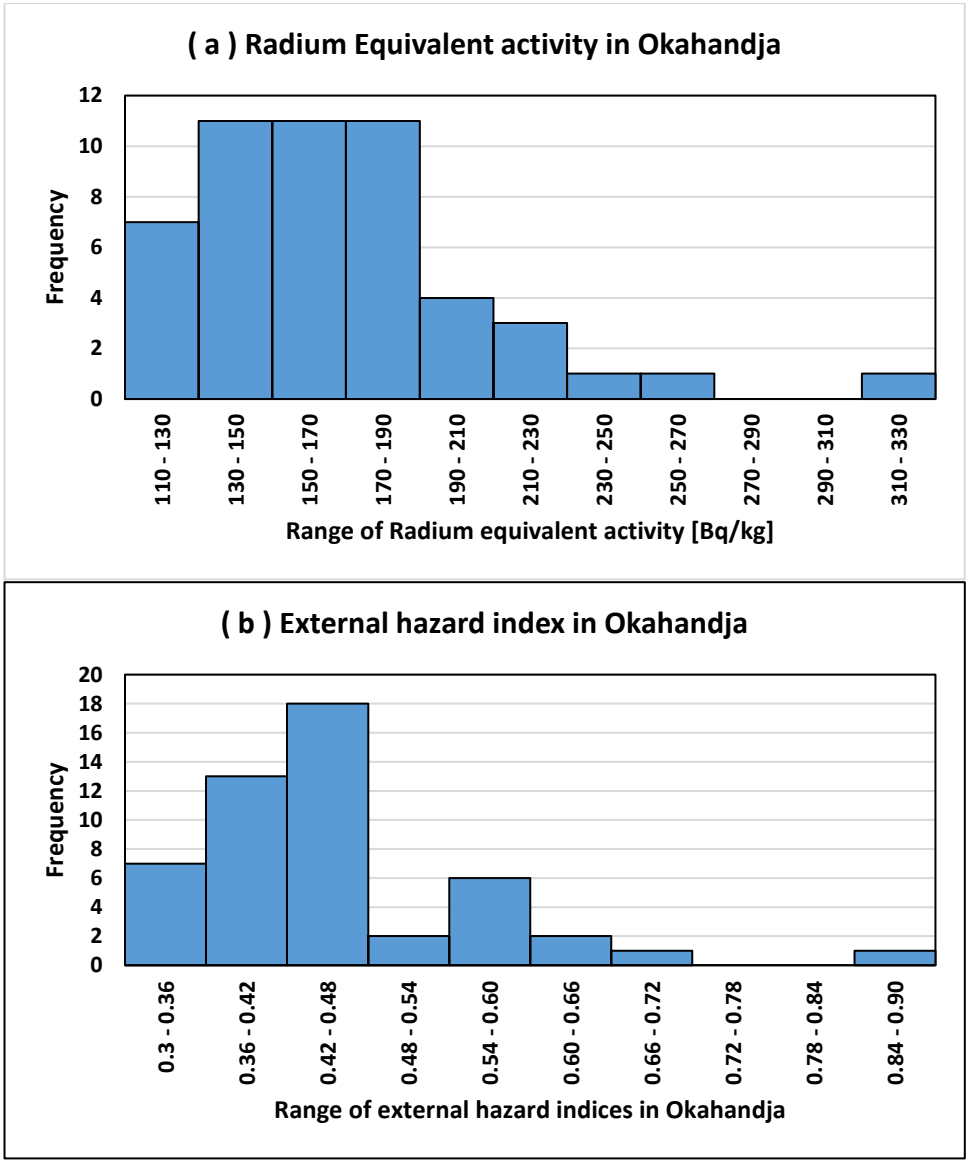

Figure 4.12: Frequency distribution of (a) Radium equivalent activity and (b) external hazard index in Okahandja.

external hazard indices are above 0.6 and the most frequently occurring range of external hazard index is 0.42 and 0.48. These relatively low values again show that the radiation hazard in the town of Okahandja is negligible.

4.3 Comparison of natural radioactivity in Karibib and Okahandja

4.3.1 Radionuclide Concentrations

The mean activity concentrations of ^{238}U, ^{232}Th and ^{40}K in the soil samples from the towns of Karibib and Okahandja are summarised in Table 4.7 and shown in Figure 4.13. As could be seen in the Table and Figure, the average activity concentration of ^{238}U is higher in Okahandja (with a value of 40.9 ± 8.6 Bq/kg) than in Karibib (with a value of 29.4 ± 5.8 Bq/kg). In fact, the activity concentration of ^{238}U in Okahandja is 1.4 times that of Karibib. Also, the average activity concentration of ^{232}Th is higher in Okahandja (with a value of 57.9 ± 19.4 Bq/kg) than in Karibib (with a value of 49.0 ± 8.6 Bq/kg). In contrast to the higher concentrations of ^{238}U and ^{232}Th in Okahandja, the average concentration of ^{40}K is much higher in Karibib (with a value of 824.3 ± 153.5 Bq/kg) than in Okahandja (with a value of 562.4 ± 125.4 Bq/kg). Also, the activity concentration of ^{40}K is much higher than those of ^{238}U and ^{232}Th in both towns. Similarly in both towns, ^{238}U has the lowest activity concentration among the three primordial radionuclides.

Table 4.7 Average radionuclide concentrations in the towns of Karibib and Okahandja. The range of values are given in parenthesis.

Town	Radionuclide concentrations [Bq/kg]		
	^{238}U	^{232}Th	^{40}K
Karibib	29.4 ± 5.8 (14.3 – 43.1)	49.0 ± 8.6 (29.0 – 69.9)	824.3 ± 153.5 (505.3 – 1168.4)
Okahandja	40.9 ± 8.6 (25.9 - 71.7)	57.9 ± 19.4 (34.6 - 138.8)	562.4 ± 125.4 (307.4 - 857.9)

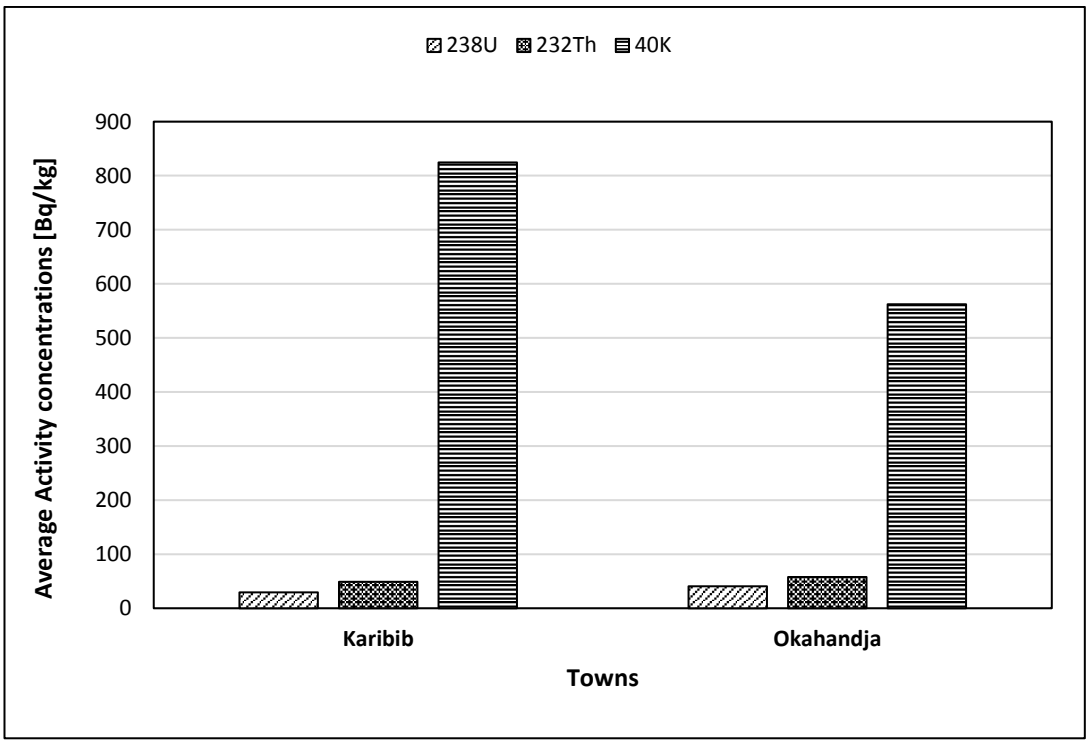

Figure 4.13 Comparison of the mean activity concentrations of ^{238}U, ^{232}Th and ^{40}K in the towns of Karibib and Okahandja.

4.3.2 Absorbed dose rate and annual effective dose.

A comparison of the average absorbed dose rate and average annual effective dose in Karibib and Okahandja are shown in Figure 4.14. As could be seen in Figure 4.14 (a), the absorbed dose rate in Karibib is slightly higher than that of Okahandja. In fact, the difference between the two values is only 0.3 nGy/h. The subsequent effective dose rates in the two towns are the same with an average value of 0.095 mSv/year as shown in Figure 4.14 (b). This result is not surprising since the average absorbed dose rates in the two towns are just about equal. The average effective dose rates in the towns are both below the recommended limit of 1.0 mSv thus showing that there is negligible radiation hazard in the towns.

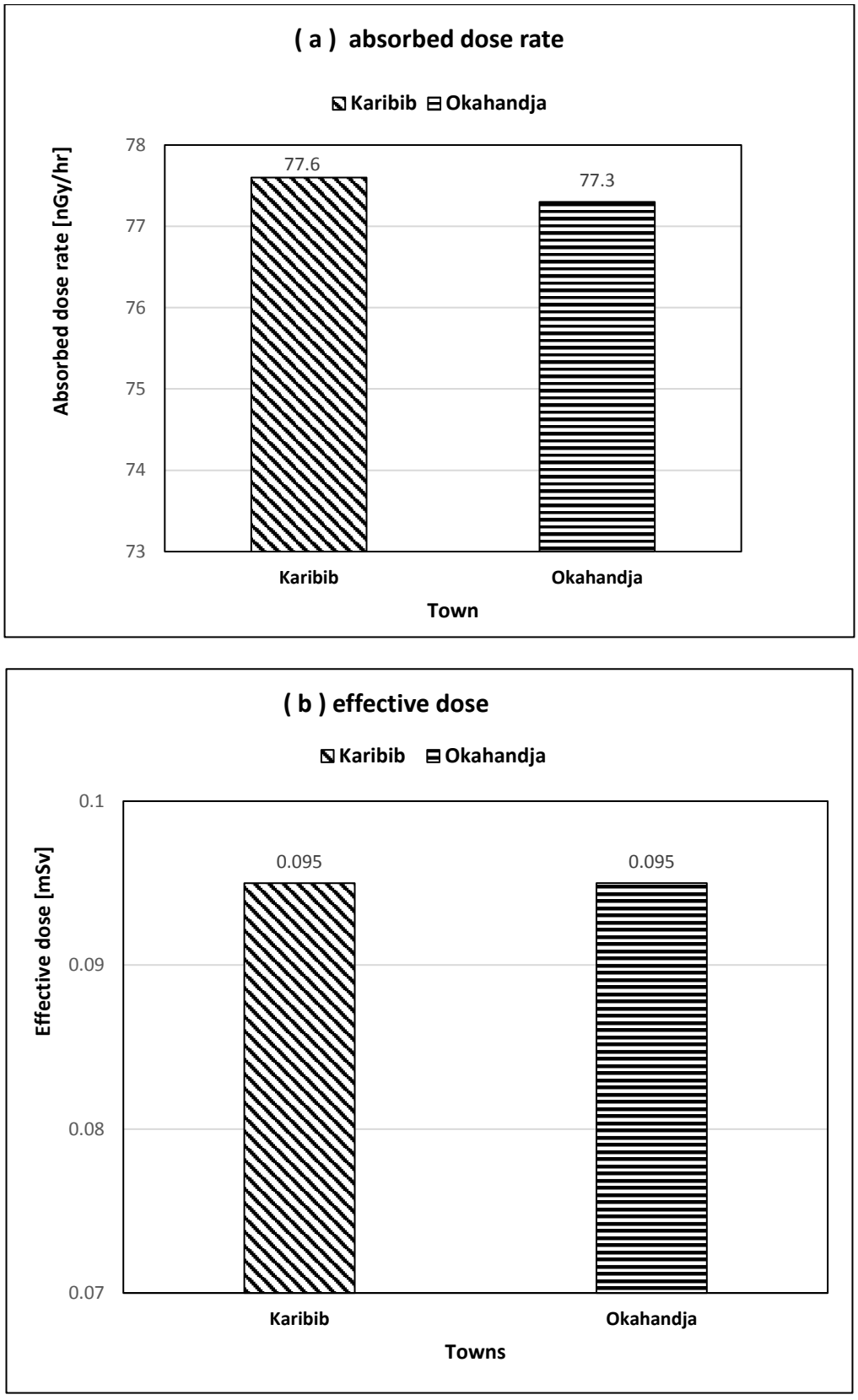

Figure 4.14 Comparison of (a) absorbed dose rate and (b) annual effective dose in the towns of Karibib and Okahandja.

4.3.3 Radium equivalent activity and external hazard index comparison

The average Radium equivalent activity and external hazard index in the towns of Karibib and Okahandja are shown in Figure 4.15. As could be observed in Figure 4.15 (a), the Radium equivalent activity is slightly higher in the town of Okahandja than Karibib. The difference in the values of the Radium equivalent activity in the towns is only 4.1 Bq/kg. Also, the average external hazard indices in the two towns (0.44 in Karibib and 0.45 in Okahandja) are almost the same as shown in Figure 4.15 (b). This result confirms that the natural radioactivity in the two towns are not much different from each other.

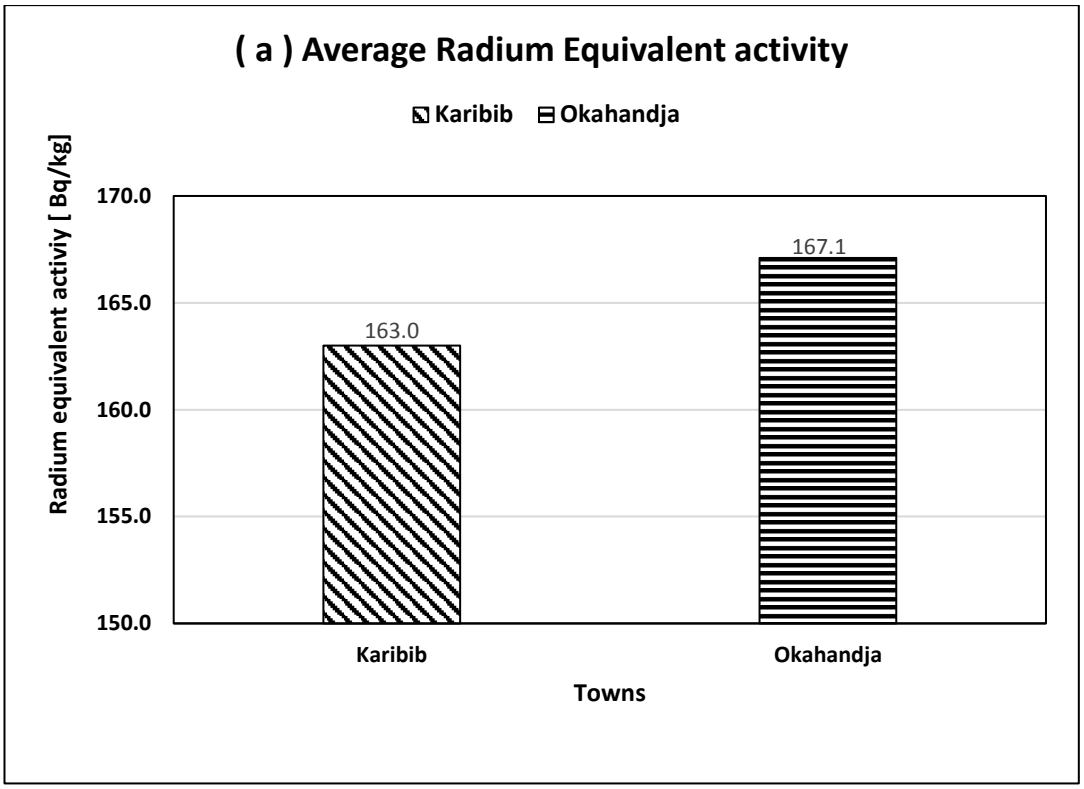

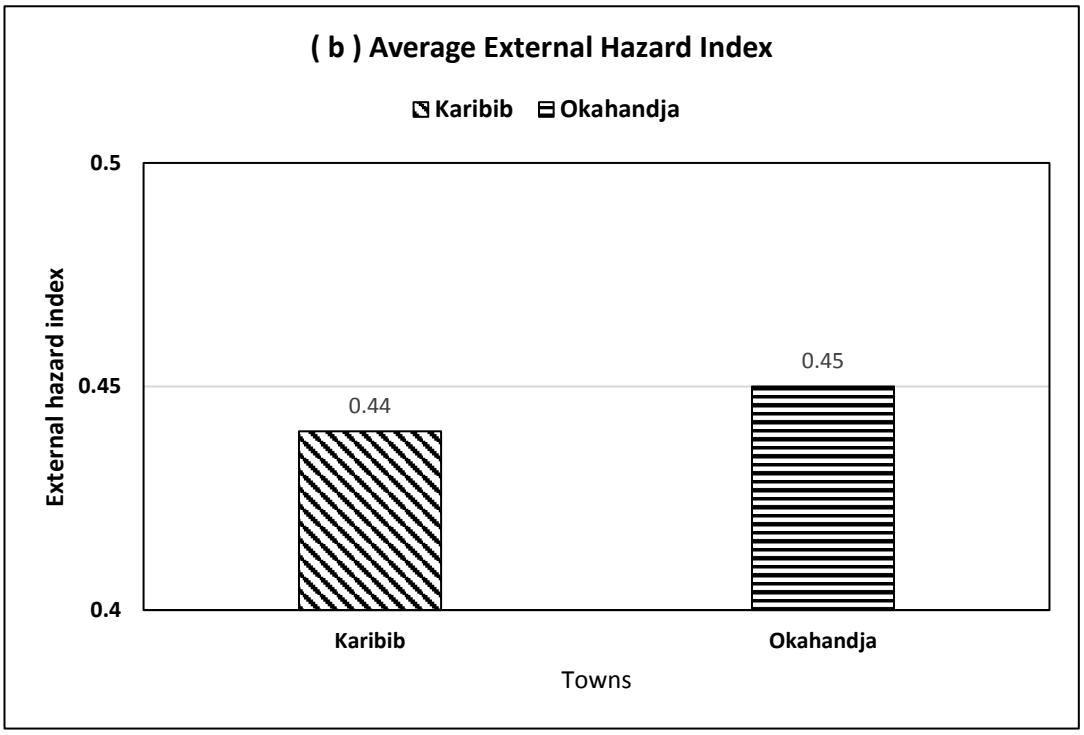

Figure 4.15 Comparison of (a) Radium equivalent activity and (b) external hazard indices in the towns of Karibib and Okahandja.

4.4 Comparison of the activity concentrations of ^{40}K in Karibib and Okahandja with those measured in neighbouring towns.

A comparison of the mean activity concentrations of ^{40}K in the soils of Karibib and Okahandja with those determined by other researchers in the soils of four major towns in the same part of Namibia is shown in Figure 4.16 [14]. The four towns are Walvis Bay, Swakopmund, Wlotzkasbaken and Usakos. With the exception of one town (Wlotzkasbaken) all the six towns are on the popular B2 road and next to each other in western Namibia. These towns are at different latitudes, and earlier studies have shown an increase in the average activity concentration of ^{40}K with decreasing latitude in four towns (Walvis Bay, Swakopmund, Wlotzkasbaken and Usakos) as could be observed in Figure 4.16 (a) to (d) [14]. However, the increase in the activity concentration of ^{40}K with decreasing latitude does not extend to Karibib and Okahandja as could be observed in Figure 4.16 (e) and (f). As could be seen in the figure, the average activity concentration of ^{40}K increases from one town to another (decreasing latitude) until it is maximum at Usakos, and it is subsequently smaller in Okahandja and Karibib. It therefore follows that the observed increase in the average activity concentration of ^{40}K with decreasing latitude in some towns in western Namibia cannot be generalised to all the towns in the area.

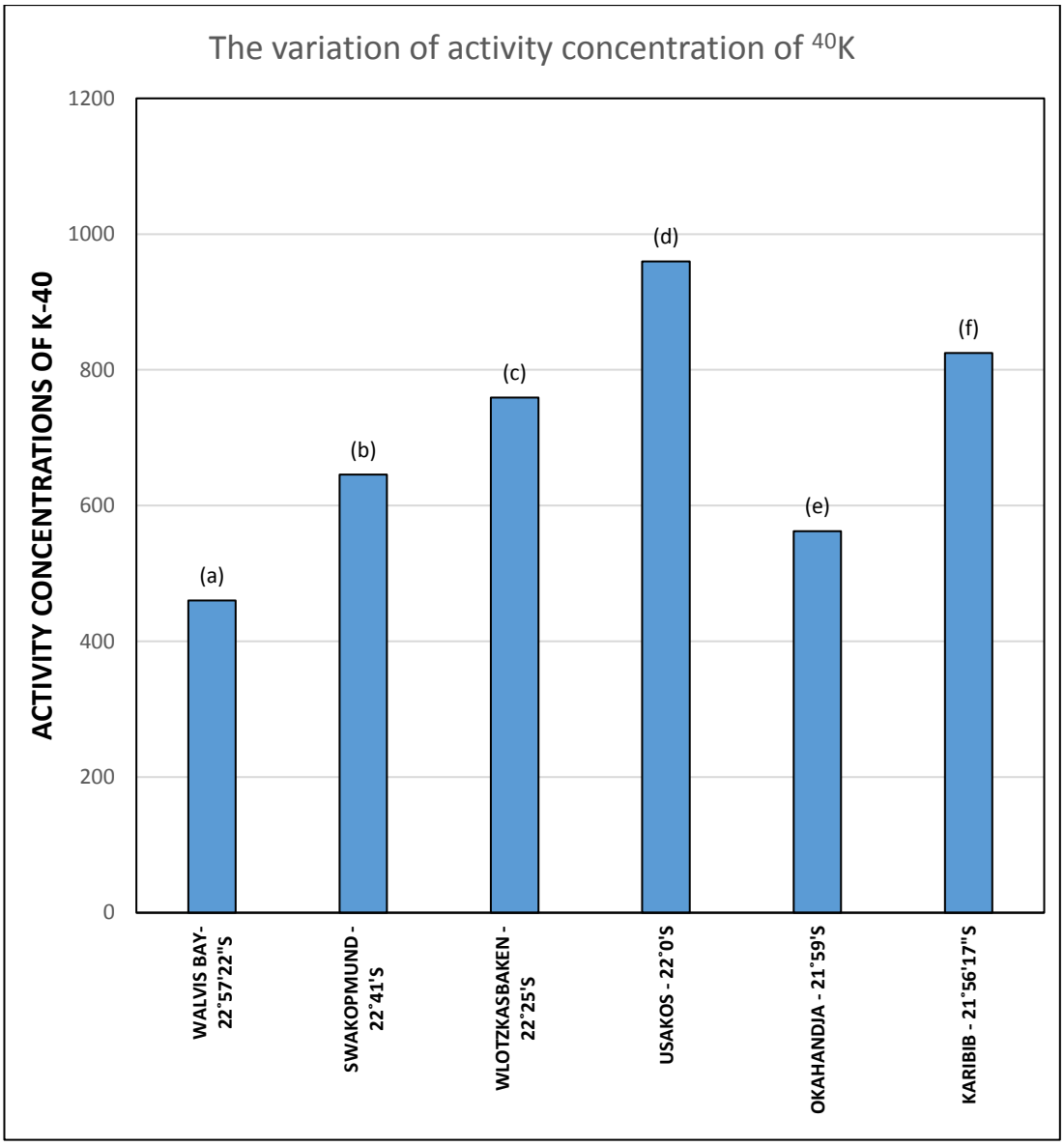

Figure 4.16 Variation of the activity concentration of ^{40}K with decreasing lattitude.

CHAPTER 5

5. CONCLUSION AND RECOMMENDATIONS

5.1 Conclusion

Gamma ray spectrometry has been used to study natural radioactivity in the soils of the towns of Karibib and Okahandja in Namibia. Each town was divided into ten geographical areas and five soil samples were collected across each geographical area (giving a total of 50 samples in each town). The activity concentrations of the primordial radionuclides ^{238}U, ^{232}Th and ^{40}K in the 50 soil samples collected from each town were determined and used to calculate the mean absorbed dose rates, effective dose rates, radium equivalent and external hazard indices. In Karibib the mean activity concentration of ^{238}U is 29.4 ± 5.8 Bq/kg (and ranges from 14.3 Bq/kg to 43.1 Bq/kg). Also, the mean activity concentration of ^{232}Th is 49.0 ± 8.6 Bq/kg (and ranges from 29.0 Bq/kg to 69.9 Bq/kg) while the mean activity concentration of ^{40}K is 824.3 ± 153.5 Bq/kg (and ranges from 505.3 Bq/kg to 1168.4 Bq/kg). Similarly, in Okahandja, the mean activity concentration of ^{238}U is 40.9 ± 8.6 Bq/kg (and ranges from 25.9 Bq/kg to 71.7 Bq/kg). Also, the mean activity concentration of ^{232}Th is 57.9 ± 19.4 Bq/kg (and ranges from 34.6 Bq/kg to 138.8 Bq/kg) while the mean activity concentration of ^{40}K is 562.4 ± 125.4 Bq/kg (and ranges from 307.4 Bq/kg to 857.9 Bq/kg). In both towns, ^{238}U has the least mean activity concentration in the soils while ^{40}K has the highest mean activity concentration in the soils. However, the mean activity concentration of ^{238}U and ^{232}Th are higher in Okahandja than in Karibib while the mean activity concentration of ^{40}K is higher in Karibib than in Okahandja. A comparison of the mean activity concentration of ^{40}K in both towns with those determined by other researchers in some towns in western Namibia shows that the

observed increase in the mean activity concentration of ^{40}K with decreasing latitude does not extend to the towns of Karibib and Okahandja.

The mean absorbed dose rates in Karibib and Okahandja are 77.6 ± 10.9 nGy/h and 77.3 ± 18.0 nGy/h and the corresponding mean effective dose rates are respectively 0.095 ± 0.013 mSv/year and 0.095 ± 0.022 mSv/year. The absorbed dose rates in the two towns are higher than the worldwide average value of 51 nGy/hr. However, the corresponding mean effective dose rates in the towns are far below the maximum permissible value of 1.0 mSv/year. This result implies that the towns of Karibib and Okahandja has normal background radiation. Also, the mean Radium equivalent activities in Karibib and Okahandja are 163.0 ± 22.6 Bq/kg and 167.1 ± 40.1 Bq/kg. Both of these values are much lower than the recommended value of 370 Bq/kg thus confirming that both towns have normal background radiation. The average external hazard indices determined for Karibib and Okahandja are 0.44 ± 0.06 and 0.45 ± 0.11 respectively. These values are again far less than the recommended safe level of unity. This result further confirms that radiological hazard is negligible in both Karibib and Okahandja. The results obtained in this study will be useful in establishing a baseline data on the activity concentrations of ^{238}U, ^{232}Th and ^{40}K in selected towns in Namibia which will be useful as a reference in assessing changes in environmental radioactivity in future.

5.2 Recommendations

Further study may be necessary to estimate internal doses and external doses from other sources like Radon-222 gas from dwellings for the population of Okahandja and Karibib. Also, studies on radiation exposure due to building materials in Okahandja and Karibib can be conducted since all building materials contain various amounts of

natural radioactive nuclides [69–75]. Furthermore, this study can be extended to other major towns in Namibia.

REFERENCES

[1] United Nations Scientific Committee on the Effects of Atomic Radiation.(UNSCEAR) 2000 *SOURCES AND EFFECTS OF IONIZING RADIATION,(ANNEX: B) Exposures from Natural Radiation Sources* (New York: United Nations)

[2] Malain D, Regan P H, Bradley D A, Matthews M, Al-Sulaiti H A and Santawamaitre T 2012 An evaluation of the natural radioactivity in Andaman beach sand samples of Thailand after the 2004 tsunami *Appl. Radiat. Isot.* **70** 1467–74

[3] Chandrasekaran A, Ravisankar R, Rajalakshmi A, Eswaran P, Vijayagopal P and Venkatraman B 2015 Assessment of natural radioactivity and function of minerals in soils of Yelagiri hills, Tamilnadu, India by Gamma Ray spectroscopic and Fourier Transform Infrared (FTIR) techniques with statistical approach *Spectrochim. Acta. A. Mol. Biomol. Spectrosc.* **136** 1734–44

[4] Oyedele J A, Shimboyo S, Sitoka S and Gaoseb F 2010 Assessment of natural radioactivity in the soils of Rössing Uranium Mine and its satellite town in western Namibia, southern Africa *Nucl. Instrum. Methods Phys. Res.* **619** 467–9

[5] El Samad O, Baydoun R, Nsouli B and Darwish T 2013 Determination of natural and artificial radioactivity in soil at North Lebanon province *J. Environ. Radioact.* **125** 36–9

[6] Almayahi B A, Tajuddin A A and Jaafar M S 2014 Measurements of natural radionuclides in human teeth and animal bones as markers of radiation exposure from soil in the Northern Malaysian Peninsula *Radiat. Phys. Chem.* **97** 56–67

[7] Ngachin M, Garavaglia M, Giovani C, Kwato Njock M G and Nourreddine A 2008 Radioactivity level and soil radon measurement of a volcanic area in Cameroon *J. Environ. Radioact.* **99** 1056–60

[8] Alazemi N, Bajoga A D, Bradley D A, Regan P H and Shams H 2016 Soil radioactivity levels, radiological maps and risk assessment for the state of Kuwait *Chemosphere* **154** 55–62

[9] Ahmed N K and El-Arabi A G M 2005 Natural radioactivity in farm soil and phosphate fertilizer and its environmental implications in Qena governorate, Upper Egypt *J. Environ. Radioact.* **84** 51–64

[10] International Atomic Energy Agency (IAEA) 2011 *Radiation Protection and Safety of Radiation Sources: International Basic Safety Standards* (Vienna: IAEA Division of public information)

[11] Sohrabi M 2013 World high background natural radiation areas: Need to protect public from radiation exposure *Radiat. Meas.* **50** 166–171

[12] Shimboyo S A and Oyedele J A 2015 Determination of natural radioactivity in soils of Henties Bay, Namibia. *Int. Sci. Technol. J. Namib.* **5** 104–10

[13] Oyedele J A, Nanghonga T T and Shimboyo S 2014 Natural Radioactivity Measurements In Soil Samples Of The Kupferberg Waste Landfill Site, Windhoek, Namibia. *Int. Sci. Technol. J. Namib.* **4** 23–30

[14] Shimboyo S A, Oyedele J A and Sitoka S S 2016 Soil radioactivity levels and associated hazards in selected towns in uranium-rich western Namibia *Int. Sci. Technol. J. Namib.* **7** 73–84

[15] Namibia Statistics Agency 2011 *Namibia 2011 Population & Housing Census Main Report* (Windhoek: Namibia Statistics Agency)

[16] New Era Publication 2016 Air force capability impresses President *New Era Newsp. Namib.* 1

[17] Martin B R 2008 *Nuclear and particle physics: [an introduction]* (Chichester: Wiley)

[18] Khan F M 2010 *The Physics of Radiation Therapy* (Lippincott Williams & Wilkins)

[19] Cember H and Johnson T E 2009 *Introduction to health physics* (New York: McGraw-Hill Medical)

[20] Bailey D L and American Association of Physicists in Medicine 2014 *Nuclear medicine physics: a handbook for teachers and students* (Vienna: International Atomic Energy Agency)

[21] Jevremovic T 2009 *Nuclear Principles in Engineering* (Boston, MA: Springer US)

[22] Socratic 2017 https://socratic.org/questions/how-does-beta-emission-positron-emission-affect-the-neutron-protron-capture

[23] Vogel D M 2011 Introduction to Nuclear Science *Contemp. Phys.* **52** 95–6

[24] ck12 2017 https://www.ck12.org/chemistry/alpha-decay/lesson/Alpha-Decay-MS-PS/

[25] Thomas Jefferson National Accelerator Facility 2017 education.jlab.org/faq/index.html

[26] Loveland W D, Morrissey D J and Seaborg G T 2006 *Modern nuclear chemistry* (Hoboken, NJ: Wiley-Interscience)

[27] Herdberg V 2017 http://perso.numericable.fr/vincent.hedberg/nuclear/nuke_sl.htm *Numericable*

[28] Oregon State University 2004 https://courses.ecampus.oregonstate.edu/ne581/three/index2.htm

[29] Griffith C 2015 http://www.atomicarchive.com/Company/Company.shtml

[30] T. H. Wu E 2015 Subatomic Particle Structures and Unified Field Theory Based on Yangton and Yington Hypothetical Theory *Am. J. Mod. Phys.* **4** 189

[31] Podgorsak E . 2006 *Radiation Physics for Medical Physiscists* (Germany: Springer)

[32] Turner J E 2007 *Atoms, radiation, and radiation protection* (Weinheim: Wiley-VCH)

[33] Zschornack G 2007 *Handbook of X-ray data: with 161 tables* (Berlin: Springer)

[34] Hall E J and Giaccia A J 2012 *Radiobiology for the radiologist* (Philadelphia: Wolters Kluwer Health/Lippincott Williams & Wilkins)

[35] Nuclear power for every body 2012 http://www.nuclear-power.net/nuclear-power/reactor-physics/interaction-radiation-matter/interaction-gamma-radiation-matter/photoelectric-effect/ *Nucl. Power*

[36] Anon 2009 http://hyperphysics.phy-astr.gsu.edu/hbase/quantum/compton.html *HyperPhysics*

[37] Knoll G F 1999 *Radiation Detection and Measurement* (New York: John Wiley & Sons, Inc.)

[38] Nuclear power for everybody 2012 http://www.nuclear-power.net/nuclear-power/reactor-physics/interaction-radiation-matter/interaction-gamma-radiation-matter/compton-scattering/ *Nucl. Power*

[39] Massachusetts Institute of Technology 2006 http://www.flickriver.com/photos/mitopencourseware/4706123553/

[40] Nuclear power for every body 2012 http://www.nuclear-power.net/nuclear-power/reactor-physics/interaction-radiation-matter/interaction-gamma-radiation-matter/pair-production/ *Nucl. Power*

[41] Stack Exchange Inc 2017 https://physics.stackexchange.com/questions/282163/why-does-the-cross-section-for-compton-scattered-photons-decrease-with-increasin

[42] Lam S 2012 http://large.stanford.edu/courses/2012/ph241/lam1/

[43] Fullonstudy Blog 2017 http://www.fullonstudy.com/2017/10/gas-filled-detectors-nuclear-radiation.html *Full Study*

[44] Mirion Technologies 2017 http://www.canberra.com

[45] Khandaker M U 2011 High purity germanium detector in gamma-ray spectrometry *Int. J. Fundam. Phys. Sci.* **1** 42–6

[46] Anon 2013 PN Junction Diode and Diode Characteristics *Basic Electron. Tutor.*

[47] Debertin K and Helmer R G 1988 *Gamma- and X-Ray Spectrometry with Semiconductor Detectors* (North Holland)

[48] National Research Council 2006 *Health risks from exposure to low levels of ionizing radiation: BEIR VII Phase 2* (Washington, DC: National Acad. Press)

[49] Ledingham K W D, Bolton P R, Shikazono N and Ma C-M C 2014 Towards Laser Driven Hadron Cancer Radiotherapy: A Review of Progress *Appl. Sci.* **4** 402–43

[50] ICRP 2007 ICRP publication 103 *Ann ICRP* **37** 2

[51] Dörr W and Hendry J H 2001 Consequential late effects in normal tissues *Radiother. Oncol.* **61** 223–31

[52] IAEA 1997 IAEA-TECDOC-870 Methods for estimating the probability of cancer from occupational radiation exposure *Int. At. Energy Agency IAEA*

[53] Katz A S 2014 The Chemistry and Toxicology of Depleted Uranium *Toxics* **2**

[54] Aliyu A S and Ramli A T 2015 The world's high background natural radiation areas (HBNRAs) revisited: A broad overview of the dosimetric, epidemiological and radiobiological issues *Radiat. Meas.* **73** 51–59

[55] Lauria D C and Godoy J M 2002 Abnormal high natural radium concentration in surface waters *J. Environ. Radioact.* **61** 159–68

[56] Wang Z, Boice J D Jr, Wei L, Beebe G W, Zha Y, Kaplan M M, Too Z, Maxon H R III, Zhang S, Schneider A B, Tan B, Wesseler T A, Chen D, Ershow A G, Kleinerman R A, Littlefield L G and Preston D 1990 Thyroid Nodularity and Chromosome Aberrations Among Women in Areas of High Background Radiation in China *JNCI J. Natl. Cancer Inst.* **82** 478–85

[57] Das D B and Karuppasamy C V 2009 Spontaneous frequency of micronuclei among the newborns from high level natural radiation areas of Kerala in the southwest coast of India *Int. J. Radiat. Biol.* **85** 272–80

[58] Ghiassi-Nejad M, Beitollahi M M, Fallahian N and Saghirzadeh M 2005 New findings in the very high natural radiation area of Ramsar, Iran *Int. Congr. Ser.* **1276** 13–6

[59] National Research Council (U.S.) and Committee on the Biological Effects of Ionizing Radiations 1990 *Health effects of exposure to low levels of ionizing radiation* (Washington, D.C.: National Academy Press)

[60] Karahan G and Bayulken A 2000 Assessment of gamma dose rates around Istanbul (Turkey) *J. Environ. Radioact.* **47** 213–21

[61] Tzortzis M and Tsertos H 2004 Determination of thorium, uranium and potassium elemental concentrations in surface soils in Cyprus *J. Environ. Radioact.* **77** 325–38

[62] Mendelsohn J, Jarvis A, Robertson T and Roberts C 2002 *Atlas of Namibia, A Portrait of the Land snd its People* (Capetown: David Philip)

[63] Dalet D 2017 http://d-maps.com/carte.php?num_car=26891&lang=en *Repub. Namib.*

[64] Amptek inc. 2017 http://amptek.com/charge-trapping-in-xr-100t-cdte-cadmium-telluride-detectors-application-note/

[65] Beck H, De campo J and Gogolak C 1972 In situ Ge (Li) and Na (Tl) gamma-ray spectrometry *US Dep. Energy Environ. Meas. Lab.*

[66] Agbalagba E O and Onoja R A 2011 Evaluation of natural radioactivity in soil, sediment and water samples of Niger Delta (Biseni) flood plain lakes, Nigeria *J. Environ. Radioact.* **102** 667–71

[67] Diab, H.M., Nouh, S.A., Hamdy, A. and EL-Fiki, S.A. 2007 Evaluation of natural radioactivity in a cultivated area around a fertilizer factory *J. Nucl. Radiat. Phys.* **3** 53–62

[68] Spiegel M R and Stephens L J 1998 *Schaum's Outlines Theory and Problems of Statistics* (McGraw-Hill)

[69] Ravisankar R, Vanasundari K, Chandrasekaran A, Rajalakshmi A, Suganya M, Vijayagopal P and Meenakshisundaram V 2012 Measurement of natural radioactivity in building materials of Namakkal, Tamil Nadu, India using gamma-ray spectrometry *Appl. Radiat. Isot.* **70** 699–704

[70] Sharaf J M and Hamideen M S 2013 Measurement of natural radioactivity in Jordanian building materials and their contribution to the public indoor gamma dose rate *Appl. Radiat. Isot.* **80** 61–6

[71] Kayakökü K, Karatepe Ş and Doğru M 2016 Measurements of radioactivity and dose assessments in some building materials in Bitlis, Turkey *Appl. Radiat. Isot.*

[72] Papaefthymiou H and Gouseti O 2008 Natural radioactivity and associated radiation hazards in building materials used in Peloponnese, Greece *Radiat. Meas.* **43** 1453–7

[73] Stojanovska Z, Nedelkovski D and Ristova M 2010 Natural radioactivity and human exposure by raw materials and end product from cement industry used as building materials *Radiat. Meas.* **45** 969–72

[74] El-Mageed A I A, Farid M E-A, Saleh E E, Mansour M and Mohammed A K 2014 Natural radioactivity and radiological hazards of some building materials of Aden, Yemen *J. Geochem. Explor.* **140** 41–5

[75] Szabó Z, Völgyesi P, Nagy H é., Szabó C, Kis Z and Csorba O 2013 Radioactivity of natural and artificial building materials – a comparative study *J. Environ. Radioact.* **118** 64–74

APPENDIX 1

Isotope concentrations in Karibib						
Area	U-238 concentration (Bq/Kg)	U-238 concentration error (Bq/Kg)	Th-232 concentration (Bq/Kg)	Th-232 concentration error (Bq/Kg)	K-40 concentration (Bq/Kg)	K-40 concentration error (Bq/Kg)
TL	14.34	2.26	60.88	4.14	505.26	23.42
TL	35.85	2.27	53.38	3.98	826.32	34.12
TL	43.09	2.70	69.85	5.01	1168.42	45.06
TL	27.30	1.83	33.09	3.24	715.79	30.26
TL	33.68	2.23	42.21	4.10	789.47	32.64
NP	32.69	2.26	43.68	3.67	694.74	29.56
NP	32.36	2.26	40.44	3.70	815.79	33.71
NP	36.18	2.17	36.91	3.41	821.05	34.08
NP	30.98	2.10	48.97	4.02	726.32	30.54
NP	31.05	2.05	48.82	3.87	710.53	30.18
KH	28.68	2.09	51.62	4.22	1057.90	41.31
KH	39.53	2.37	54.71	4.25	1026.32	40.48
KH	19.80	1.68	32.79	2.92	621.05	27.39
KH	27.30	2.14	28.97	3.30	752.63	31.54
KH	23.42	1.76	36.32	3.38	652.63	28.46
KT	30.06	2.09	56.47	4.17	857.90	35.00
KT	42.30	2.39	54.41	3.55	994.74	39.41
KT	29.14	2.03	54.56	4.13	921.05	36.91
KT	24.40	1.98	56.03	4.22	736.84	31.16
KT	25.52	2.03	43.82	3.54	778.95	32.54
HG	33.48	2.09	53.68	4.04	878.95	35.70
HG	24.93	2.03	39.12	3.40	773.68	32.17
HG	39.01	2.27	47.94	3.88	873.68	35.52
HG	23.09	2.01	51.47	4.04	621.05	27.46
HG	30.78	2.07	46.76	3.75	857.90	34.93
TF	22.43	2.09	56.32	3.97	652.63	28.56
TF	27.69	2.12	61.62	4.51	731.58	30.88
TF	30.72	2.15	45.29	3.92	784.21	32.47
TF	29.14	2.15	57.94	4.09	773.68	32.12
TF	21.18	2.06	55.74	4.04	578.95	25.91
CB	29.27	2.37	55.88	3.21	884.21	35.68
CB	29.53	2.04	51.32	3.83	736.84	30.96
CB	25.65	2.13	54.26	4.04	742.11	31.22
CB	21.58	1.63	38.38	3.44	731.58	30.87
CB	24.67	2.14	41.62	3.60	821.05	33.80
OG	20.46	1.75	60.74	3.67	605.26	26.51
OG	25.06	1.93	47.94	3.22	673.68	29.01
OG	29.21	2.13	40.00	3.73	742.11	31.03
OG	34.01	2.37	40.59	3.98	710.53	30.43
OG	30.32	2.01	39.12	3.49	805.26	33.23
LM	27.56	2.00	51.47	3.94	968.42	38.60
LM	33.74	2.04	46.47	4.07	1057.90	41.28
LM	36.38	2.29	52.50	3.96	1057.90	41.45
LM	30.52	2.06	51.03	3.97	926.32	37.08
LM	31.18	2.09	48.09	4.07	1015.79	39.98
EP	32.96	2.05	51.62	4.02	1052.63	41.16
EP	36.51	2.28	60.44	4.07	1063.16	41.68
EP	25.85	1.92	56.62	4.69	1078.95	42.25
EP	28.61	2.07	43.53	3.83	1026.32	40.48
EP	28.88	2.06	53.38	4.09	815.79	33.90

APPENDIX 2

Isotope Concentrations in Okahandja							
S/N	*Area*	U^{238} conc (Bq/kg)	U^{238} conc error (Bq/kg)	Th^{232} conc (Bq/kg)	Th^{232} conc error (Bq/kg)	K^{40} conc (Bq/kg)	K^{40} conc error (Bq/kg)
1	BE	41.37	2.28	48.97	3.78	815.79	32.52
2	BE	45.91	2.34	53.68	3.75	460.53	21.55
3	BE	48.41	2.34	95.29	5.21	678.95	28.02
4	BE	35.52	2.08	46.32	3.95	531.58	23.67
5	BE	45.65	2.46	49.41	3.85	480.00	22.08
6	NP	35.72	2.32	57.06	3.85	382.63	18.97
7	NP	39.99	2.32	47.06	3.49	376.32	18.54
8	NP	33.48	2.07	53.09	3.92	320.00	16.80
9	NP	34.73	2.10	41.76	3.70	307.37	16.53
10	NP	29.73	1.86	39.12	3.15	355.79	17.88
11	FE	49.33	2.60	48.53	3.83	726.32	29.51
12	FE	52.62	2.70	72.79	4.63	636.84	26.85
13	FE	51.37	2.56	46.76	4.11	652.63	27.21
14	FE	44.73	2.28	50.74	4.15	689.47	28.28
15	FE	54.79	2.55	72.94	4.75	578.95	25.10
16	AE	43.15	2.29	63.68	3.87	547.37	24.08
17	AE	41.64	2.40	61.47	4.17	568.42	24.77
18	AE	36.84	2.33	52.06	4.64	517.37	23.13
19	AE	36.38	2.21	51.32	3.89	573.68	24.88
20	AE	35.32	2.06	46.18	3.52	470.53	21.85
21	VO	40.85	2.36	71.18	4.29	721.05	29.53
22	VO	29.27	1.98	40.44	3.66	497.90	22.32
23	VO	28.55	1.85	34.56	3.13	857.90	33.30
24	VO	31.77	2.15	40.74	3.70	621.05	26.36
25	VO	25.92	2.00	35.15	3.23	445.26	20.71
26	CE	30.19	1.99	44.56	3.69	420.00	19.91
27	CE	34.47	2.22	41.91	3.94	520.53	23.23
28	CE	34.07	1.91	52.06	3.82	460.53	21.26
29	CE	43.09	2.36	56.47	4.03	557.90	24.43
30	CE	44.66	2.34	63.24	4.27	657.90	27.84
31	DE	46.70	2.36	63.38	4.32	474.21	21.89
32	DE	47.30	2.56	58.53	4.19	547.37	24.04
33	DE	44.80	2.48	57.35	4.40	573.68	25.06
34	DE	32.03	2.27	41.91	3.73	515.79	23.22
35	DE	33.28	1.98	37.94	3.76	521.58	22.95
36	GE	45.85	2.50	86.91	4.93	642.11	26.93
37	GE	42.76	2.15	60.29	4.20	482.11	22.18
38	GE	71.70	3.22	138.82	6.74	763.16	31.37
39	GE	49.40	2.60	101.91	5.56	768.42	31.05
40	GE	40.98	2.32	38.53	3.58	600.00	25.54
41	OP	51.04	2.61	72.94	4.71	621.05	26.62
42	OP	38.55	2.38	55.74	3.88	513.16	22.80
43	OP	32.63	2.34	60.74	4.43	726.32	29.66
44	OP	49.47	2.41	83.24	4.97	647.37	27.28
45	OP	51.04	2.71	88.53	5.36	668.42	28.10
46	NC	29.27	1.88	42.94	3.58	417.90	20.01
47	NC	44.20	2.52	60.59	4.36	471.05	22.05
48	NC	41.18	2.40	63.97	4.29	513.68	23.35
49	NC	42.36	2.21	47.5	4.23	584.21	25.13
50	NC	31.97	2.11	56.18	4.29	636.84	26.68

APPENDIX 3

Python Program to calculate activity concentrations

```
#!/usr/bin/env python2
# -*- coding: utf-8 -*-
"""
Created on Tue Feb 14 08:30:44 2017
@author: midzi
"""
# Program to calculate concentrations, Dose rate and Anual effective dose from the isotopes U-238, Th-232 and K-40
import numpy as np
f = open ('full-kar-results.txt','r')     # opens the textfile with results for U, Th and K Net peak Areas and their errors
contents = f.readlines()       # list the contents of the opened file as string
U = []                    # create empty list to input Net Peak Area of U in sample
U1 = []                    # create empty list to input error Net Peak Area of U in sample
Th = []                    # create empty list to input Net Peak Area of Th in sample
Th1= []                    # create empty list to input error Net Peak Area of Th in sample
K = []                    # create empty list to input Net Peak Area of K in sample
K1 = []                    # create empty list to input error Net Peak Area of K in sample
for lines in contents:
    spl = lines.strip().split()          # split the lines into columns
    if len(spl)==6:                    # split lines in 6 columns
        a,b,c, d, e, g = lines.split()    # different columns assigned to a,b, ..g
        U.append(float(a))              # append column a into empty U list
        Th.append(float(c))             # append column c into empty Th list
        U1.append(float(b))             # append column b into empty U1 list
        Th1.append(float(d))            # append column d into empty Th1 list
        K.append(float(e))              # append column e into empty K list
        K1.append(float(g))             # append column g into empty K1 list
U = np.array(U)                    # create array of U Net Peak Area values
U1 = np.array(U1)                    # create array of U1 Net Peak Area error values
Th = np.array(Th)                    # create array of Th Net Peak Area error values
```

```
Th1 = np.array(Th1)                # create array of Th1 Net Peak Area error values
K = np.array(K)                    # create array of K Net Peak Area error values
K1 = np.array(K1)                  # create array of K1 Net Peak Area error values

As_U = 73700.0                     # Net peak area in RGU standard
Cs_U = 4940.0                      # Concentration of U in Bq/kg in RGU standard
k_U = As_U/Cs_U                    #k standard for U-238
ke_U = 0.11                        # error in k standard in U
As_Th = 21700.0                    # Net peak area in RGTh standard
Cs_Th = 3250.0                     # Concentration of U in Bq/kg in RGTh standard
k_Th = As_Th/Cs_Th                 #k standard for Th-232
As_K = 27800.0                     # Net peak area in RGk standard
Cs_K = 14000.0                     # Concentration of U in Bq/kg in RGK standard
ke_Th = 0.19                       # error in k standard in Th
k_K = As_K/Cs_K                    #k standard for K-40
ke_K = 0.06                        #  error in k standard in K
for n in U, U1, Th, K, K1:         # for Loop calculation of Isotope concentration
   U_concn = U/k_U
   U_concn_er = U_concn*(((U1/U)**2 + (ke_U/k_U)**2)**0.5)
   Th_concn = Th/k_Th
   Th_concn_er = Th_concn*(((Th1/Th)**2 + (ke_Th/k_Th)**2)**0.5)
   K_concn = K/k_K
   K_concn_er = K_concn*(((K1/K)**2 + (ke_K/k_K)**2)**0.5)
for p in U_concn, Th_concn, K_concn, U_concn_er, Th_concn_er, K_concn_er:
   Dt = 0.042* K_concn + 0.429*U_concn + 0.666*Th_concn
   Dt_er = ((0.042*K_concn_er)**2 + (0.429*U_concn_er)**2 + (0.666*Th_concn_er)**2)**0.5
for q in Dt, Dt_er:
   A_eff_Dose = Dt*0.00876*0.7*0.2
   A_eff_Dose_er = Dt_er*0.00876*0.7*0.2
z = open ('results-karibib.txt','w')
```

```
z.write ('U_cn \t U-cn_er \t Th_cn \t Th_cn-er \t \t K_cn \t \t \t K_cn_er \t Dse_rt \t Dse_rt_er \t A_ef_dse \t A_ef_dse_er \n')

i = 0

for i in range (0,50):

    z.write ('%2.2f \t %2.2f \t \t %2.2f \t \t %2.2f\t \t %2.3f \t \t %2.2f \t \t %2.2f \t \t %2.2f \t \t %2.3f \t \t %2.3f \n'%(U_concn[i], U_concn_er[i],Th_concn[i], Th_concn_er[i], K_concn[i], K_concn_er[i], Dt[i], Dt_er[i], A_eff_Dose[i], A_eff_Dose_er[i]))

    i += 1

f.close
```

UNAM
UNIVERSITY OF NAMIBIA

ETHICAL CLEARANCE CERTIFICATE

Ethical Clearance Reference Number: FOS/173/2017 **Date: 28 March, 2017**

This Ethical Clearance Certificate is issued by the University of Namibia Research Ethics Committee (UREC) in accordance with the University of Namibia's Research Ethics Policy and Guidelines. Ethical approval is given in respect of undertakings contained in the Research Project outlined below. This Certificate is issued on the recommendations of the ethical evaluation done by the Faculty/Centre/Campus Research & Publications Committee sitting with the Postgraduate Studies Committee.

Title of Project: An Evaluation Of The Natural Radioactivity In The Soils Of Okahandja And Karibib, Namibia-

Nature/Level of Project: Masters

Researcher: Wilfred Midzi

Student Number: 201406379

Faculty: Faculty of Science

Supervisor: Professor J Oyedele

Take note of the following:

(a) Any significant changes in the conditions or undertakings outlined in the approved Proposal must be communicated to the UREC. An application to make amendments may be necessary.

(b) Any breaches of ethical undertakings or practices that have an impact on ethical conduct of the research must be reported to the UREC.

(c) The Principal Researcher must report issues of ethical compliance to the UREC (through the Chairperson of the Faculty/Centre/Campus Research & Publications Committee) at the end of the Project or as may be requested by UREC.

(d) The UREC retains the right to:

(i) Withdraw or amend this Ethical Clearance if any unethical practices (as outlined in the Research Ethics Policy) have been detected or suspected,

(ii) Request for an ethical compliance report at any point during the course of the research.

UREC wishes you the best in your research.

Prof. P. Odonkor: UREC Chairperson

Ms. P. Claassen: UREC Secretary

CENTRE FOR POSTGRADUATE STUDIES

University of Namibia, Private Bag 13301, Windhoek, Namibia
340 Mandume Ndemufayo Avenue, Pioneers Park
☎ +264 61 206 3275/4662; Fax +264 61 206 3290; URL.: http//www.unam.edu.na

UNAM
UNIVERSITY OF NAMIBIA

RESEARCH PERMISSION LETTER

Student Name: Wilfred Midzi

Student number: 201406379

Programme: MSc Nuclear Science

Approved research title: AN EVALUATION OF THE NATURAL RADIOACTIVITY IN THE SOILS OF OKAHANDJA AND KARIBIB, NAMIBIA

TO WHOM IT MAY CONCERN

I hereby confirm that the above mentioned student is registered at the University of Namibia for the programme indicated. The proposed study met all the requirements as stipulated in the University guidelines and has been approved by the relevant committees.

The proposal adheres to ethical principles as per attached Ethical Clearance Certificate. Permission is hereby granted to carry out the research as described in the approved proposal.

Best Regards

Dr Marius Hedimbi
Director: Centre for Postgraduate Studies
Tel: +264 61 2063275
E-mail: mhedimbi@unam.na

Centre for Postgraduate Studies
Office of the Director
2017 -04- 05
University of Namibia
UNAM